UNIVERSITÉ DE GRENOBLE

THÈSE

Pour obtenir le grade de

DOCTEUR DE L'UNIVERSITÉ DE GRENOBLE

Spécialité : **Physique subatomique & astroparticules**

Arrêté ministériel : 7 août 2006

Présentée par

Vincent Lamirand

Thèse dirigée par **Eric Liatard**
et codirigée par **Vincent Gressier**

préparée au sein du **Laboratoire de Métrologie et de Dosimétrie des Neutrons (IRSN)**
dans **l'École Doctorale de Physique de Grenoble**

Détermination de sections efficaces pour la production de champs neutroniques monoénergétiques de basse énergie

Thèse soutenue publiquement le **18 novembre 2011**,
devant le jury composé de :

Dr. Gérard Barreau
Docteur émérite CNRS, CENBG, Rapporteur
Dr. Frank Gunsing
Ingénieur-chercheur CEA, SPhN, Rapporteur
Pr. Eric Liatard
Professeur, Université Joseph Fourier, Grenoble, Membre
Dr. Vincent Gressier
Ingénieur-chercheur IRSN, LMDN, Membre
Dr. David J. Thomas
Docteur, National Physical Laboratory, Membre
Dr. Ralf Nolte
Docteur, Physikalisch-Technische Bundesanstalt, Membre
Dr. Stephan Oberstedt
Docteur, Institute for Reference Materials and Measurements, Membre

À mes sœurs

Le vrai miracle n'est pas de marcher sur les eaux ni de voler dans les airs : il est de marcher sur la terre.

惠能

Remerciements

Bonne lecture aux courageux, le reste du français est à la fin !

Résumé

La réponse d'un détecteur de neutrons varie avec l'énergie du neutron incident. La détermination expérimentale de cette variation se réalise au moyen de champs neutroniques monoénergétiques. Ceux-ci sont produits par l'interaction entre un faisceau d'ions accélérés et une cible fine constituée d'un dépôt réactif sur un support métallique. En utilisant différentes réactions telles que $^7Li(p,n)$, $^3H(p,n)$, $^2H(d,n)$ et $^3H(d,n)$, il est possible de produire des neutrons entre 120 keV et 20 MeV dans la direction du faisceau incident (0°).

Pour atteindre des énergies inférieures, il est possible d'augmenter l'angle du point de mesure par rapport à la direction du faisceau d'ions. Cependant, cette méthode présente des problèmes d'homogénéité en énergie et en fluence des neutrons à la surface du détecteur, ainsi qu'une augmentation de la proportion de neutrons diffusés. Une alternative est l'utilisation d'autres réactions nucléaires, notamment la réaction $^{45}Sc(p,n)$ qui permet de descendre jusqu'à des énergies de 8 keV à 0°.

Une étude complète de cette réaction et de sa section efficace a été menée au sein d'une coopération scientifique entre le laboratoire de métrologie et de dosimétrie des neutrons (LMDN) de l'IRSN, deux instituts de métrologie européens, le NPL (National Physical Laboratory, RU) et le PTB (Physikalisch-Technische Bundesanstalt, All), et l'IRMM (Institute for Reference Materials and Measurements, CEE).

Parallèlement, d'autres réactions envisageables ont été étudiées : $^{65}Cu(p,n)$, $^{51}V(p,n)$, $^{57}Fe(p,n)$, $^{49}Ti(p,n)$, $^{53}Cr(p,n)$ et $^{37}Cl(p,n)$. Elles ont été comparées en termes d'émission neutronique et d'énergie minimale des neutrons produits.

Mots-clés : Neutron ; section efficace ; champ neutronique monoénergétique ; accélérateur ; réaction nucléaire ; détecteur de neutrons ; $^{45}Sc(p,n)$; métrologie.

Abstract

The response of a neutron detector, defined as the reading of the device per unit of incident fluence or dose, varies with neutron energy. The experimental determination of this variation, i.e. of the response function of this instrument, has to be performed by facilities producing monoenergetic neutron fields. These neutrons are commonly produced by interaction between accelerated ions (proton or deuteron) onto a thin target composed of a reactive layer deposited on a metallic backing. Using the $^7Li(p,n)$, $^3H(p,n)$, $^2H(d,n)$ and $^3H(d,n)$ reactions, monoenergetic neutrons are obtained between 120 keV and 20 MeV in the ion beam direction (0°).

To reach lower neutron energies, the angle of the measuring point with respect to the ion beam direction can be increased. However, this method presents several problems of neutron energy and fluence homogeneities over the detector surface, as well as an important increase of the scattered neutron contribution. Another solution is to investigate other nuclear reactions, as $^{45}Sc(p,n)$ allowing to extend the neutron energy range down to 8 keV at 0°.

A complete study of this reaction and its cross section has been undertaken within the framework of a scientific cooperation between the laboratory of neutron metrology and dosimetry (IRSN, France), two European national metrological institutes, the National Physical Laboratory (UK) and the Physikalisch-Technische Bundesanstalt (Germany), and IRMM, the Institute for Reference Materials and Measurements (EC).

In parallel, other possible reactions have been investigated: $^{65}Cu(p,n)$, $^{51}V(p,n)$, $^{57}Fe(p,n)$, $^{49}Ti(p,n)$, $^{53}Cr(p,n)$ and $^{37}Cl(p,n)$. They were compared in terms of neutron fluence and minimum energy of the produced neutrons.

Keywords: Neutron ; cross section ; monoenergetic neutron fields; electrostatic accelerator; nuclear reaction ; neutron detector; $^{45}Sc(p,n)$; metrology.

Table of Contents

Introduction
Monoenergetic neutron fields for detector calibration

The response of a neutron detector, defined as its reading per unit of incident neutron fluence or dose, varies with neutron energy. This variation, called response function, is usually calculated using Monte-Carlo codes and determined through experiments at facilities producing monoenergetic neutron fields.

These kinds of neutron fields can be produced with radioactive sources, nuclear reactors or accelerators (Ma60). Radioactive sources such as antimony-beryllium sources can be employed. The neutrons are produced by (γ,n) reactions between 1691 keV and 2091 keV γ rays of ^{124}Sb and beryllium. The main neutron group has an energy of 22.8 ± 1.3 keV. Since this source also produces a higher energy group (378 keV, 3 percent of the main contribution), it can only be considered a quasi-monoenergetic source. Its half-life is only 60 days, so ^{124}Sb is usually produced immediately prior to any measurement (Th10-2).

Reactor-based sources consist in filtering the neutron beam coming from the reactor with different materials (Sc, Fe, Al, Si) in order to obtain quasi-monoenergetic neutron sources between the thermal range and 144 keV (ISO 8529). Their use is mainly limited by the need for and constraints of a nuclear reactor.

Accelerator-based neutron sources, resulting from two-body reactions, are a convenient way to produce monoenergetic fields. The neutrons are obtained from nuclear reactions between accelerated charged particles (like protons and deuterons) and targets of specific material. As a result of the collisions, neutrons are emitted in every direction, creating a neutron field. Each projectile energy and emission angle correspond to a single neutron energy; therefore, they are sources of monoenergetic neutron fields. It allows for various uses such as detector calibration and scientific experiments.

Protons and deuterons accelerated up to 3.5 MeV and driven onto appropriate targets produce monoenergetic neutrons between 120 keV and 19 MeV in the ion beam direction (0°), as described in Table 1.

Table 1: *Commonly employed nuclear reactions for the production of monoenergetic neutron fields. Available neutron energy ranges in the ion beam direction (0°) are indicated, as well as the corresponding projectile energy ranges. In brackets the energy range for ion beam energy range limited to 100 keV-4 MeV is given.*

Reaction	Ion energy range (MeV)		Neutron energy range (at 0°, MeV)	
^{7}Li(p,n)^{7}Be	1.92	2.37	0.12	0.65
^{3}H(p,n)^{3}He	1.15	8.35	0.29	7.58 (3.2)
^{2}H(d,n)^{3}He	0	4.45	2.45 (2.85)	7.71 (7.26)
^{3}H(d,n)^{4}He	0	3.71	14.1 (14.7)	20.5

These latter nuclear reactions are not suitable for the production of monoenergetic neutron fields below 120 keV in the ion beam direction. Several other solutions are employed instead.

Low-energy neutron ranges are possible at other angles with the ^{7}Li(p,n) reaction (Gi60). However, the use of these angles presents problems, as the neutron energy and fluence vary rapidly across the detector surface, and the relative scattered-neutron contribution increases with angles (Ro77).

An original approach has been developed by NMIJ for 24 keV-neutron energy. It consists in the iron resonance filtering of neutrons produced in a thick lithium target by the ^{7}Li(p, n)^{7}Be reaction below the monoenergetic threshold (Ha10).

An alternative solution is to use other nuclear reactions to produce low energy monoenergetic neutron fields at 0°. The main drawback of these neutron fields is the low neutron yield as compared to that of ^{7}Li(p,n). The ^{45}Sc(p,n) reaction appears to be one of the most favourable candidates, capable of extending the neutron energy range down to 8 keV at 0° with a neutron yield that is sufficient for the calibration of radiation protection devices.

The importance of low-energy calibration can be illustrated by the following:
- The over response of survey meters and dosimeters in the 10^{-5}-10^2 keV range, as already demonstrated in previous simulations and measurements (see Fig. 1, Al94, Kl97 and also 5.2)
- International Electrotechnical Commission (IEC) standards recommend one energy below 100 keV and one between 1 keV and 50 keV for the calibration of personal dose devices (IEC 61526) and ambient dose devices (IEC 61005), respectively. ISO standard 8529 (ISO 8529-1) recommends ^{7}Li(p,n) and ^{45}Sc(p,n) reactions within this energy range.
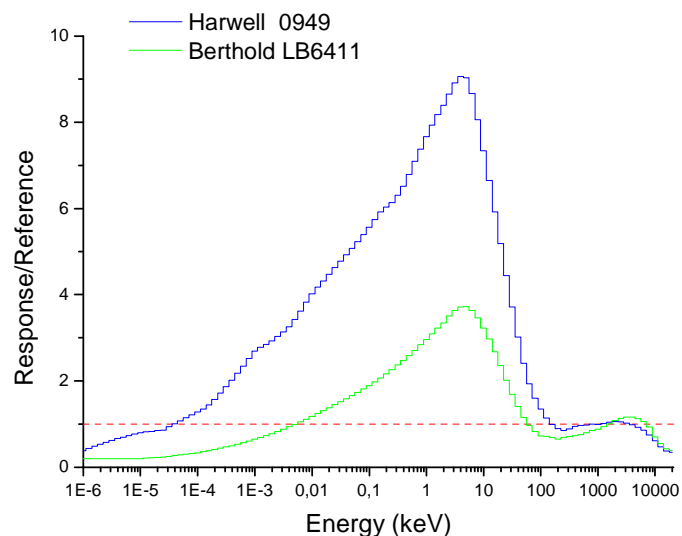
Fig. 1: *Simulated responses (normalised with ^{252}Cf) of Harwell and Berthold survey meters.*

The aim of this study is therefore to investigate nuclear reactions capable of producing low-energy monoenergetic neutron fields suitable for the calibration of neutron detectors. This includes a comprehensive study of the ^{45}Sc(p,n) reaction and the investigation of other suitable reactions for calibration in the keV neutron range. In particular, differential cross section and cross section structure will be determined. The study is also motivated by the next international comparison exercise for neutron fluence references in monoenergetic neutron fields (CCRI K11), which is planned for 2011 and will include 27-keV neutron energy.

This study is undertaken within the framework of European scientific cooperation between the Institute for Reference Materials and Measurements (IRMM, EC), the National Physical Laboratory (NPL, United Kingdom), the Physikalisch-Technische Bundesanstalt (PTB, Germany) and the Institute for Radiological protection and Nuclear Safety (IRSN, France).

1 NEUTRON PRODUCING NUCLEAR REACTIONS

1.1 NUCLEAR REACTIONS

When particles enter matter, they can interact in various ways, depending on the energy and nature of the particles in play. At low energy, interaction with the electron cloud of the atoms prevails. When particles of higher energy, from accelerator, nuclear source or cosmic rays hit matter, they can interact with the nuclei of the material, leading to nuclear reactions.

A two-body nuclear reaction is an interaction process between a projectile and a nucleus. It results in transformations induced by nuclear forces. It can be written as follows:

$$a + X \rightarrow b + Y$$
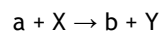
Where:

- a is the accelerated ion, the projectile
- X is the target nucleus
- b is the light product of the reaction
- Y is the heavy product of the reaction, the resulting nucleus.

These reactions are conventionally written X(a,b)Y.
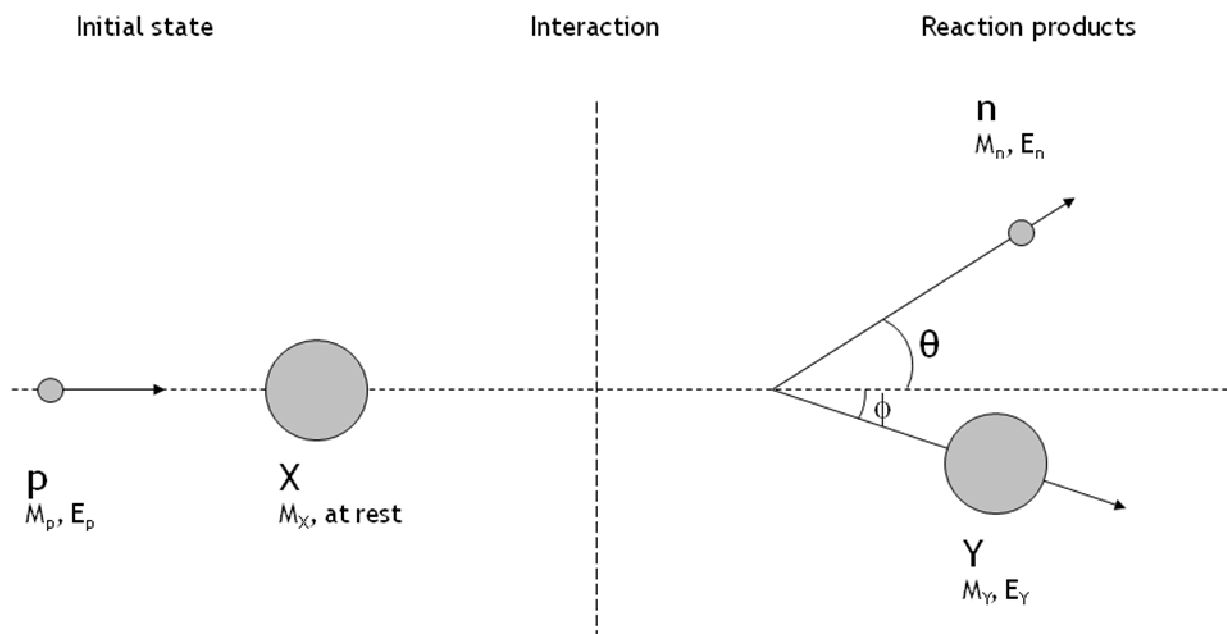
Fig. 2: *Two-body nuclear reaction with neutron production, in the laboratory frame of reference. The kinematics of the reaction does not depend on the interaction process (direct exchange, formation of a compound nucleus) but rather on the masses M and energies E of the initial particles.*

Nuclear reactions used to produce monoenergetic neutron fields are interaction processes between accelerated ions and nuclei of a target. A large number of reactions are therefore possible, depending on the accelerator's capabilities (type and energy of the ions, intensity of the beam) and the chosen target. For monoenergetic neutron field production, one condition is that the heavy product Y is in its fundamental state. If this nucleus is in an excited state Y*, it emits new particles through various decay modes, and monoenergeticity can be lost.

In a first part are described the main interactions that can occur when a particle approach the nucleus of an atom, as well as the possible interaction mechanisms. In a second part are presented the conservation laws ruling those interactions. A full description of these phenomena can be found in (Be04), the aim of these parts is to introduce the needed concepts.

1.1.1 INTERACTION BETWEEN CHARGED PARTICLES AND ELECTRONS

An atom can be described by a nucleus surrounded by electrons. The size of a nucleus is comprised between a few and a few tens of femtometres (10^{-15} m). It has a positive electric charge Z.e, with Z being the atomic number of the atom and e the elementary electric charge. Z negatively charged electrons orbit around the nucleus at a distance about one Angstrom (10^{-10} m). The atom at rest is thus electrically neutral.

When a charged particle approaches an atom, it first meets its electron cloud. The interaction between the electric charges induces electric forces deflecting the projectile. The particle can directly escape or hit an electron and interact with it. It slows down through inelastic collisions, losing energy at each interaction. If it possesses sufficient energy, it can break the bond of the electron trapped inside the electric potential barrier, which is then free to move. This process is called ionisation.

These interactions with electrons are the most probable for a charged particle with matter. It slows or stops charged particles, energy lost being about a few tens of eV per interaction. The average energy loss of the particle per length unit is called stopping power. It depends on the energy of the projectile, and the types of particles in play. These interactions define the electronic stopping power, as opposed to the nuclear stopping power (see next part). At a macroscopic level, this energy loss is responsible of the heating of the material.

1.1.2 RUTHERFORD SCATTERING

When a charged particle crosses the electronic potential barrier of the atom to pass around the nucleus, it can be deflected due to the interaction between its charges and those of the nucleus. The particle does not hit the nucleus, an elastic scattering occurs: there is no energy exchange, direction only is affected.

This interaction defines the nuclear stopping power, as opposed to the electronic stopping power (see previous part). Nuclear stopping power is negligible at low energy and increases when the mass of the projectile increases compared to the mass of the target nucleus.

The electrostatic potential formed by the interaction between the incident particle and the target nucleus is called the Coulomb barrier. It is given by the electrostatic potential energy:

$$U_{Coul} = \frac{1}{4\pi\varepsilon_0} \frac{q_p q_t}{r}$$

Where

- $k = \frac{1}{4\pi\varepsilon_0} = 8.99 \times 10^9 \, Nm^2 C^{-2}$ is the Coulomb constant, with ε_0 the permittivity of vacuum.
- $q_p = Z_p e$ and $q_t = Z_t e$ are the electronic charges of respectively the projectile and the target nuclei.
- r is the interaction radius.

When the incident particle (positive charge q_p) and the target nuclei (positive charge q_t) move closer, the repulsive potential increases. At the distance $r = d_0$, the attractive strong interaction takes place upon electrostatic interaction.

$$d_0 = R_p + R_t \approx r_0 (A_p^{1/3} + A_t^{1/3})$$

Where:

- $R_i \approx r_0 A_i^{1/3}$ is the radius of nucleus i, with A_i its mass number
- r_0 is an empirical constant between 1 and 1.5 fm.

To undergo nuclear reaction, the two interacting nuclei of projectile and target must overcome this barrier or tunnel through it. Many nuclear reactions are indeed observed with the projectile energy below the Coulomb barrier, such as ^{2}H(d,n) and ^{3}H(d,n) reactions.

1.1.3 DIRECT AND SEMI-DIRECT REACTIONS

In direct reactions a projectile transfers energy or exchange nucleons with the target nucleus in a single event in a very short time (10^{-21} s), i.e. approximately the time for the particle to travel across the target nucleus. Semi-direct reactions are equivalent reactions with more than one interaction between nucleons.

Inelastic scattering and reactions with nucleon exchange

In the case of inelastic scattering, the energy transferred by the incident particle excites a collective mode of the nucleus. The excited nucleus decays through various modes, like in the case of (p,p') reactions.

Transfer reactions involve nucleon exchange. For a stripping reaction, the projectile loses one or more nucleons when passing around the target nucleus. On the contrary, in a pick-up reaction the projectile gains one or more nucleons. D(d,n)^{3}He is a stripping reaction commonly employed for producing monoenergetic neutrons. A knockout reaction results in three reaction products: an incident particle extracts a nucleon from the target nucleus but does not absorb it.

1.1.4 COMPOUND NUCLEUS

Some nuclear reactions occur through the formation of a compound nucleus. This model was proposed by Niels Bohr in 1936. The reaction is divided in two different stage comprising formation and decay.

The incident particle is absorbed by the target nucleus. Nucleons of the projectile and target nucleus interact until all the energy of the projectile nucleons is shared in the new nucleus. This latter one is called compound nucleus, and possess $A_a + A_X$ nucleons. The compound nucleus is highly excited and unstable. It decays after a relatively long period of time (typically from 10^{-19} to 10^{-15} s) through particle evaporation. It usually results in a light particle and heavy product nucleus.

The probability of its formation is much more important if the projectile energy gives access to an excited state of the compound nucleus. Since a new nucleus is formed, the decay is fully independent for the formation mode and the initial nuclei. Particle emission is isotropic, memory of the incident particle is lost through the numerous interactions leading to thermalisation of the nucleus.

1.2 MONOENERGETIC NEUTRON FIELDS

Neutron production by nuclear reaction depends on several interdependent parameters, such as the energy of the reaction (or Q-value), ion beam energy and the reaction cross section, among others. Some quantities such as the energy of the reaction and thresholds can be calculated using kinematics laws. This results in a simple reaction description, for which details are given in the first part of this chapter. In the second part, several important properties of accelerator-based monoenergetic neutron fields are discussed: the degree to which the neutron energy distribution is truly monoenergetic (improperly named monoenergeticity in this document, for practical reason), energy spread, yield and target characteristics.

Several important features of these reactions can be obtained from elementary classical mechanics using conservation laws. Details and relativistic corrections are not included here and can be found in (Be04) and (Ma60).

1.2.1 KINEMATICS OF NEUTRON-PRODUCING REACTIONS

1.2.1.1 Conservation laws

Kinematics of nuclear reaction arises from conservation laws. In all nuclear reactions, including neutron-producing reactions, quantities conserved in a X(a,b)Y reaction* are:

Total energy

In the general case, and for any kind of particles including photons, the conservation of total energy is given by:

$$E_a + E_X = E_b + E_Y \tag{1}$$

Where $E_i = \sqrt{p_i^2 c^2 + m_i^2 c^4}$ is the total relativist energy of the particle i.

In the non-relativistic case, the conservation of total energy is given by:

$$M_a + T_a + M_X + T_X = M_b + T_b + M_Y + T_Y \tag{2}$$

Where M_i and T_i are the mass (in eV) and kinetic energy of the particle i.

Total momentum

In all case, the conservation of total momentum is given by:

$$\vec{p}_a + \vec{p}_X = \vec{p}_b + \vec{p}_Y \tag{3}$$

Where $\vec{p}_i$ is the momentum of particle i.

---

* All reaction products are in their fundamental state.

Electric charge

In all case, the conservation of electric charge is given by:

$$q_a + q_X = q_b + q_Y \tag{4}$$

Where q_i is the electric charge of particle i.

Total angular momentum and parity

In classical mechanics, the angular momentum $\vec{l}$ is the quantity describing a rotational state, like an electron around its nucleus. This is the cross product of the position and the linear momentum of a particle: $\vec{l} = \vec{r} \times \vec{p}$.

In quantum mechanics, the angular momentum is a quantized quantity, a multiple or half-multiple of the reduced Planck constant $\hbar$. The total angular momentum $\vec{j}$ is the sum of the angular momentum $\vec{l}$ and the intrinsic momentum or spin $\vec{s}$:

$$\vec{j} = \vec{l} + \vec{s} \tag{5}$$

The angular momentum $\vec{l}$ can be seen as the associated vector to the quantum number l. Its projection m_l is comprised between $-l$ and $+l$.

By analogy with classical mechanics, the intrinsic momentum would correspond to the rotation of the particle on itself. For an electron, a proton or a neutron, its projection is $m_s = \pm 1/2$.

In all case, conservation of the total angular momentum is given by:

$$\vec{j}_a + \vec{j}_X = \vec{j}_b + \vec{j}_Y \tag{6}$$

In the case of an X(a,b)Y reaction, the angular momentum $\vec{l}$ is the relative angular momentum of the two particles. The relation is then given by:

$$\vec{l} + \vec{s}_a + \vec{s}_X = \vec{l}\,' + \vec{s}_b + \vec{s}_Y \tag{7}$$

Parity is the transformation consisting in flipping all spatial coordinates, from $\vec{r}$ to $-\vec{r}$. If the properties of system are unchanged through parity transformation, it is called even, otherwise the system is odd. In quantum mechanics, parity transformation P is related to the angular momentum l through the relation $\pi = (-1)^l$.

For a two-body reaction, conservation of the parity is expressed on each side by the composition of the particles parities and parity of the relative angular momentum:

$$\pi_a * \pi_X * (-1)^l = \pi_b * \pi_Y * (-1)^{l'} \tag{8}$$

Mass number

The mass number A (or baryonic number) of a particle is the total number of nucleons in its nucleus. This number is conserved through strong interaction, *i.e.* the number of protons and neutrons contained in the initial particles is equal to the final number of nucleons. This quantity may change in case of weak interaction.

1.2.1.2 Energy of the reaction Q

Considering the target nucleus X at rest, and the conservation of total energy, the mass difference Q is defined as:

$$Q = (M_a + M_X) - (M_b + M_Y) = E_b + E_Y - E_a \qquad (9)$$

Q is the energy of the reaction, i.e. the energy difference between initial and final states. The sign of the quantity Q determines the type of reaction:

- If Q>0, the reaction is exothermic. Part of the energy of the initial state is directly transmitted as kinetic energy of the reaction products.

- If Q<0, the reaction is endothermic. The energy of the final state is higher than the energy of the initial state. The reaction needs an energy contribution to occur above a specific energy threshold.

In the rest of this document, including next equations, is discussed only the case of two-body reactions which produce neutrons, i.e. X(p,n)Y reactions with p standing for projectile.

Exothermic reactions

For exothermic neutron-producing reactions, the minimal neutron energy allowed by the reaction is:

$$E_{n,min} = Q \; \frac{M_Y}{M_Y + M_n} \qquad (10)$$

Since energy is easily transferred to the reaction products, exothermic reactions are more likely to produce high neutron energies. Such is the case, for example, of the ^{2}H(d,n) and ^{3}H(d,n) reactions (Q-values of 3 268.914 ± 0.0004 and 17 589.293 ± 0.0004 keV, respectively). They are not well suited for low-energy neutron production and are not discussed in this document. More details on their kinetics can be found in (Ro55).

Endothermic reactions

For endothermic reactions, the projectile threshold for neutron production energy at 0° is (limited to proton or deuteron in this study):

$$E_{p,th} = - Q \; \frac{M_n + M_X}{M_X} \qquad (11)$$

1.2.1.3 Energy of the emitted neutrons

Using conservation laws, energy of the neutrons emitted at the angle θ with respect to the ion beam direction is given by the solution of the polynomial equation of the second degree:

$$\sqrt{E_n(\theta)} = \frac{\sqrt{M_p M_n E_p} \cos(\theta) \pm \Delta}{M_n + M_Y} \qquad (12)$$

Where

$$\Delta = \sqrt{M_p M_n E_p \cos^2(\theta) + (M_n + M_Y)\left((M_n - M_Y)E_p - M_Y Q\right)} \qquad (13)$$

Two solutions, (±) in the formula, appear because of centre-of-mass motion. Until the neutron velocity in the centre of mass equals and then exceeds the velocity of the centre of mass, two groups are emitted for the same angle in the laboratory reference (as illustrated in Fig. 3).
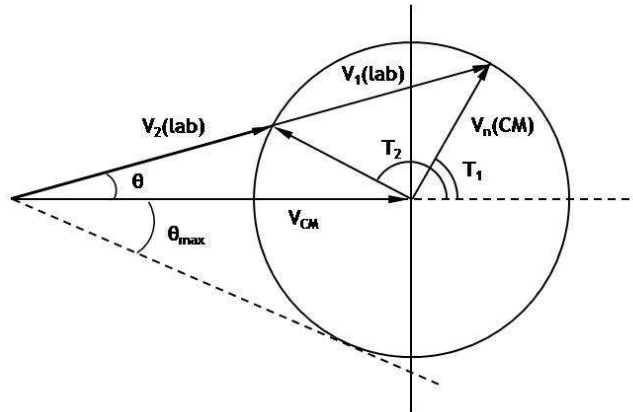
Fig. 3: *Relationship between velocities and angles in laboratory and centre-of-mass references. For $V_n(CM)$ lower than V_{CM}, the neutron velocity V(lab) has two values at a given laboratory θ angle ($V_1(lab)$ and $V_2(lab)$). These two velocities correspond to two emission angles (T_1 and T_2) in the centre-of-mass system. The emission angle θ_{max} is the maximum angle available at a given projectile energy.*

From Eq. 12 can be deduced variations of neutron energy with emission angle and with proton or deuteron energy:

$$\left|\frac{\partial E_n}{\partial \theta}\right| = 2E_p \cdot \left(\sin\theta \frac{M_p M_n}{\varpi (M_p + M_X)^2}\right) \cdot (\cos\theta \pm \varpi)^2 \qquad (14)$$

$$\left|\frac{\partial E_n}{\partial E_p}\right| = \left(\frac{\cos\theta \pm \varpi}{(M_X + M_n)^2}\right) \cdot \left(M_p M_n (\cos\theta \pm \varpi) \pm \frac{M_Y M_X E_{th}}{\varpi E_p}\right) \qquad (15)$$

Where:

$$\varpi^2 = \alpha^{-2} - \sin^2(\theta) \quad \text{and} \quad \alpha^2 = \frac{M_p M_n}{M_X M_Y} \frac{E_p}{E_p - E_{th}}$$

<u>*Double-valued range and monoenergetic threshold*</u>

At the exact threshold energy ($\Delta = 0$), only one group of neutrons is emitted at 0° at a unique neutron energy, achieving a specific monoenergetic point. Above the threshold energy, two groups of neutrons of different energies are emitted exclusively in raising forward cone. The emission cone of the neutrons opens with neutron energy up to cover the whole solid angle. The energy of the first neutron group increases, whereas the energy of the second group decreases to 0. The maximum angle of emission for a projectile energy is given by:

$$\theta_{max} = sin^{-1}\left(\sqrt{\frac{M_X M_Y}{M_p M_n} \frac{E_p - E_{th}}{E_p}} \right) \tag{16}$$

When θ_{max} reaches 90°, the neutrons produced have a unique energy for a given angle and proton energy. Above this point, neutrons are emitted in every direction; the source surpasses its monoenergetic threshold and reaches its monoenergetic range:

$$E_{mono} = -Q \frac{M_Y}{M_Y - M_p} \tag{17}$$

The monoenergetic range of a neutron-producing reaction is kinetically limited by this low threshold. Limitations and other limits, upper limits in particular, are discussed in the next part (1.2.2).

The different specific cases and ranges from reaction threshold to monoenergetic range are all illustrated in the same way as Fig. 3 in Appendix A.

As an instance, on Fig. 4 are graphically represented the solutions of equation (12) for ^{45}Sc(p,n) reaction. Following the variation of neutron energy with proton energy, one observes the specific ranges delimitated by both reaction and monoenergetic thresholds. The reaction starts when emission at 0° is possible, with emission of two neutron groups of different energy. For any emission angle below 90°, *i.e.* 0° and 45° on the figure, two neutron energies are possible before the monoenergetic threshold, here around 2910 keV. Above this threshold, only one neutron group is emitted per angle. Larger emission angles are as well available, altogether and directly monoenergetic.
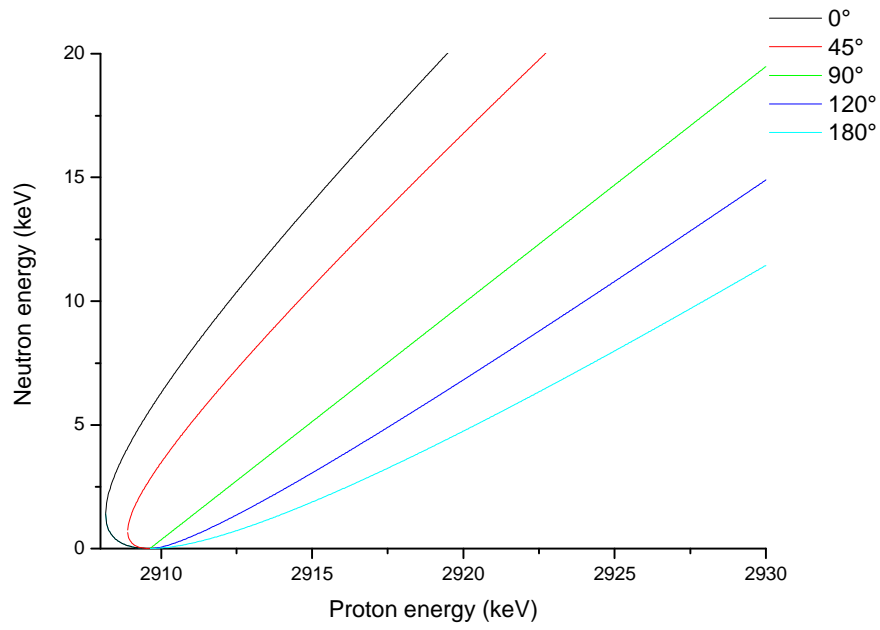
Fig. 4: *Variation of neutron energy with proton energy for several emission angles for a (p,n) endothermic reaction according to reaction kinematics (here for $^{45}Sc(p,n)$ reaction).*

1.2.2 GENERAL PROPERTIES OF ACCELERATOR-BASED MONOENERGETIC NEUTRON FIELDS

A monoenergetic neutron source has different general characteristics depending on reaction physics and experimental configuration. These properties are interdependent, as discussed in this chapter.

1.2.2.1 Yield, fluence, cross section and intensity

The yield *Y* of a two-body reaction is defined as the flux of produced neutrons compared to the flux of incident particles in set conditions. This yield depends on:

- The neutron cross section σ of the reaction used
- Target thickness, i.e. the energy loss ΔE_t of the incident particles in the target material,
- The target material stopping power, related to the stopping cross section per atom ε.

$$Y(E_p,\theta) = \sigma(E_p,\theta).\frac{\Delta E_t}{\varepsilon} \qquad (18)$$

This quantity should be expressed per incident particle (Ut83 III.B.2), but is generally expressed per microcoulomb, in proportion to the number of incident (and charged) particles. The usual unit is then $(sr.\mu C.keV)^{-1}$ or $(\mu C.keV)^{-1}$ (steradian is a dimensionless unit), taking into account the target thickness in keV.

For practical purposes, reactions are usually compared in terms of neutron intensity.

Cross section

The neutron cross section depends on the reaction itself. It is one main characteristics of a two-body neutron reaction. Expressed in barn, it is the probability of interaction between the incident ion and the target nucleus. It cannot be calculated using kinematics; it has to be measured or calculated from nuclear models. For accelerator-produced neutron fields, angular differential cross sections are usually employed. According to equation (12), the maximum available yield is usually at 0°. Some reactions have cross sections that are highly dependent on the incident ion energy, i.e. with resonant structure (see 1.2.2.2), such as the ^{45}Sc(p, n) reaction.

The influence of target thickness and stopping power

The target thickness employed depends on the monoenergeticity required. Yield increases with target thickness as well as energy width. Target thickness must be chosen according to needs and adjusted for the stopping power of the reactive layer.

Neutron intensity

Compared to neutron yield, the notion of neutron intensity includes also the maximum usable ion beam current which can be deposed onto the target. It is the maximum achievable fluence rate for a reaction in a given experimental setup (distance, solid angle, etc.). It depends on two distinct limits:

- accelerator specifications: maximum available beam current delivered by the accelerator,
- target resistance: it depends mostly on the energy loss in the target (how fast it warms up) and the maximum power that could be dissipated by the target in a specific setup (how it is cooled).

A comparison of different usable reactions is usually made theoretically in terms of yield, i.e. $(\mu C.keV)^{-1}$. For a practical use of monoenergetic fields, a comparison must then be made in terms of neutron intensity, i.e. $(keV.s)^{-1}$ including maximum usable beam current (Dr99).

1.2.2.2 Resonance structures in nuclear reactions

Some reactions have a cross section highly dependent on projectile energy. Such is the case for most of the reactions considered in this document for the production of low-energy neutrons (see parts 2 and 3).

These rapid variations of the cross section are called resonances and result from the discrete level distribution of the nuclei participating in the reactions. Identifying the neutron production process (direct nuclei interaction or compound nucleus) and knowing precisely the level spectrum of the nuclei involved should make it possible to predict the resonance energies.

The energies of the different resonances are usually measured using a thick target and the time-of-flight method. This consists in measuring the time needed by the neutrons to cover a set distance. Knowing this distance and time-of-flight, neutron speed and thus energy is determined, as illustrated in Fig. 5.
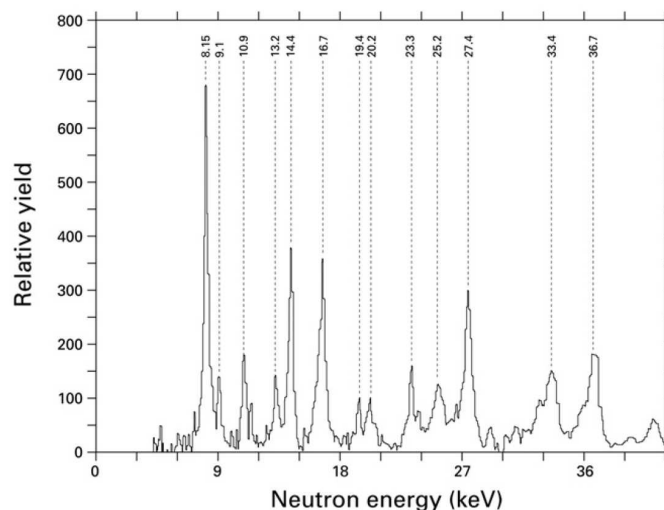
Fig. 5: *Neutron spectrum as obtained by Cosack et al. using the time-of-flight method with a thick target in the ion beam direction. (Co85)*

Another method for observing the cross section structure is to measure the change of neutron production (or yield) while scanning an ion beam energy range. The resulting figure detailing yield variation with projectile energy is called excitation function.

There are several advantages in using reactions with such resonant cross sections:
- Lower impact of both biggest sources of neutron energy spread:
  - If the resonances are thin and well-spaced, a significant projectile energy spread, larger than the energy width of the selected resonance, has significantly reduced fallout (see Fig. 6).
  - In the same way, an increase of target thickness, in order to obtain a higher neutron yield, has less impact on the energy spread.
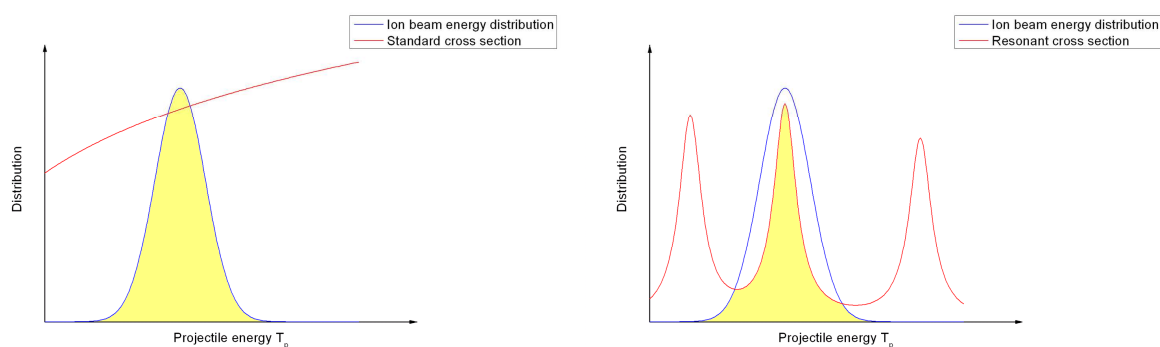
Fig. 6: *As shown in the case on the left, for an infinitely thin target, a monotonic cross section directly undergoes the ion beam energy spread (yellow surface). A cross section with a resonant structure reduces the effective projectile energy spread, as long as the energy spread does not cover several resonances.*

- Selection of neutron energy: for this kind of reaction, neutron energy selection is performed by selecting a given resonance of known neutron energy. One scans the yield by varying projectile energy around the resonance energy, the maximum yield corresponding to the resonance energy. This allows one to choose neutron energy directly and precisely without depending on the accelerator energy accuracy and calibration. The mean energy is always the resonance energy.

- Projectile energy variation: if the ion beam energy varies a few hundred eV from the resonance energy, the neutron production falls abruptly. This important fluence variation is immediately noticeable on any neutron monitor, allowing for on-line energy adjustment. This is of primary importance for any use of this kind of neutron source.

The main drawbacks are:
- Using such reactions requires scanning the range of the resonance for its selection, complicating the accelerator setup.

- If the total projectile energy spread covers several resonances, several neutron energies are produced. The neutron source is no longer a monoenergetic source, but rather a mix of several monoenergetic neutron groups. This limits the target thickness.

1.2.2.3 Differential angular cross section

In the case of radioactive sources, particles are emitted in an isotropic way in the laboratory frame of reference. Either the laboratory frame of reference is also the centre of mass of the reaction, like in the case of a spontaneous decay; or the reaction is induced by the particle of another reaction in the surroundings: the emission direction is then statistically isotropic. This is the case of [241]Am-Be neutron sources:

$$^{241}_{95}Am \longrightarrow \, ^{237}_{93}Np + \, ^{4}_{2}He + \gamma$$
$$^{9}_{4}Be + \, ^{4}_{2}He \longrightarrow \, ^{12}_{6}C + \, ^{1}_{0}n + \gamma$$
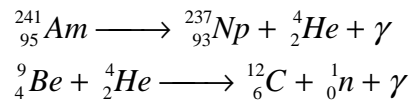
In the case of nuclear reaction induced by an accelerated particle, the centre of mass of the reaction is moving with respect to the ion beam direction. The momentum of the projectile is transferred, inducing directionality. Thus particle emission through nuclear reaction is not isotropic in the laboratory frame of reference.

However some reactions are still isotropic in the centre of mass: the probability of emitting a neutron does not depend on the emission angle in this frame of reference. This is the case of reactions with formation of a compound nucleus (see 1.1.4). Relative yield can be calculated for any emission angle at the expense of a change of frame of reference, using kinematics (see Fig. 3) as described in (Ma68). The relative yield is determined by the ratio of the differential cross sections in the centre of mass (emission angle T) and in the laboratory frame of reference (emission angle θ):

$$\frac{\sigma(\theta)}{\sigma(T)} = \frac{(AC)^{\frac{1}{2}}(D/B - sin^2 \, T)^{\frac{1}{2}}}{E_n/E_T}$$

(19)

Where:
$$E_T = E_p + Q = E_n + E_Y \, ,$$

$$A = \frac{M_p M_Y (E_p/E_T)}{(M_p + M_X)(M_n + M_Y)}, \qquad C = \frac{M_X M_n}{(M_p + M_X)(M_n + M_Y)}\left(1 + \frac{M_p Q}{M_X E_T}\right)$$

$$B = \frac{M_p M_X (E_p/E_T)}{(M_p + M_X)(M_n + M_Y)}, \qquad D = \frac{M_X M_Y}{(M_p + M_X)(M_n + M_Y)}\left(1 + \frac{M_p Q}{M_X E_T}\right)$$

For direct reactions (see 1.1.3), angular distribution depends on the interaction modes.

1.2.2.4 Target specifications

The target is where the nuclear reaction for neutron production takes place and is located at the end of the beamline. There are basically two kinds of targets for accelerator-based neutron sources: solid and gaseous. Gaseous targets are mainly used for achieving pure targets of hydrogen isotopes for DD reaction. They are therefore not discussed in this report.

Solid targets can be:
- A simple volume of a given material
- Composed of a backing supporting a layer of the chosen reactive element.

The monoenergeticity requirement usually demands the use of thin reactive layer.

Ideally, a target should be isotopic, self-supporting and able to stop incident particles, as indicated in the next paragraphs (Dr99). In addition, it should preferably be easy to prepare and handle.

The reactive layer

Ideally, the reactive layer should be isotopically and chemically pure. However, an isotopic layer may be prohibited for cost or structural reasons. Other constituents may be needed to:
- Provide a matrix for the implantation of elements like tritium in titanium (TiT targets)
- Generate chemical species not sensitive to oxidisation, such as LiF compared to metallic Li

These elements can produce secondary reactions, as is the case with lithium fluoride targets, where a significant quantity of gammas are created by the $^{19}F(p,\gamma)$ reaction.

The presence of other isotopes or constituents in the reactive layer also increases the energy spread. For a given yield, there are proportionally more incident particles slowed before interacting. In other words, for a given target thickness, there is a corresponding decrease in the neutron yield. For example, a pure Li target produces three times more neutrons than a LiF target of same thickness (see 2.2.1.5). Furthermore, this is a source of additional straggling.

Backing

A backing serves as beam stop and is usually chosen for its good thermal conductivity. Aluminium, silver, tungsten, molybdenum, gold and copper among others, are commonly employed. This kind of backing allows the beam power to be dissipated by air or water cooling. These cooling methods are highly necessary to enable the target to withstand the high temperatures generated by beam currents up to 50 µA without deterioration. For low-energy neutrons, water cooling is not considered, as it would induce important scattering.

In practice, the target is the cap of the beamline. The side with the reactive layer is in the accelerator vacuum, whereas the blank side is in air and cooled by air spray. The backing should thus have sufficient mechanical resistance (i.e. Young modulus) in order to withstand 1 bar pressure without deformation.

If the backing is deformed, the neutron emission position is changed and the vacuum can be lost. To obtain sufficient rigidity or temperature resistance, a minimum backing thickness is required, resulting in an unavoidable neutron scattering level. Some materials, like aluminium, induce fewer scattered neutrons, but are more deformable. A compromise has to be made between minimal scattering and target integrity.

Ideally, the backing should be chosen to avoid, as much as possible, any reaction producing neutrons (as well as minimising photons) with the projectile at the given energy. Reaction thresholds and yield for the backing material must then be checked before selection.

Target production

There are basically two ways of producing solid targets with layer and backing. One consists in evaporating and laying down the reactive material on the backing in an oven. The second uses accelerator facilities for the selection and implantation of the reactive material in the backing set at the end of the beamline. These methods are discussed in detail in 4.2.

1.2.2.5 Monoenergeticity

A neutron field is considered monoenergetic when it is constituted by only one group of neutrons having one defined mean energy E_n. In addition, the energy variation ΔE_n within this group is negligible compared to the mean neutron energy:

$$\frac{\Delta E_n}{E_n} << 1 \, .$$

This group of neutrons forms a monoenergetic peak. The main parameters influencing monoenergeticity are:
- Target thickness
- Ion beam energy spread and stability
- Energy variation with emission angle

Energy spread due to beam energy spread, target thickness and solid angle variation are taken into account by simulation codes like *TARGET* (SC05). All contributions are folded resulting into a final theoretical energy distribution of monoenergetic peak.

Influence of target thickness

In accelerator-based sources, the thickness of the target can be considered an intrinsic source of increase in energy width. After hitting the target, the accelerated ions are progressively slowed down, depending on the stopping power of the material. The energy lost by the ion in the reactive layer of the target increases with layer thickness. Therefore, the probability that the ion energy is significantly reduced when producing a neutron by

nuclear reaction increases also with target thickness. As a result, the mean neutron energy decreases, and the energy spread of the monoenergetic peak increases. However, as long as the reactive layer thickness is smaller than the range, increasing the thickness increases the probability of interaction and therefore the production of neutrons. In summary, when using a thicker target, one can observe:

- Increase in fluence

- Decrease in mean neutron energy (for a given projectile energy)

- Increase of the monoenergetic peak FWHM (full width half maximum)

The choice of the most suitable target thickness always requires a compromise between the intensity of the neutron emission and the energy broadening (see Fig. 7).
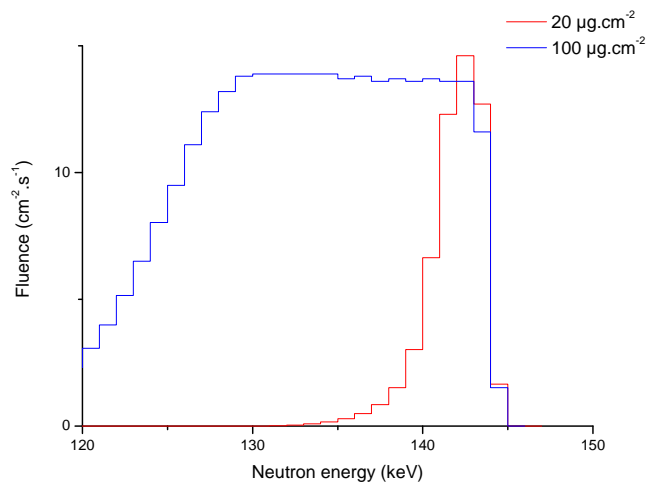
Fig. 7: *Simulations with the TARGET code (SC05) of the neutron fluence energy distribution obtained with LiF targets having two different thicknesses (all other parameters being identical).*

Ion beam energy spread and stability

The second source of energy spread comes from the energy spread of the ion beam. The ion beam does not have a single energy but an energy distribution which can be approximated by a Gaussian distribution. The Gaussian FWHM is generally between a few hundred of eV and a few keV for electrostatic accelerators in continuous mode (such as Van de Graaff, tandetron or singletron). It can be experimentally determined using thin resonances of (p,γ) reactions (^{27}Al(p,γ) for example, cf. Br94).

In addition to its energy spread, the beam's mean energy can vary:
- For a given time t: this is a result of the previously described ion beam energy spread and the influence of target thickness
- Over time: it depends on accelerator stability (typically of a few hundreds of eV with electrostatic accelerators)

The variation of projectile energy modifies the neutron energy to an extent depending on the reaction. This dependence of neutron energy on projectile energy is described by equation (15) (see 1.2.1.3).

The impact of ion beam stability and spread are reduced when employing reactions with well-defined (p,n) or (d,n) resonance structure in the cross section. There are two advantages in that case:

- A smaller amount of neutrons produced by the projectiles of non-desired energy

- An immediate decrease in fluence, which can be observed using appropriate neutron monitors, in the event of sudden projectile energy change.

Resonant structure in cross section of nuclear reactions is presented in 1.2.2.2.

Energy variation with emission angle

Another parameter influencing monoenergeticity is the energy variation within a solid angle defined by the detector with respect to the neutron producing target. This variation is given by equation (14) (see 1.2.1.3).

From this equation, it can be deduced that:

- The heavier the target element X, the lower the centre-of-mass velocity. As a consequence, the angular variation is slower. For a given kinetic energy of the projectile, reactions with medium-weight nuclei are thus preferable to those with light nuclei. One can note that this variation is more significant for high ion beam energy.
- This angular dependence is comparatively smaller in the ion beam direction. It is therefore preferable that a 0° emission angle be used.

1.2.2.6 <u>Parasite radiations</u>

<u>Background neutrons</u>

Intrinsic contaminations

Any two-body reaction can theoretically produce monoenergetic neutron fields. In practice, there are many sources of background neutrons. As presented in 1.2.1.3, unlike exothermic reactions, endothermic reactions do have a monoenergetic threshold. Below this threshold two groups of neutrons are emitted due to kinematics. Above specific thresholds, the interaction between projectile and nucleus can intrinsically produce secondary neutrons of different energy or other reaction products. These contaminations can result from different competing reactions:

- Reactions of accelerated ions with the target nucleus: multiple-body break-up, gamma production, etc.
- Reactions between the accelerated ions and the heavy product Y of the initial reaction
- Deuteron break-up
- Above some thresholds, excited levels of the target nucleus can be reached. Nucleus de-excitation can result in new reactions, possibly emitting neutrons of different energy or other reaction products.

The latter competing reactions generally determine the upper limit of the monoenergetic range of the reaction. It can occur just above the monoenergetic threshold, considerably limiting the available energy range. A neutron-producing nuclear reaction is thus monoenergetic only in a specific energy range.

Some reactions can be considered quasi-monoenergetic when used in a range where multiple groups of neutrons would be emitted, if the contamination is known and small. This is the case of the first resonance of the ^{65}Cu(p,n) reaction, allowing keV neutrons with ten percent contamination from a second neutron group (see 2.2.4., Sc89).

Many neutron-sensitive devices do not separate neutron and gamma contributions. The knowledge of the photon contribution to the neutron field is then of primary importance.

Contaminations from interaction with facility and target materials

Neutron background arises also from unwanted interactions in the path of the ion beam. These neutrons are produced by the interaction of the ion beam with the accelerator and target structure. Another source of neutron background is the neutron scattering of the primary neutrons with materials in the irradiation area. They of course depend on the facility used.

- *Interaction of ions with beamline and target structures:*

The contribution from reactions between projectiles and experimental environment is reduced by selecting proper target materials (especially backing) and fine tuning the beam through the beamline and apertures.

Some materials needed in the target structure have unknown neutron or gamma production cross sections, especially when used at unusual energy ranges (like Mo, see 4.1.1.1). If their contribution is not too significant, it can be easily subtracted by measurements with blank targets, i.e. targets without any reactive layer.

- *Resulting from neutron scattering:*

Facilities dedicated to monoenergetic neutron field production are designed to limit neutron scattering. The number of materials and instruments around the nuclear reaction location, i.e. the target, are reduced as much as possible. Several experimental setups and facilities are detailed in 3.1.
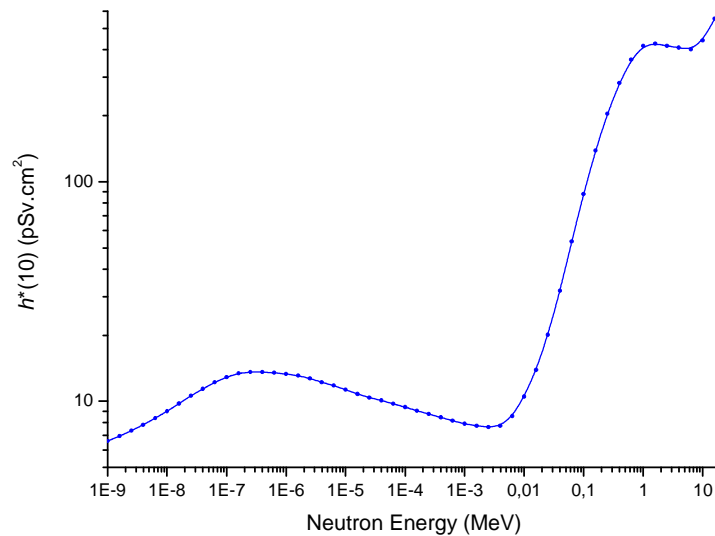
Fig. 8: *Fluence to dose conversion factor*.

For monoenergetic neutron fields in the keV range, neutrons scattered in the materials around the target (especially at backward angles) contribute more to the total dose equivalent than in the higher energy ranges, due to a relatively constant fluence-to-dose conversion factor (see Fig. 8 below a few keV). In order to take into account this contribution to the fluence and dose equivalent, a complete detailed simulation of both neutron emission and transportation in the surrounding structures and building must be performed using Monte Carlo codes. As a prerequisite for these simulations, the differential cross sections with neutron emission angle and proton energy must be known.

1.2.2.7 Sources of photons

As discussed in the previous parts, (p,n) reactions are well suited for producing monoenergetic neutron fields. However, (p,n) interaction is only one among many other possible interactions between ion beam and target materials. Besides, it requires that protons cross the coulomb barrier to interact with nuclei, which is not the predominant process in the studied energy range. Many of the competitive interactions can be sources of photons, depending on their branching probability.

As the neutron fluence to dose equivalent conversion coefficients are low below a few keV energies, the photon contribution to the dose equivalent could be important in that energy range. It has to be known in order to use any nuclear reaction to calibrate accurately neutron detectors.

The proton inelastic scattering due to the coulomb barrier of the atoms at rest induces photon emission through two interaction modes:
- Ionisation of the atom by Compton scattering: the deflected proton ejects one electron of the atom.
- Excitation of the atom: the proton interacts with an electron which shifts between excitation levels.

In all cases, the electron cloud is then rearranged. The electron transitions generate X-ray emission. These interactions are described by Bethe and Bloch formula and the concept of stopping power. The interaction with

the electron cloud is much more probable than interaction between proton and nucleus at the considered energies.

The inelastic scattering of protons with nuclei, so called (p,p'γ) reaction, consists in the excitation and decay of the target nucleus by a proton and γ-ray emission. The energy of the γ-rays, as well as the branching probability of each transition, depends on the nuclear structure of the hit nucleus.

The photon emission can happen from the decay of a new nucleus formed by the interaction with the proton. This is the case of the (p,γ) reaction, where a new nucleus in excited state is formed through proton capture: Z→Z+1. It decays through the emission of one or several energetic photons. The energy and branching probability of the γ rays depend then of the new nucleus structure. For a (p,nγ) reaction, the first step is the same: proton capture, Z→Z+1. However, it emits first a neutron, decaying toward a third nucleus: A→A-1. The remaining nucleus is left in an excited state, above its energy of first excitation, and decays through gamma emission.

The last contribution is due to secondary reactions involving the produced neutrons, i.e. (n,γ) and (n,n'γ) reactions. The γ-rays energy and the transition branching depends on the level structure of the nucleus (A+1).

1.2.3 CONCLUSION ON NEUTRON FIELDS PROPERTIES

Some important characteristics of usable nuclear reactions can be calculated *a priori*, limiting the range of search for new reactions. This allows for the selection of reactions producing neutrons in the desired energy range, as well as predictions of a few other main features like neutron fluence and energy variations in a selected solid angle.

Such specifications need to be complemented by experiments to determine the achievable neutron intensity, including cross section measurements and target behaviour under irradiation studies.

2 <u>REACTIONS SELECTION</u>

As briefly mentioned in the introduction, there are several known methods for producing monoenergetic neutrons. The production of keV neutrons is usually performed with accelerator-induced nuclear reactions.

In this chapter we first briefly list the requirements for a reaction to be an acceptable source of monoenergetic keV neutrons (3.1). In the second part (3.2) we discuss some properties of several reactions used, from the literature and calculations using *Drosg2000* (Dr00) and *TARGET* (SC05) codes. At the end of this part, other possible reactions are reviewed.

2.1 REQUIREMENTS

Nuclear reactions and characteristics of monoenergetic neutron fields are discussed respectively in parts 1.1 and 1.2. Here are presented the criteria we determined from these latter parts for selecting the reactions.

2.1.1 MAIN CRITERIA

<u>*Feasibility and experimental needs*</u>

- The threshold energy must be low enough to be reachable with an energy ion beam of only a few MeV.

The selected reactions must be achievable at the facilities commonly employed for neutron metrology, such as those of the scientific cooperation. The upper limit for the proton energy is thus set at 4 MeV.

- The target must be easy to produce and handle.

The requirements related to contamination monitoring (for tritium-based reactions, for example) or inert gas, to avoid oxidation and target deterioration, (as for Li targets, see part 2.2.1.5), can be serious drawbacks for any use.

<u>*Neutron energy*</u>

- The monoenergetic range of the selected reaction should cover the desired neutron energy range.

Here, the aim is to investigate reactions producing monoenergetic neutrons below 50 keV, and preferentially as closed as possible to 1 keV.

- Achievable energy resolution must be as low as possible.

Depending on the stopping power of the target material, cross section structure of the reaction, and dependence of energy to proton emission, achievable monoenergeticity can vary.

<u>*Neutron intensity*</u>

Neutron intensity is the maximum achievable neutron fluence rate as defined in 1.2.2.1. It must be large enough to allow for scientific use, such as neutron device calibration. It is not predictable by standard kinematics calculations and must be therefore determined through experiments (see part 3):

- Reaction yield

It depends itself on cross section and target thickness. This gives the achievable flux of neutrons for specific incident particle intensity (i.e. beam current) and target thickness (for low neutron energies).

- Beam current

It is mainly limited by target resistance. The target must withstand the high temperatures generated by beam currents from a few to several tens of micro-amperes. Cooling systems are needed.

2.1.2 SECONDARY CRITERIA

Some other properties are helpful, such as a slow variation with incident particle energy (neutron energy), or with emission angle (neutron energy and fluence).

- A slow variation of the neutron energy with incident particle energy
- A slow variation of the neutron energy and fluence with emission angle: energy and fluence homogeneities

To the extent possible, there must not be any background neutrons from target material (reactive layer and possibly backing) or competing reactions. Gamma can be detected along neutrons by many detection devices; their production must be as low as possible.

2.2 STUDY AND SELECTION OF KNOWN REACTIONS FOR KEV NEUTRON PRODUCTION

Several reactions are currently or were previously employed for keV neutron production. In this part we discuss data and results obtained in related studies.

First of all, a description of the use of ^{7}Li(p,n) for low-energy neutron production is provided. This is followed by a description of ^{45}Sc(p,n). More exotic and therefore less studied reactions such as ^{51}V(p,n) and ^{65}Cu(p,n) reactions are presented in the following parts.

2.2.1 THE ^{7}LI(P,N)^{7}BE REACTION

The ^{7}Li(p,n) reaction has been used for decades (Ha40) and is still employed due to its numerous qualities:

- Significant yield
- Minimal neutron energy at 0°: 120 keV
- Low energy variation with angle around the ion beam direction (0°)

It can be employed for producing neutrons of lower energy by increasing the angle of the measuring point with respect to the ion beam direction. This is the most common source for monoenergetic neutron fields below 650 keV.

Since this document is dedicated to the production of neutrons of keV energy, the use of ^{7}Li(p,n) far above the threshold is not described here and can be found in (Gi60).

2.2.1.1 Threshold and monoenergetic range

The reaction is endothermic. Its reaction threshold has been calculated and measured starting in the 1950s (Jo54, Va57). Q-value and threshold have been calculated with best constant data using the *QCalc* tool from NNDC (QC03), while the monoenergetic threshold was taken from the IRMM *Kinematics* tool:

$$Q = -(1\ 644.24 \pm 0.07)\ \text{keV}$$
$$E_{th} = (1\ 880.36 \pm 0.08)\ \text{keV}$$
$$E_{mono} = 1\ 920.336\ \text{keV}$$

At the reaction threshold, due to kinematics, two collimated groups of neutrons are emitted at 29.7 keV. Beyond 1.9204 MeV, the reaction is monoenergetic; the minimal monoenergetic neutron energy available in the ion beam direction (i.e. at 0°) is 120 keV. It remains monoenergetic up to 650 keV neutrons.

At that energy the ^{7}Li(p,n)^{7}Be* reaction can occur: the 0.429 MeV level of ^{7}Be gets excited. It results in three neutron groups of different energies, the only one from ^{7}Li(p,n)^{7}Be reaction (here above monoenergetic threshold), and the two groups from the new reaction (still below monoenergetic threshold). The contamination is typically less than 10 percent (Dr90, p33).

The ^{7}Li break-up takes place at neutron energy of 2.015 MeV. The binding energy of ^{7}Li is sufficiently low so that the nucleus breaks up when hitting the target. The threshold of the competing reaction ^{7}Li(p,n'γ)^{7}Be lies at 2.378 MeV, once again far above our range of interest.

2.2.1.2 Neutron energy

As explained in the previous part, the minimum neutron energy at 0° using ^{7}Li(p,n) reaction is 120 keV. It can be used for producing neutrons in our range of interest by two means:

- Increasing the neutron emission angle of the measuring point with respect to ion beam direction
- Setting proton energy just above the reaction threshold, allowing for the production of 30 keV neutrons

This last method makes use of kinematics at the reaction threshold. As explained in 1.2.1.3, at the exact reaction threshold one only group of neutrons is emitted. Then it splits in two groups of different energies when the projectile energy is increased. Through the very fine tuning of the proton energy, it is possible to use the very rapidly rising cross section before the separation of the two neutron groups. The neutrons are collimated in a forward cone; the neutron background is very low at this moment. This very subtle method for obtaining 30 keV neutrons is discussed in (Mo09) and in the review article of Drosg (Dr99). It is highly dependent on the accuracy of the setup and facility used.
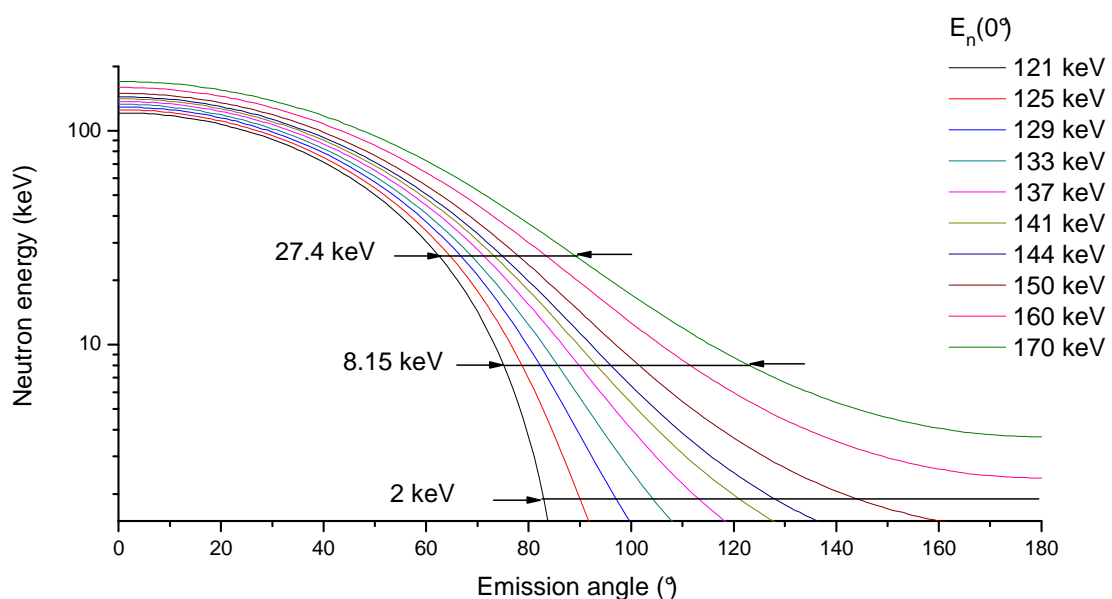
Fig. 9: *Calculated neutron energy variation with emission angle for several neutron energies at 0°.*

The study detailed here is limited to the use of ^{7}Li(p,n) reaction with angle for producing three selected neutron energies among all those available:

- 27.4 keV: energy of one of the main resonance of ^{45}Sc(p,n) reaction at 0°, close to the 24 keV ISO standard
- 8.15 keV: energy at 0° of ^{45}Sc(p,n) first resonance
- 2 keV: energy recommended in ISO standards

The suitable energy of the incident particles must be chosen according to the influence of kinematics and cross section to the neutron field characteristics. Possible ion beam energy beginning at reaction threshold and the related reaction characteristics are listed in Table 2.

Table 2: *Variation of cross section with angle and proton energy to obtain 27.4, 8.15 and 2 keV neutrons with* ^{7}*Li(p,n) reaction (determined using Drosg2000).*

Proton energy (keV)	Neutron energy at 0° (keV)	27.4 keV		8.15 keV		2 keV	
		Angle (°)	σ_{diff} (mbarn.sr^{-1})	Angle (°)	σ_{diff} (mbarn.sr^{-1})	Angle (°)	σ_{diff} (mbarn.sr^{-1})
1 920.5	121.4	62	40.63	75	22.74	**83**	10.76
1 923.0	125.3	64	37.22	79	17.43	**90**	5.39
1 925.5	129.1	66	34.25	82	14.86	97	3.56
1 928.0	132.9	68	31.63	85	12.96	104	2.65
1 931.0	137.4	70	29.33	90	10.21	112	2.11
1 933.5	141.0	72	27.29	93	9.22	120	1.70
1 935.5	144.0	**74**	25.43	**96**	8.27	126	1.54
1 939.5	149.7	77	23.03	101	7.17	141	1.22
1 946.5	159.6	82	19.84	111	5.55	-	-
1 954.0	170.0	88	16.83	122	4.52	-	-

2.2.1.3 Cross section and yield

The cross section of the ^{7}Li(p,n)^{7}Be reaction has an extremely rapid rise above threshold (Gi60). This is followed quickly by a plateau and a sharply peaked resonance around E_p=2.25 MeV (E_n~518 keV). The cross section then decreases to a second plateau (Ep: 2.6-4 MeV) before rising to another peak at higher energies (see Fig. 10).

The quantity $\sigma_{p,n}(E)/E_n^{1/2}$ (referred to as the reduced cross section) is more or less constant for the neutron energy between 17 and 30 keV (therefore, below the monoenergetic threshold, two neutron groups are emitted). At the top of the rise (i.e. the monoenergetic threshold), the total cross section is approximately 250 mbarn (EXFOR database). The differential cross section in the ion beam direction is approximately 75 mbarn.sr^{-1} (Dr90).
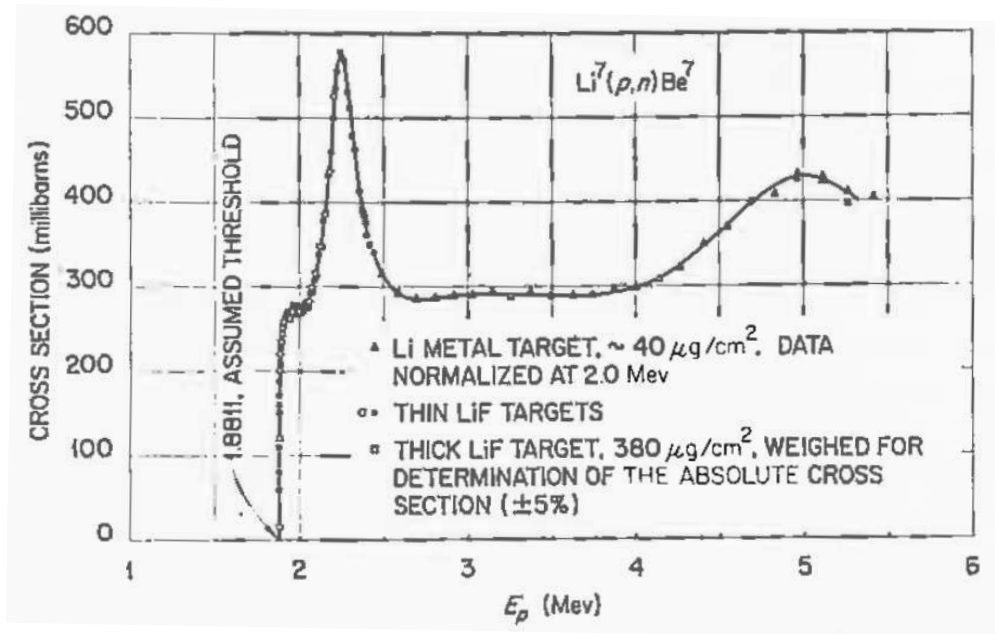
Fig. 10: *Total cross section for $^7Li(p,n)^7Be$, $^7Be^*$ from threshold to 5.5 MeV. (Gi59)*

When the reaction is used at emission angles higher than 0°, the differential cross section depends on the ion beam energy and the emission angle. The variation of this cross section with proton beam energy to obtain selected neutron energies is shown in Fig. 9, and the values reported in Table 2.

The differential cross section decreases with proton energy, with a significant drop just above reaction threshold. The ion beam energy has to be set as low as possible to maximise neutron fluence rate.
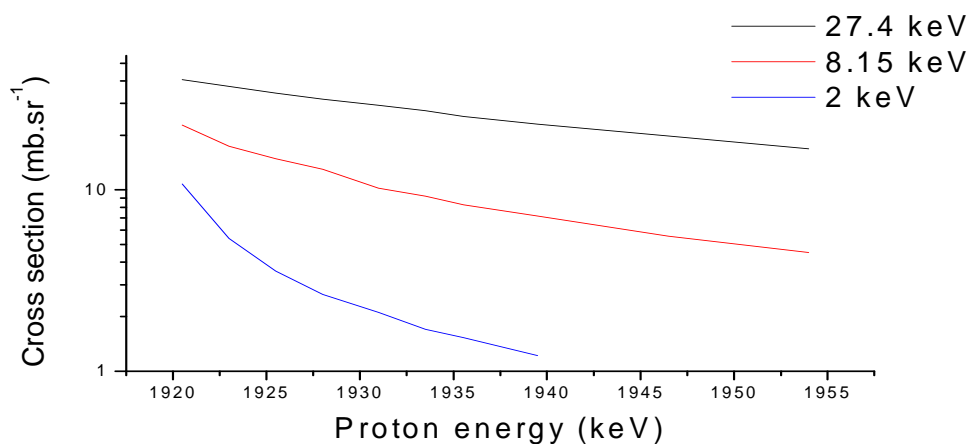
Fig. 11: *Variation of differential cross section to produce 27.4, 8.15 and 2 keV with a $^7Li(p,n)$ reaction as a function of the proton energies, calculated with the code* Drosg2000 *(the emission angle is not constant and related to this energy).*

2.2.1.4 Angular distribution

Isotropy and homogeneity

The ^{7}Li(p,n) reaction is isotropic in the centre of mass up to 2 MeV proton energy (Ta48, Gi60), *i.e.* in the energy range of interest of this study. The number of neutrons per energy interval depends only on proton energy and can be calculated. Kinematics can be used to determine energy and fluence variation with angle.

According to the literature, the kinematics energy spread is low: Drosg shows that for an opening angle of ± 5 degrees, the relative energy resolution is close to 0.15 percent of the neutron energy (Dr99) in the ion beam direction (*i.e.* 0°).
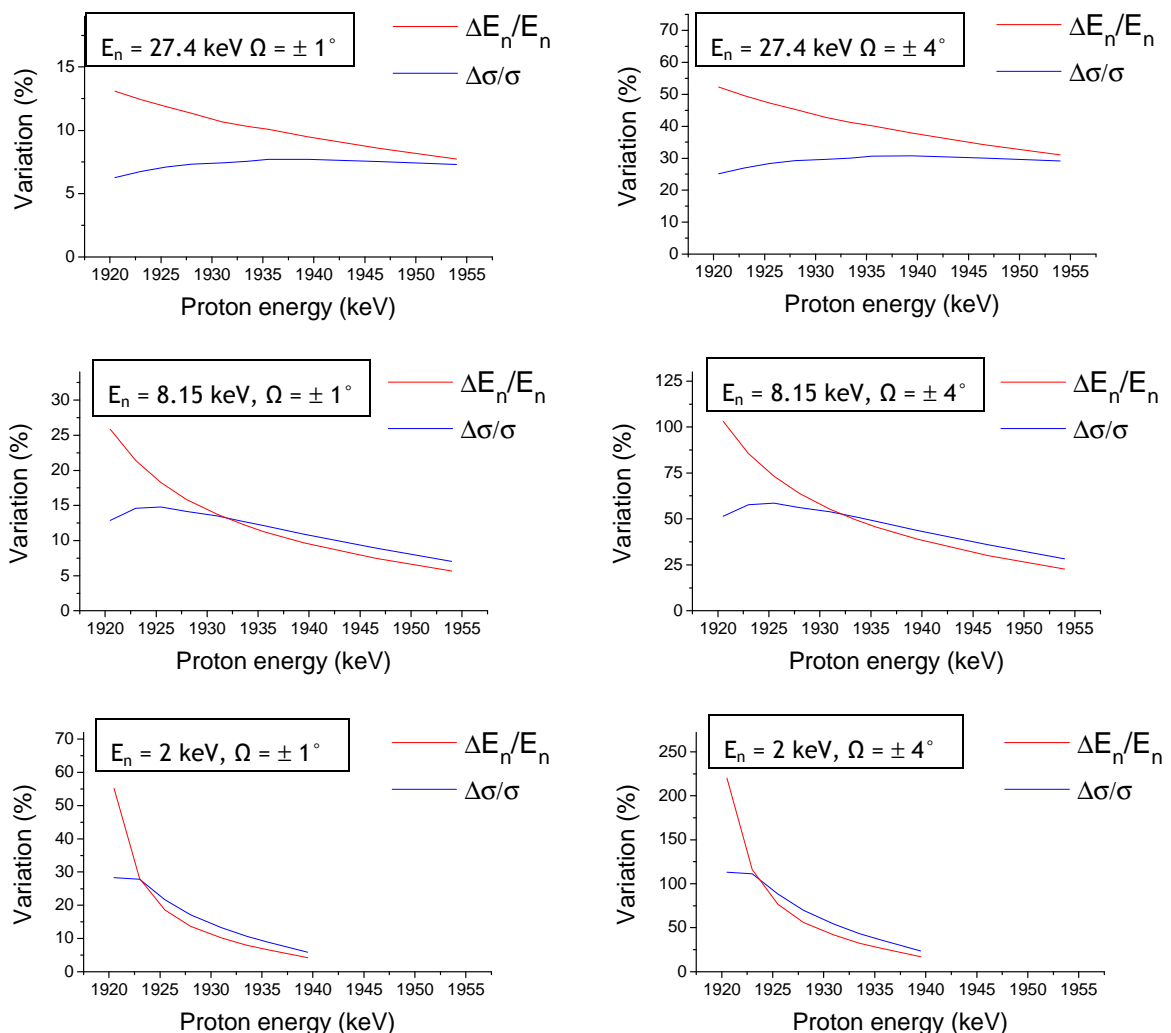
Fig. 12: *Variation of energy and cross section homogeneities with proton energy for three neutron energies and two solid angles (1° and 4°) obtained with a Li(p,n) reaction (calculation performed with* Drosg2000 *code).*

However, at the emission angles needed for low energies, neutron fluence and energy variations with angle are much larger over the detector surface. These homogeneity variations depend on the kinematics, thus depend strongly on the energy of the ion beam, as shown in Fig. 12 for two solid angles (1° and 4°). Expressed in energy or fluence unit, the homogeneity is the difference between values at minimum and maximum emission angle within the cone.

In Fig. 12, one can see that energy homogeneity is better at higher proton energies. The behaviour of cross section homogeneity with proton energy depends on the neutron energy. It does in any case increase greatly with proton energy, and decrease after some distance from the threshold. This leads to favouring higher proton energies. However, as seen in the previous subsection, cross section is more significant at lower proton energies. A compromise must then be made between maximum fluence (and poor energy homogeneity) and homogeneities (but lower yield).

Neutron attenuation in materials

Produced neutrons are attenuated when going through the target material. This attenuation depends on the emission angle and material thickness that the neutrons have to cross. Fig. 13 presents the variation of target thickness (in the case of a tantalum backing) crossed by the neutrons and the neutron transmission, depending on the angle of emission. At around 90°, neutrons go through a significant thickness of material: this results in a low neutron transmission, i.e. a significantly reduced fluence rate.
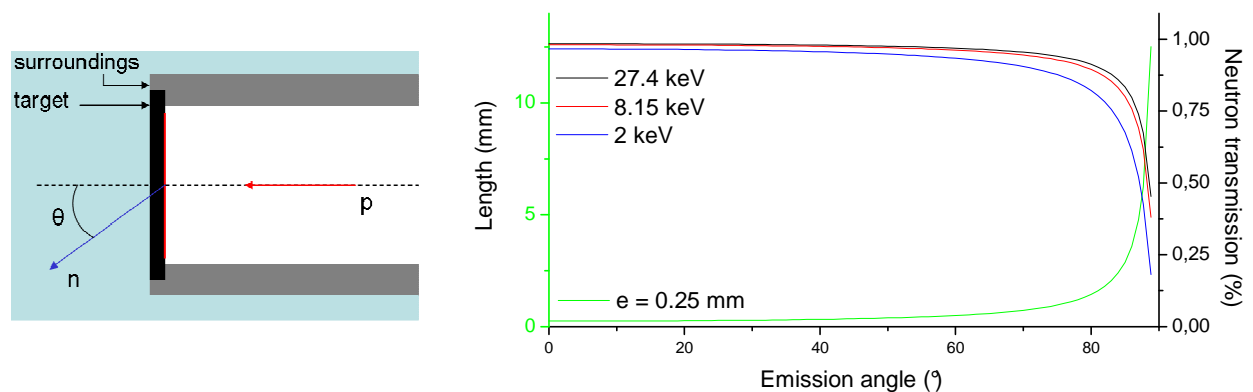
Fig. 13: *On the left side, a simplified diagram of the target and the surrounding materials. On the right side, target thickness crossed by neutrons and neutron transmission, depending on the angle for a 0.25-mm thick tantalum target (cross sections taken from ENDF/B-VI.8 database).*

At backward angles, neutrons have to go through target surrounding materials. This results in a transmission depending on the material used, a great deal of the effect coming from resonances. For example, if the target holder is made of steel, i.e. mainly iron, the absorption resonance of around 24 keV must be taken into account. Such is especially true for 27 keV monoenergetic fields, where 40% of the neutrons are stopped in 1 mm.

Selection of the studied configurations

In light of the previous observations, four configurations have been selected for the production of the three neutron energies:

- 27 keV: E_p = 1935.5 keV, i.e. $E_n(0°)$ = 144 keV and emission angle 74°. It seems to be a good compromise between keeping a high fluence rate, an acceptable homogeneity (~10 % for a 1° cone) and a reasonable distance to 90° for employing large detectors.
- 8 keV: three specific ranges can be distinguished:
  - Under 90°: since homogeneity is very poor close to the threshold, the aim is to set the angle as close as possible to 90° without experiencing attenuation in the target slice
  - Around 90°: unusable due to considerable attenuation
  - Above 90°: fluence is reduced, but homogeneity is considerably increased, which allows for setting the detector nearer to the target

  The configuration selected for this study is the one at minimal angle: E_p=1928 keV and $\theta = 85°$.
- 2 keV: homogeneity is poor; two layouts are merging: one for maximising neutron production (E_p = 1920.5, $\theta = 83°$), another for quality purposes while keeping fluence high (E_p = 1923 keV, $\theta = 90°$).

Special target design has to be considered for minimising attenuation while employing large angles. It consists in setting the target at a slant instead of perpendicular to the ion beam direction.

2.2.1.5 Target

^{7}Li targets usually consist of evaporated lithium metal or LiF on a backing (tantalum, silver, tungsten). In Table 3 common target thicknesses, corresponding ion beam energy loss and neutron energy variation are given.

Table 3: *Various ^{7}Li target thicknesses routinely employed (SRIM 2008) and corresponding neutron energy broadening for the selected configurations at 27, 8 and 2 keV, in keV and percent of the neutron mean energy.*

Thickness		ΔE_n							
Material	ΔE_p	$E_n(74°)$=27.4 keV		$E_n(85°)$=8.15 keV		$E_n(83°)$=2 keV		$E_n(90°)$=2 keV	
µg.cm^{-2}	keV	keV	%	keV	%	keV	%	keV	%
5	0.71	0.8	2.7	0.6	7.9	1.0	51.4	0.5	26.6
10	1.42	1.5	5.5	1.3	15.7	2.3	113.8	1.1	53.2
20	2.84	3.0	11.0	2.6	31.4	-	-	2.1	106.3
50	7.11	7.6	27.6	6.4	79.0	-	-	-	-

Effect of target thickness

The impact of target thickness on the neutron energy spread is compared to that of the solid angle in Fig. 14. It shows the variation of the energy resolution with solid angle for two typical target thicknesses, for all four energy configurations discussed. These results were calculated with *TARGET* code, ΔE/E corresponding to the FWHM of the monoenergetic peak.
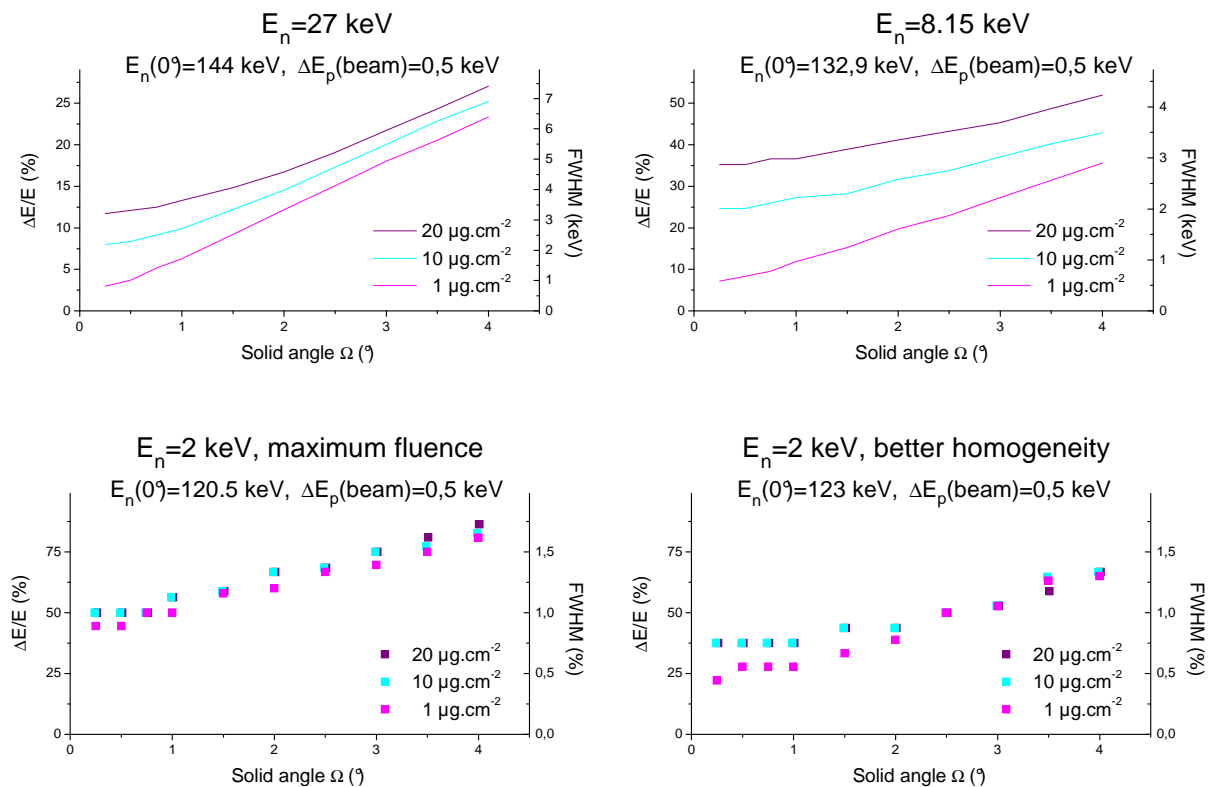
Fig. 14: *Variation of energy resolution with solid angle for the four chosen configurations and three target thicknesses.*

Each discussed configuration corresponds to different proton energy and different emission angle. As shown on Fig. 9, for each configuration neutron energy varies differently with emission angle and proton beam width. By using Fig. 14, one can observe the different layouts:

- 27.4 keV: the target thickness effect on the monoenergetic peak FWHM is negligible compared to the energy variation within the solid angle (above ±1°). FWHM is mainly due to solid angle.
- 8.15 keV: the energy variation with angle is lowered in the energy range for producing 8 keV neutrons. However, it is still paramount in percent compared to target thickness effect as soon as the solid angle exceeds ± 2°.
- 2 keV: homogeneity values for different target thickness are nearly superimposed; the effect of target thickness is completely negligible. When producing 2 keV neutrons, the energy width due to solid angle is very large (>25%).

In the end, the effect of target thickness on the energy resolution is relatively low as soon as the solid angle exceeds ±2°. This is due to the poor energy and fluence homogeneities induced by the kinematics of the reaction. As a reminder, IRSN long counter occupies ±3.8° and ±2.3° when set at 3 and 5 metres from the target, respectively.

Target composition

Natural lithium with 7.5 percent ^{6}Li can be used since the ^{6}Li(p,n) reaction threshold lies at 5.92 MeV. To avoid oxidisation difficulties when handling the target, Fluorine is commonly employed for trapping Lithium (Dr99). The resulting LiF target has a neutron yield at least three times lower than a pure Li target of the same thickness.

The upper part of Fig. 15 presents the difference of fluence variations with target thickness for both kinds of targets. These calculations with TARGET code give a ratio of approximately 3.8 for the studied configurations. The low part of Fig. 15 presents the energy resolution, which remains globally the same for a given target thickness.
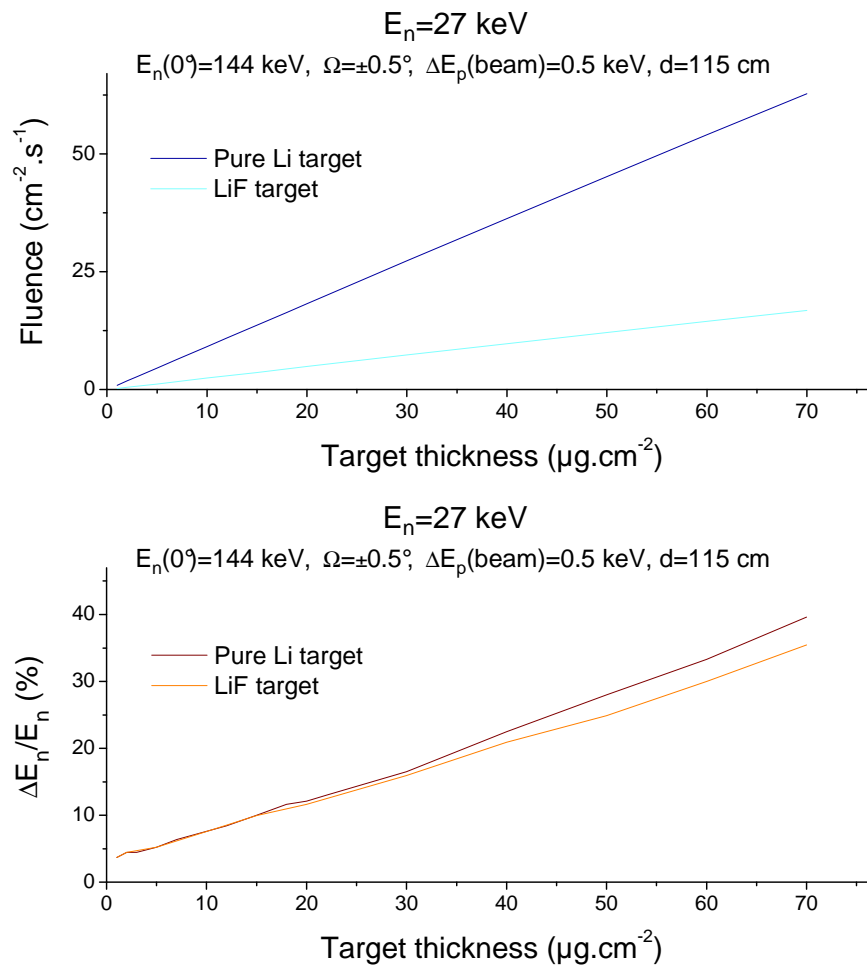
Fig. 15: *Variations of fluence (top) and neutron energy resolution (bottom)*
with target thickness for Li and LiF targets.

Fig. 16 compares the energy resolution for Li and LiF targets, allowing for the same fluence per µC at 8.15 keV - neutron energy. In this example, the lithium target thickness is 20 µg.cm^{-2}, whereas the LiF target is 70 µg.cm^{-2} thick. Energy resolution obtained with a pure Li target is at least twice better, depending on the solid angle.
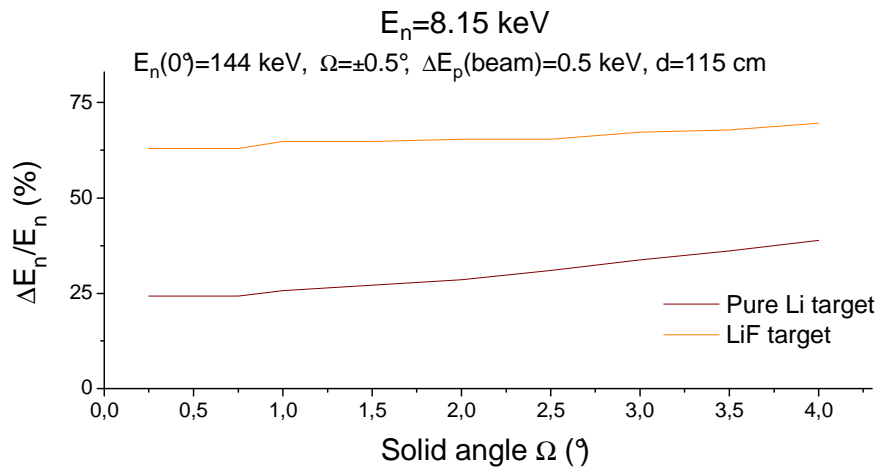
Fig. 16: *Comparison of the energy resolution with two targets of different thicknesses (20 µg.cm^{-2} for pure Li target, 70 µg.cm^{-2} for LiF target) producing same neutron emission rate.*

Measurements with LiF targets are thus done at the expense of fluence rate or energy resolution. In addition, the maximum achievable fluence rate is limited by currents targets can withstand (a few µA with pure lithium targets, around 20 µA with LiF ones).

2.2.1.6 Ion beam energy resolution and accuracy

As presented in Table 3, for ^{7}Li(p,n) reaction the effect of a beam energy spread of 1.5 keV corresponds to the energy broadening induced by a 10 µg.cm^{-2} target. It was demonstrated in the previous part that the effect of such a target thickness is small. It is indeed much less important than the energy variation observed in a finite solid angle. As for target thickness, the impact of the ion beam resolution is in this case limited.
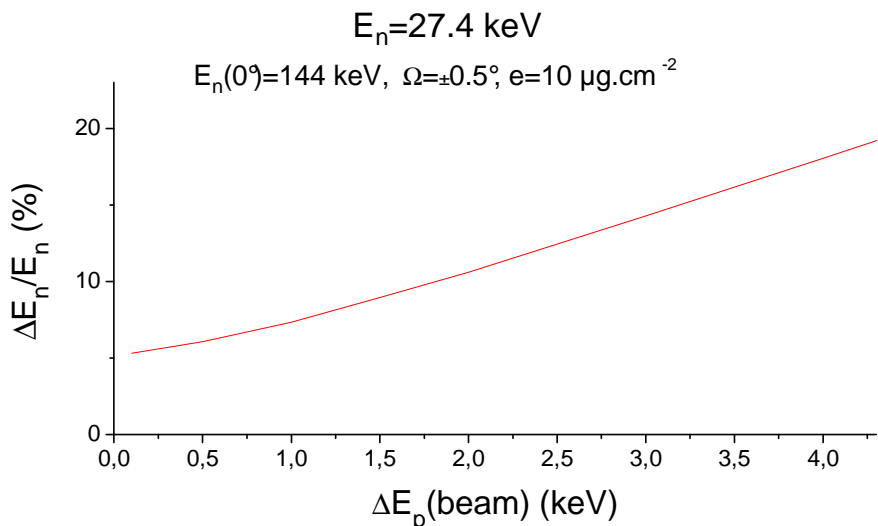
Fig. 17: *Variation of neutron energy resolution at 27 keV as a function of the ion beam energy spread.*

However, when accelerators are employed in pulse mode, the beam energy resolution is around a few keV (3 to 4 keV at AMANDE facility for example). The contribution of the ion beam resolution to the final homogeneity is no more negligible, as shown in Fig. 17.

Ion beam accuracy and stability is another source of neutron energy variation. Unlike reactions with resonance structure, cross section of ^{7}Li(p,n) reaction follows a monotonic function in the studied energy range. The uncertainty on proton energy is directly reflected on neutron energy. The significance depends on the relation between both quantities. In Table 4 neutron energy variation for a ±1 keV proton energy change are given for the four selected configurations.

Table 4: *Variation of neutron energy for a ±1 keV proton energy change with ^{7}Li(p,n) reaction. In the case of 2 keV neutrons produced at 83°, protons with 1 keV less are under reaction threshold.*

E_n	keV	27.4	8.15	2	2
Θ	°	74	85	83	90
$\Delta E_n / \Delta E_p$	-	±2.1	±1.8	+1.3/-	±1.5
	%	±7.7	±22.1	-	±74.9

2.2.1.7 <u>Measurements with angle: use of the ^{7}Li(p,n) reaction</u>

Measurements performed at a large emission angle have several drawbacks:
- Neutron energy and fluence are relatively constant around 0°, but decrease rapidly with angle. The use of high angles results in a loss in energy and fluence homogeneity within a defined solid angle.
- As demonstrated by D.W.O. Rogers in 1976, the ^{7}Li(p,n) cross section is strongly peaked at 0°, inducing a large fraction of scattered neutrons when a detector is placed at large angles. Almost 50 percent of the flux was due to scattered neutrons when set at the angle for 20 keV neutrons in the employed setup.

The achievable fluence and homogeneities have been calculated for three neutron devices of different sizes, in 27.4, 8.1 and 2keV neutron fields produced with 20 µg.cm^{-2} thick pure Li targets. These devices are:
- A standard phantom, 30x30x15 cm
- A survey meter of 10 cm radius
- A neutron detector of 2 cm radius

Results for 27.4 keV neutrons, as well as the setup, are shown in Fig. 18.

In order to maximise neutron fluence rate, neutron devices must be set as close as possible to the target. As described previously, this induces low energy and fluence homogeneities at the detector surface. Regardless of the compromise found, the homogeneities remain poor.
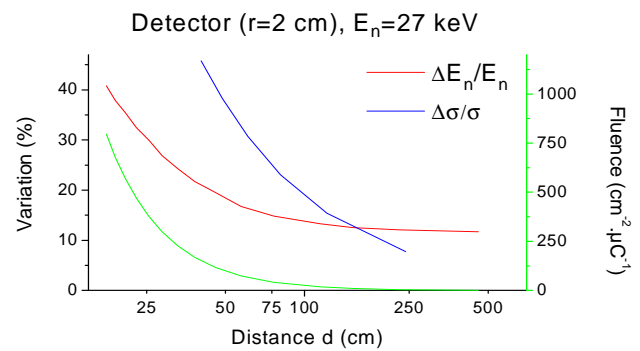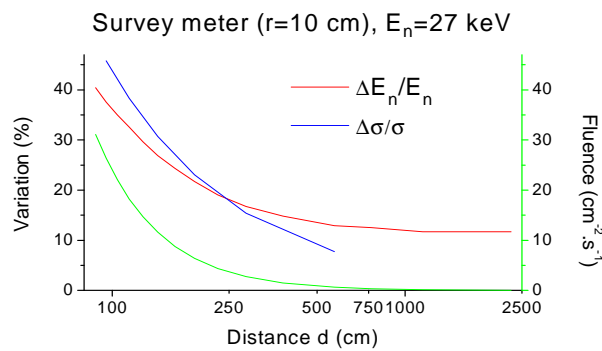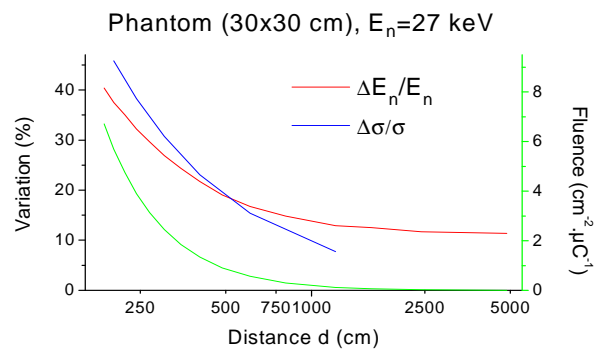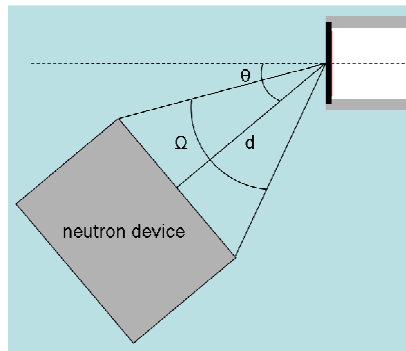
Fig. 18: *Variations of fluence (in green) and homogeneities (energy in red, cross-section in blue) at the surface of several neutron devices of different sizes as a function of the distance to the target*

2.2.1.8 Conclusion

Because of the related experimental difficulties, the use of the ^{7}Li(p,n) reaction just at the reaction threshold is limited to very specific applications.

The ^{7}Li(p,n) reaction has several advantages when employed for keV neutron production at angles other than 0°:

- Significant yield at backward angles
- Relatively easy preparation and handling of targets
- Simple shape of the excitation function and thus easy accelerator setup (no resonances)

Several drawbacks limit its use:

- Poor quality neutron spectrum at those angles:
  - Significant neutron scattering contribution
  - Significant fluence and energy variation with angle at backward angles
- Low resistance of the target to high beam current, limited to a few µA
- Simple shape of the excitation function and thus increased uncertainty on neutron energy

Those drawbacks, mainly due to setup with high angles, restrict the use of the ^{7}Li(p,n) reaction as a monoenergetic source for keV energies. As a consequence, reactions usable at 0° should be studied as alternate solutions.

2.2.2 THE ^{45}SC(P,N)^{45}TI REACTION

The ^{45}Sc(p, n) reaction has been employed for detector calibration for several years (Hu85, Ta07). This reaction allows for the production of neutrons with energy between 5.6 and 53 keV in the ion beam direction, avoiding the need to use high emission angles to calibrate neutron devices in this energy range.

Its characteristics make it an interesting alternative to the ^{7}Li(p, n) reaction for low energy monoenergetic neutron fields, as discussed in (Ro77). The neutron yield is however ten times lower than that of the lithium reaction to produce 8 keV neutron fields (Br55, Ro77), but that could be compensated by allowing for the use of higher beam current and lower distance.

2.2.2.1 Threshold and monoenergetic range

The reaction is endothermic. The most accurate measurements of its proton energy threshold for neutron production as well as of the energy of the reaction were performed by Schölermann and Siebert (Sc85) using covariance analysis. They can be compared to calculations using *QCalc* and *Kinematics* (without uncertainty) tools:

Experimental values	Calculated values
Q = -(2 845.40±0.52) keV	Q_{calc} = -(2 844.40±0.51) keV
E_{th} = (2 908.58±0.52) keV	$E_{th, calc}$ = (2 908.15±0.52) keV
	E_{mono} = 2 909.73 keV

Its monoenergetic threshold of 2909.73 keV can be easily achieved with electrostatic accelerators. The corresponding minimal neutron energy at 0° is around 5.5 keV (Ro77). These values were obtained with pure scandium targets (43 µg.cm^{-2}, i.e. 3.2 keV) and a long counter having a flat response between 5 and 200 keV (see 3.1.2).

The reaction is monoenergetic up to 2,946 keV, i.e. 53 keV neutrons in the ion beam direction. At this proton energy the first excitation level, at 37 keV, of ^{45}Ti, is reached (Ro77).

2.2.2.2 Cross section and yield

The ^{45}Sc(p,n) reaction cross section has a complex resonance structure, which may be considered either as a quality or a drawback (see 1.2.2.2).

The most detailed excitation curve, i.e. yield variation with proton energy, can be found in (Co85). In its monoenergetic range, the reaction has several main and usable resonances just above the threshold (see Fig. 19). The 8.15 and 27.4 keV neutron energy peaks are the most important and therefore the most commonly used. The differential angular cross section at 0° has been estimated at about 3 mbarn per steradian, approximately 15 percent of the cross section from the ^{7}Li(p,n) reaction at 120° (Ma60).
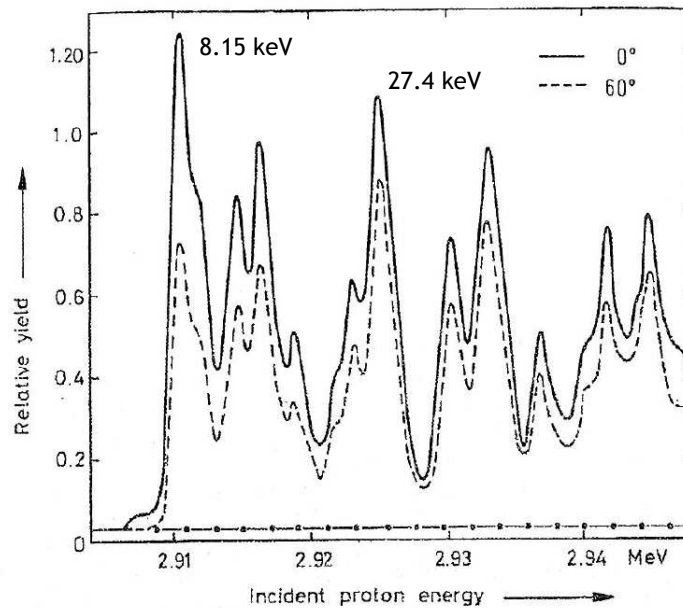
Fig. 19: *Cross section with resonant structure, example of the ^{45}Sc (p, n) reaction*
for two different emission angles: 0° and 60° with respect to the ion beam (Co85)

Setting the ion beam energy on a resonance allows for very little neutron energy uncertainty during irradiation. Due to the small width of the resonances, which is less than 0.5 keV (Co85), the promptly falling yield indicates any energy change. The beam energy can be tuned with an uncertainty lower than 100 eV.

Several cross section measurements have been reported in the literature in the past fifty years and are summarised in Table 5. One of the first estimations of differential angular cross section was made with Sc_2O_3 targets by Brugger et al. (Br55): about 1.5 mb.sr^{-1}. Rogers (Ro77) obtained a fluence rate of approximately 80 cm^{-2}.s^{-1} with an 8-keV-thick target (~100 µg/cm^2) at a distance of 80 cm. This corresponds to a cross section of 2 mb.sr^{-1} for 20 keV neutrons, which can be compared to the 15 mb.sr^{-1} of the ^{7}Li(p,n) reaction (E$_p$=1950 keV). In their search for calibration neutron fields, Tanimura et al. (Ta07) obtained a fluence of 90 cm^{-2}.s^{-1} (8 keV resonance) and 130 cm^{-2}.s^{-1} (27 keV resonance) at 50 cm from a pure scandium thick target (50 µg.cm^{-2}, i.e. 3.7 keV thick with 3 MeV protons at 50 µA).

Table 5: Obtained cross sections and fluence rates from several experiments.

Experiment	Br55	Ro77	Co85	Ta07	
Neutron energy	-	20 keV	8.2 keV	8 keV	27 keV
Target	Sc_2O_3	-	Sc	Sc	Sc
Target thickness	-	8 keV (~100 µg.cm^{-2})	0.7 keV (10 µg.cm^2)	3.7 keV (50 µg.cm^{-2})	3.7 keV (50 µg.cm^{-2})
Beam current	-		50 µA	50 µA	50 µA
Distance	-	80 cm	(50 cm)	50 cm	50 cm
Cross section	1.5 mb.sr^{-1}	2 mb.sr^{-1}			
Fluence rate	-	80 cm^{-2}.s^{-1}	10^5 sr^{-1}.s^{-1} (40 cm^{-2}.s^{-1})	90 cm^{-2}.s^{-1}	130 cm^{-2}.s^{-1}

2.2.2.3 <u>Neutron energy and time-of-flight (TOF) measurements</u>

The characterisation of the neutron energy spectrum and verification of monoenergeticity of the 8 keV resonance have been carried out by Cosack et al. using the time-of-flight technique with respectively thick and thin targets of pure scandium (Co85). The energies of the different resonances are well resolved, 8.15, 16.7, 27.4 and 36.7 being the main ones (see Fig. 20). The purity of the spectrum, shown in particular by the thin target TOF measurements, makes the reaction an excellent candidate for production of low energy monoenergetic neutron fields.
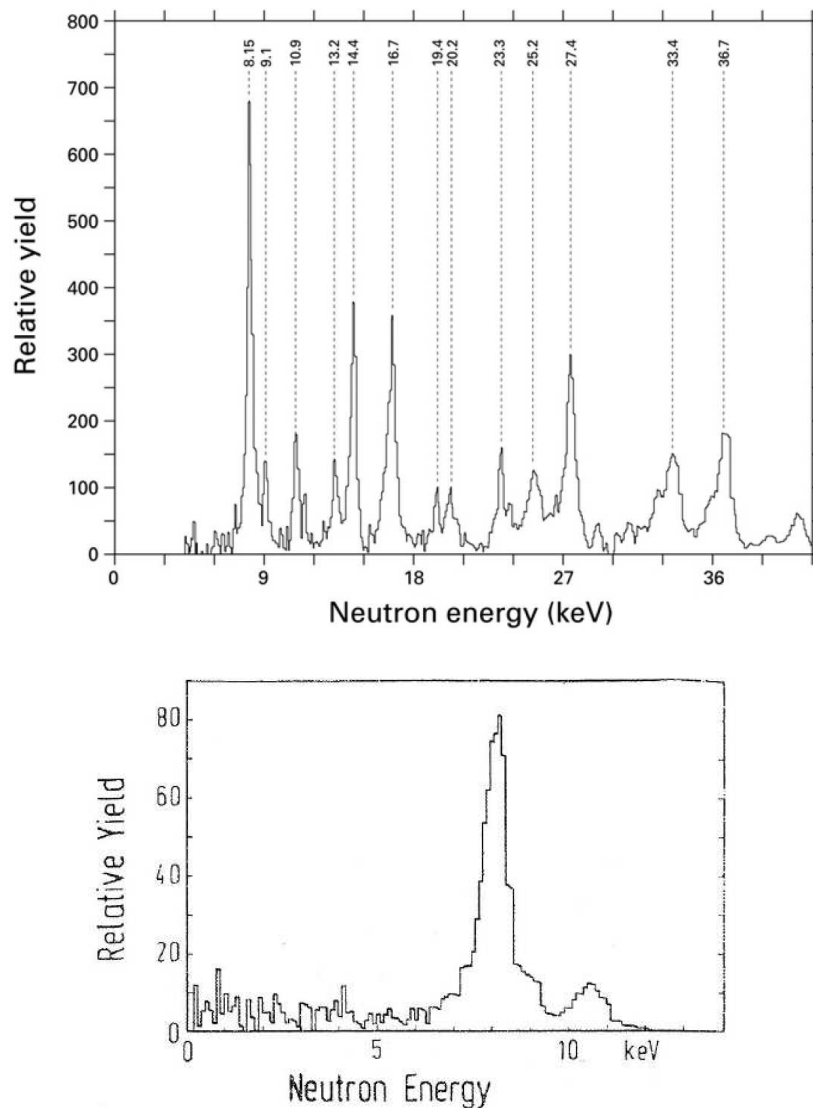
Fig. 20: *Two measurements by Cosack et al. using the time-of-flight method. On top, detailed neutron spectrum using a thick target in the ion beam direction. At the bottom, relative spectral neutron yield for a thin target measurement (Co85).*

By using the 8.15 keV resonance with a neutron emission angle higher than 0°, one can produce lower energies down to less than 1 keV (0.5 keV at 120°, see Fig. 21). Neutrons at these low energies are much more sensitive to materials on their path and the emission angle should therefore not exceed 85°. Usable 2 keV neutrons are produced around 80°, i.e. before experiencing too much interaction with the target surrounding materials.

Neutron energy (8.15 keV resonance)
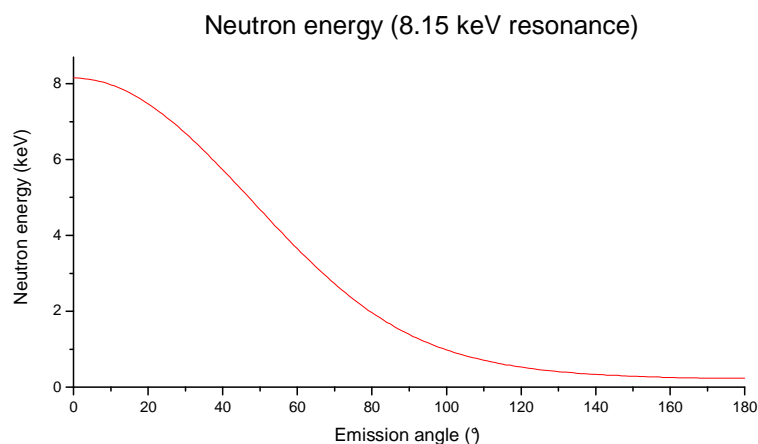
Fig. 21: *Variation of neutron energy with emission angle when the ion beam energy is set on the 8.15 keV resonance (calculated using kinematics described in (Ma68), see equation 4).*

Resonances of 8.15 keV and 27.4 keV are usually favoured for applications and studies because of their significant yield, neutron energies and easy selection:

- The 8.15 keV resonance has the best yield, is the lowest achievable energy at 0° and is easy to select by scanning from the threshold.
- The 27.4 has a good yield, has the closest energy to the 24 keV ISO standard recommended energy provided by other calibration means (reactor, SbBe) and has no other main resonance around.

2.2.2.4 Angular distribution

The formation of a compound nucleus is the more probable kind of interaction at these energies between a proton and a medium-weight nucleus (Ma60). If the reaction is considered isotropic in the centre of mass, neutron energy and relative yield can be calculated for any emission angle using kinematics (see Fig. 22) described in part 1.2.1.3. The relative yield is determined by the ratio of the differential cross sections in the centre of mass and in the laboratory frame of reference. Isotropy has been roughly confirmed by the experiments of Cosack et al. (Co85) for 8.15 and 27.4 keV resonances.
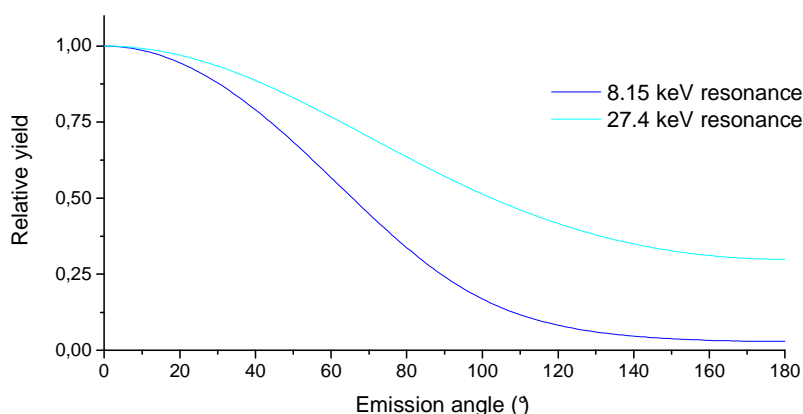
Fig. 22: *Relative yield or variation of neutron production with emission angle for 8.15 and 27.4 resonances of the ^{45}Sc(p,n) reaction (calculated by using kinematics described in (Ma68), see 1.2.1.3).*

2.2.2.5 Acceptable opening angle

According to kinematics, energy and fluence dependence on neutron emission angle is much lower with heavier elements at 0°. Fig. 23 presents the calculated relative variations of both energy and fluence in the opening angle sustained by a detector at a set distance. The results are based on kinematics and do not include the influence of target thickness and ion beam energy spread.
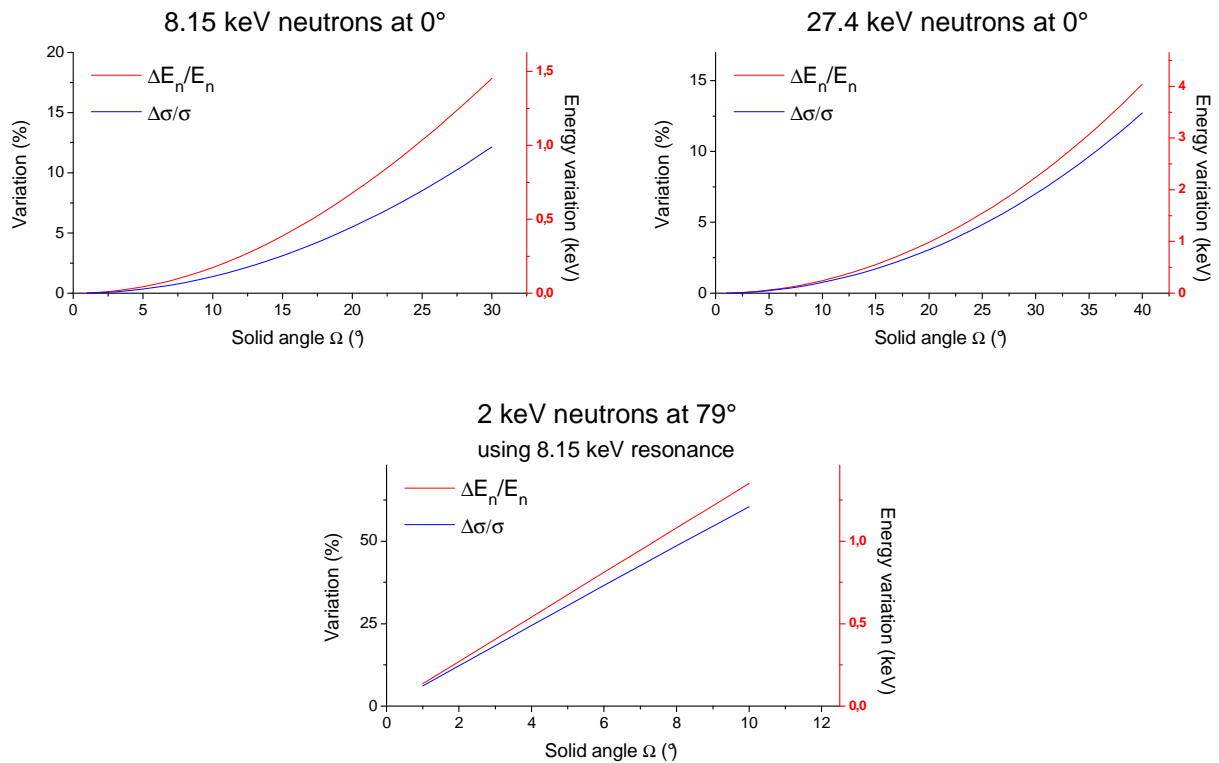
Fig. 23: *Energy and fluence homogeneity variations with detection opening angle*
for 8.15 keV (0°), 27.4 keV (0°) and 2 keV (79°) neutrons produced with $^{45}Sc(p,n)$ reaction.

When employed in the ion beam direction (0°), the $^{45}Sc(p,n)$ reaction allows for very good energy and fluence homogeneities in the detector: the variations are less than 10% for 20° and 30° opening angles, respectively, for 8.15 keV and 27.4 keV neutrons. As expected, inhomogeneities are much more significant when the reaction is used with a large angle, as in the case of 2 keV neutrons.

For a 10 percent maximum variation of fluence, solid angles with ±27°, ±35° and less than ±2° openings are acceptable for 8.15, 27.4 and 2 keV neutrons, respectively. Energy variation depends much more on target thickness; this effect must be taken into account.

2.2.2.6 Targets

Thin layers deposited on the backing are required for the production of monoenergetic neutrons. The relatively low evaporation temperature of scandium allows for target production through the evaporation of the metal using an evaporation boat on the selected backing. Pure scandium targets are preferable: Sc_2O_3 targets are 70 percent thicker in terms of energy loss with no real advantage. They were employed in the past due to the difficulty of separating the metal (Ma60).

Scandium targets are able to withstand high currents for several hours. Targets on tantalum backing employed by Rogers withstood a 50 µA beam current for twelve hours without noticeable yield decrease. This resistance property had been already speculated on by Brugger et al. (Br55) in the 1950s and pointed out by Marion & Fowler as one of the key reasons for the use of the $^{45}Sc(p,n)$ reaction.

As shown in 2.2.2.2, the $^{45}Sc(p,n)$ yield curve presents many resonances: 13 have been identified within 23 keV proton energy variation, i.e. one every 1.8 keV. If the beam energy spread is larger than this spacing, several resonances are covered at the same time. This results in producing neutrons of several energies and must be avoided (see 1.2.2.2). However very close resonances can be employed at the same time for producing monoenergetic fields, since their contributions are included in the FWHM of the monoenergetic peak.

Table 6: Proton energy loss in several target thicknesses and corresponding neutron energy variation for 27 and 8 keV neutrons produced at 0° and 2 keV neutrons produced with angle (SRIM 2008, in keV and percent of the neutron energy). These values are indicative and do not take into account the resonance structure of the reaction.

Thickness		ΔE_n					
Material	ΔE_p	$E_n(0°)=27.4$ keV		$E_n(0°)=8.15$ keV		$E_n(79°)=2$ keV	
µg.cm^{-2}	keV	keV	%	keV	%	keV	%
5	0.37	0.5	1.7	0.6	7.4	0.3	14.8
10	0.74	0.9	3.3	1.2	14.8	0.6	29.6
20	1.47	1.8	6.7	2.4	29.6	1.2	59.2
50	3.68	4.6	16.6	6.0	73.9	3.0	147.9

According to Table 6 and resonance characteristics, 5 µg.cm^{-2} targets are well suited for characterisation of the excitation function: they allow for a good resolution of each resonance. The maximum thickness for monoenergetic neutron production is 20 µg.cm^{-2}, since it allows for maximum fluence while keeping the energy resolution below the mean separation energy between two resonances. Thicker targets should be used only in TOF experiments for determination of the neutron spectrum.

The impact of target thickness on energy distribution is slightly dependant on the ion beam energy and considered emission angle. Depending on the neutron energy, it corresponds to a more or less significant variation ratio. Thinner targets should be preferred for lower energies or larger angles. Using the 8.15 keV resonance, a 20 µg.cm^{-2} target produces a 30 % variation in the neutron spectrum. The ratio is much greater when using 2 keV neutrons because of the angle; 10 µg.cm^{-2} are enough to produce this same variation.

2.2.2.7 Conclusion

Despite its low yield, the ^{45}Sc(p,n) reaction is considered to be a good candidate for neutron production and related applications. Several experiments have shown with various accuracies its general characteristics, such as reaction thresholds, excitation curves and neutron spectrum produced.

^{45}Sc(p,n) resonant cross section can be considered either as a drawback or an advantage. The difficulty for selecting the needed resonance is highly reduced with a good target voltage control system. Its principle drawback remains its low yield. It can be compensated for by maintaining a high current on the target. This is possible due to the capability of the scandium targets to withstand high beam power.

The high atomic mass of scandium as compared to lithium or other light elements is an important advantage for obtaining good energy and fluence homogeneities in the considered solid angle. Accurate knowledge of cross section (at 0° and its angular variation), target ability to withstand high currents and other general characteristics could make this reaction an alternative to ^{7}Li(p,n) reaction.

2.2.3 THE $^{51}V(P,N)$ REACTION

The $^{51}V(p,n)$ reaction has been used for various applications during the last decades (Hu85). It can be employed over a large energy range with low contamination, from a few keV to MeV in the ion beam direction, and is mainly employed for 4π measurements, as described below.

2.2.3.1 Threshold and monoenergetic range

$^{51}V(p,n)$ reaction threshold and Q-value have been measured several times since the 1950s (Gi55, De69, Sc89). Calculations of these quantities obtained with *QCalc*, as well as the monoenergetic threshold obtained using *Kinematics*, are as follows:

$$Q = -(1\ 534.92 \pm 0.24)\ keV$$
$$E_{th} = (1\ 565.28 \pm 0.24)\ keV$$
$$E_{mono\ =}\ 1\ 565.91\ keV$$

Because of its medium weight, neutrons produced in the ion beam direction are only 2.36 keV according to De69 (or 2.41 keV according to kinematics calculation) at monoenergetic threshold. The first excitation level of the residual nucleus ^{51}Cr is at more than 750 keV, thus the needed proton energy for forming a competing and second neutron group is 2.335 MeV (De69). This threshold corresponds to an energy of the first neutron group around 790 keV, according to calculations with the IRMM *Kinematics* software.

Some contaminations occur if natural vanadium is used as target. It is mainly composed of 99.75 percent ^{51}V and 0.25 percent ^{50}V. The $^{51}V(p,n)$ reaction is then systematically contaminated by the $^{50}V(p,n)^{50}Cr$ and $^{50}V(p,\gamma)^{51}Cr$ reactions. These latter reactions are exothermic, having Q-values of 0.25 MeV and 9.50 MeV (Ha65), respectively.

This results in a non-strictly monoenergetic field, even over the monoenergetic range of $^{51}V(p,n)$ reaction. However, the contamination is very low, less than 0.2 percent from the $^{50}V(p,n)$ reaction with no significant γ production, according to Ha65.

Several neutron groups arise at higher energies (De69). Depending on the needs, the reaction can be used for neutron energies up to 1.5 MeV, since contamination from other neutron groups represents only a fifth of the neutron production (De69).

2.2.3.2 Cross section and yield

The residual nucleus ^{51}Cr is radioactive with a 27.8-day half-life; it emits 0.322 MeV γ rays. This γ production can be easily detected after completion of the measurements determining the emitted fluence with the associated nucleus method (Ha65).

For neutron production with protons between 2 and 4 MeV, total cross section represents a fifth of those of ^{7}Li and T(p,n) (De69). At lower proton energies from 1.579 to 2.276 MeV, total cross section is from less than 1 mb to about 10 mb (Ha65). Gibbons et al. measured a 1-mb total cross section for the production of 100 keV neutrons, corresponding to proton energy of 1655 keV. This has to be compared to the several hundred of mbarn for T(p,n) and ^{7}Li(p,n) reactions.
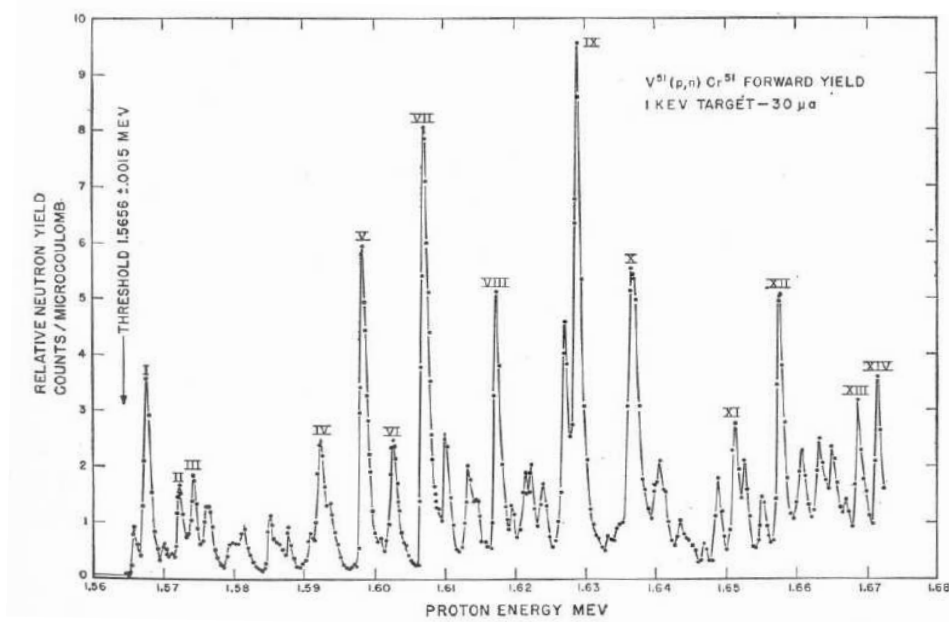
Fig. 24: *^{51}V(p,n) forward neutron yield, for a target thickness around 1 keV and proton beam current of around 30 μA. (Gi55)*

The ^{51}V(p,n) cross section has a resonance structure near threshold (see Fig. 24). From 1.55 to 1.65 MeV proton energy, the average spacing between resonances is less than 2 keV (Gi55). Gibbons et al. obtained an experimental width of the peaks including just that of their 1 keV thick target: the natural width of the resonances should be lower than 1 keV. The effective shape of the cross section is then somewhat dependent upon target thickness, beam energy spread and solid angle (Gi65), as always for reactions with a resonant structure but especially when resonances are thin and close to each other.

2.2.3.3 <u>Neutron energy and time-of-flight (TOF) measurements</u>

Schölermann and Böttger determined the resonance structure of the ^{51}V(p,n) cross section just above threshold by time-of-flight measurements. They bombarded a 50-keV-thick target with protons approximately 50 keV above the reaction threshold. One low noticeable peak corresponding to a neutron energy of 6.44 ± 0.195 keV was determined (see Fig. 25).
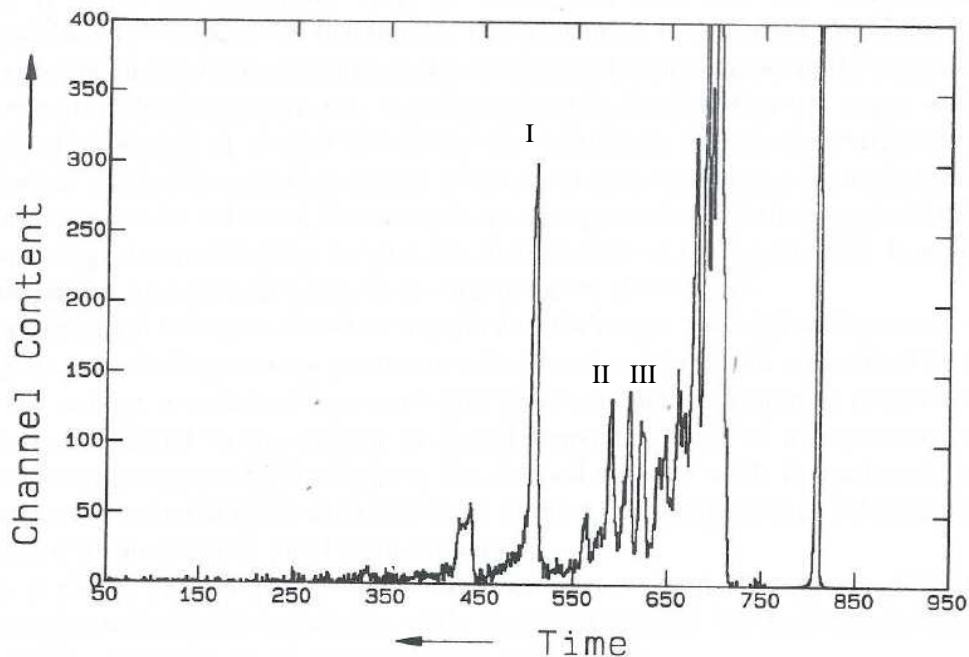
Fig. 25: *TOF spectrum of neutrons from ^{51}V(p,n) for proton energy near threshold.*
The peak at channel 508 (I) corresponds to the 6.44 keV neutrons. (Sc89)

2.2.3.4 <u>Angular distribution</u>

Due to its comparatively high atomic weight for neutron production, vanadium induces low energy spreads and small fluence variation with angle (Gi65 and De69). The ^{51}V(p,n) reaction was found to be nearly isotropic between 1.579 and 2.276 MeV by Harris et al. (Ha65). Only a few peaks (identified as IV and V in Fig. 25) present some departures from isotropy.

Deconninx *et al.* described a slow variation of neutron energy with emission angle (De69). This reaction was therefore employed for 4π-applications without introducing large energy spreads of around a few percent (Gi65). It has been used as a pulsed isotropic neutron source in this energy range, corresponding to neutrons between 20 and 750 keV (De69).

For monoenergetic field production, this reaction could be interesting when used at rear angle to reach very low energies. However, it will depend on the neutron emission rate (see 4.2.3).
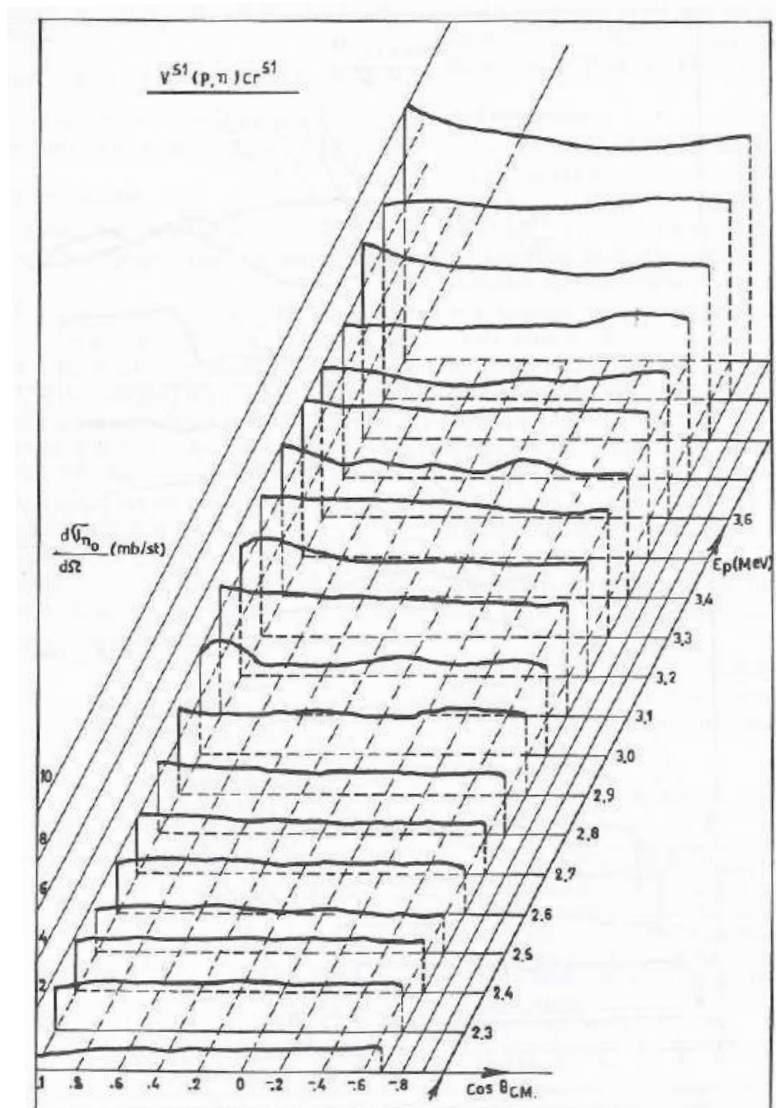
Fig. 26: *Angular distributions of first neutron group for ^{51}V(p,n) reaction (De69)*

2.2.3.5 Target production and use

Vanadium has a high fusion point (1 710°C) and is a good conductor of heat and electricity. This allows for the use of relatively high beam currents (De69) able to compensate partly the lower cross section of the ^{51}V(p,n) reaction.

The production of thin vanadium targets is relatively easy using vacuum evaporation, from tungsten, for example (Gi55). Harris et al. cooled the target backing for a better bond between vanadium and platinum backing. They noted the necessity of both mechanical and chemical cleanings of the surface of the backing to obtain for allowing the use of the target with beam current around 10 µA. Gibbons et al. achieved measurements with a 30 µA proton beam.

Relatively pure ^{51}V used to be a cheap material (De69). However, the cost of this isotope has considerably increased, leading to new production method requiring less material than the evaporation technique (see 4.2.2.1).

2.2.3.6 <u>Conclusion</u>

Due to the relatively high mass number of ^{51}V, the ^{51}V(p,n) reaction exhibits many interesting characteristics for low-energy monoenergetic neutron production, especially for 4π applications:

- Low variation of energy and fluence with emission angle, due to its medium-weight
- Low neutron energy: first main peak at 6.44 keV

However, the neutron yield seems very low and could not be sufficient for calibration of radiation protection devices.

2.2.4 THE ^{65}CU(P,N) REACTION

Natural copper is composed of 30.83 % ^{65}Cu and 69.17 % ^{63}Cu (BerkeleyLab online database). Both isotopes can produce monoenergetic neutron fields. However, the ^{63}Cu(p,n) reaction has a threshold above 4 MeV, which is slightly higher than that available in standard neutron calibration facilities. It is therefore not detailed in this part but with other conceivable reactions in 2.2.5.

The ^{65}Cu(p,n) reaction has been largely studied by Schölermann and Böttger (Sc89) and this brief review is mainly based on their work.

2.2.4.1 Threshold and monoenergetic range

The ^{65}Cu(p,n) reaction Q-value was experimentally determined by Schölermann and Böttger in 1989 using a covariance analysis method. The reaction threshold of the first neutron group can be found in (Br55), as well as the experimental thresholds of the three next groups. The values calculated using *QCalc* and *Kinematics* tools are the following:

$$Q = -(2\ 134.41 \pm 0.34)\ keV$$
$$E_{th} = (2\ 167.531 \pm 0.34)\ keV$$
$$E_{mono} = 2\ 168.11\ keV$$

A second neutron group is formed at 2,970 ± 0.03 keV proton energy (Br55). According to (Br55) and based on the work of Crasemann on ^{65}Ga (Cr54), there should be no other specific reaction in this energy range. The reaction should then allow for the production of monoenergetic neutrons from a few keV to 825 keV.

2.2.4.2 Cross section and yield
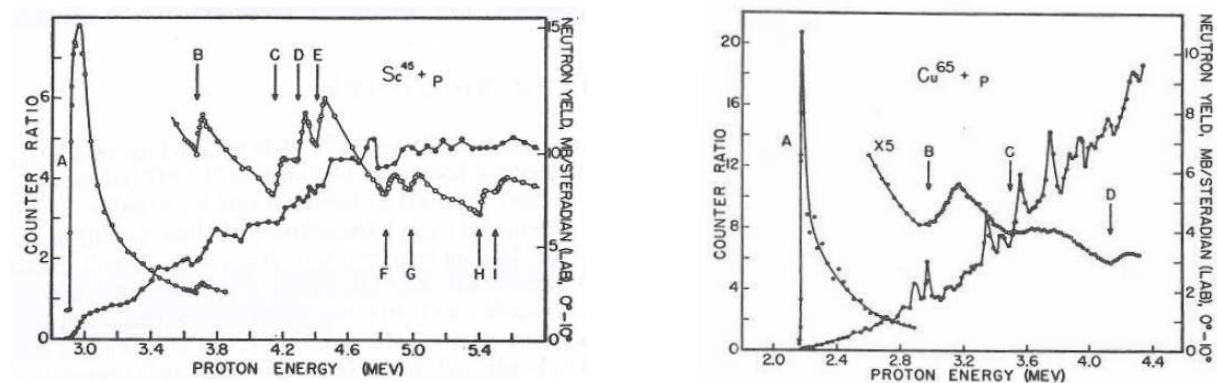
Fig. 27: *Counter ratio and neutron yield for ^{45}Sc(p,n) (left) and ^{65}Cu(p,n) (right) reactions as presented in (Br55). Letters corresponds to neutron thresholds, characterised by Brugger et al. Neutron yield just above threshold is visibly around 2 mb.sr^{-1} for ^{45}Sc(p,n), whereas the yield of ^{65}Cu(p,n) is below 1 mb sr^{-1}. Note: counter ratios have been multiplied by 5 for proton energies above a given value.*

The cross section for the neutrons in the forward direction averaged over proton energy from 2,710 to 2,750 has been estimated at 1.1 mb.sr^{-1} by (Br55). This corresponds to a neutron energy range of 56-60 keV, far above our range of interest. This latter article provides a comparison of ^{45}Sc(p,n) and ^{65}Cu(p,n) reactions: the neutron yield of ^{65}Cu(p,n) seems noticeably lower (see Fig. 27).

The cross section of the ^{65}Cu(p,n) reaction presents a resonance structure just above threshold. This structure shows a first main peak, followed by several much smaller ones. This first peak looks interesting for keV energy neutron production.

2.2.4.3 Neutron energy and time-of-flight (TOF) measurements
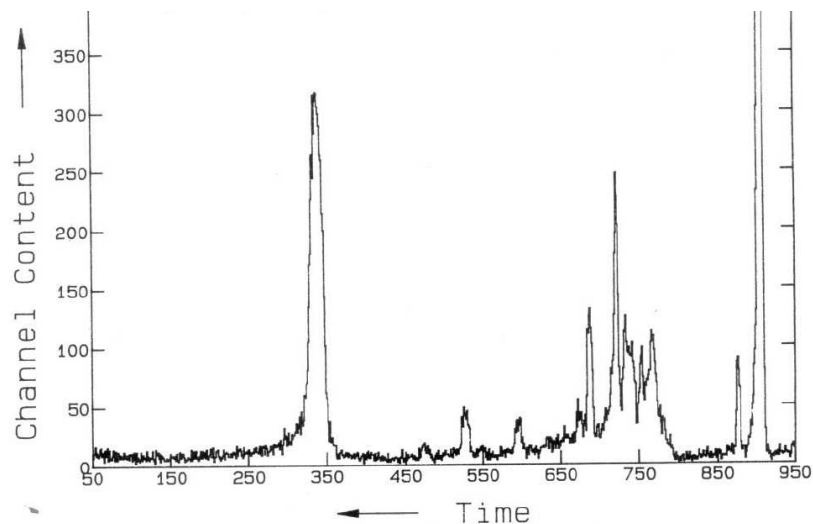
Fig. 28: *TOF spectrum of neutrons from ^{65}Cu(p,n) reaction for proton energy near threshold. The flight time runs from right to left. The peak at channel 333 corresponds to the 1.17 keV neutrons (Sc89)*

Schölermann and Böttger identified several peaks close to the threshold in the cross section of ^{65}Cu(p,n) through TOF measurements (see Fig. 28). They bombarded a 50 keV thick target with protons approximately 50 keV above the reaction threshold, obtaining the detailed resonance structure up to the threshold. One main peak corresponding to a neutron energy of 1.17 ± 0.1 keV was determined.

However, this low-energy peak cannot be, strictly speaking, employed as monoenergetic neutron source, since it rises before the monoenergetic threshold: a contribution of about 10 percent to the fluence arises from the second neutron group (E_n=0.116 keV) (Sc89).

2.2.4.4 Conclusion

The ^{65}Cu(p,n) reaction is a good candidate for mono- or quasi-monoenergetic neutron production around 1 keV neutron energy. Copper targets seem able to withstand significant ion beam currents (around tens of μA). However, their use may be restricted by a low yield and contaminations from other neutron groups.

2.2.5 OTHER REACTIONS

Other nuclear reactions have been suggested and/or partly studied for production of low-energy monoenergetic neutron fields, but only limited information is available from literature. Those reactions are reported in Table 7.

Table 7: List of considered reactions and related monoenergetic threshold, minimum neutron energy at 0° and cross section estimation, when available.

Reaction	Monoenergetic threshold (keV)	Minimal neutron energy at 0° (keV)	Cross section estimation (mb)	
			Near threshold	Around 100 keV
^{57}Fe(p,n)Co	1647.46	2.04	A fifth of ^{51}V	~0.1
^{37}Cl(p,n)Ar	1641.00	4.70	~1	~2
^{12}C(d,n)^{13}N	333.58	13		
^{39}Ar(p,n)	223.12	0.58		
^{36}Cl(p,n)	74.76	0.23		
^{53}Cr(p,n)Mn	1405.97	2.01	< 0.1	
^{77}Se(p,n)Br	2175.55	1.50	< 0.1	~0.3
^{59}Co(p,n)Ni	1887.41	2.19	< 0.1	
^{49}Ti(p,n)V	1413.33	2.35	< 0.2	
^{63}Cu(p,n)Zn	4 216.43	4.29		
^{48}Ca(p,n)Sc	511.11	0.88		
^{25}Mg(p,n)Al	5271.78	31.97	3->9	9->20
^{26}Mg(p,n)Al	4979.91	28.03	10^-2	0.2->1mb

The possibility of using such reactions as monoenergetic neutron sources was mainly found in the proton strength functions achieved by Johnson *et al.* (Jo57), like the ^{49}Ti(p,n) one illustrated in Fig. 29, and in the neutron sources review of Drosg (Dr99). The details for the ^{57}Fe(p,n) reaction were found in the article of C.A. Uttley on neutron sources (Ut83). Those for the ^{12}C(d,n) reaction were found in (Ma60).

The strength functions allow for the selection of reactions with the best yields. However, since major part of (p,n) reactions has resonant cross sections near reaction threshold, cross sections averaged over several keV can be misleading. The first indication given by those articles was the presence of a neutron production and monochromaticity.

Reactions were thus first selected for producing monoenergetic fields, their minimal neutron energy and then their cross section value. Reactions with known competing reactions were not considered. As available data are very limited, the reaction selection must be done by performing new experiments.
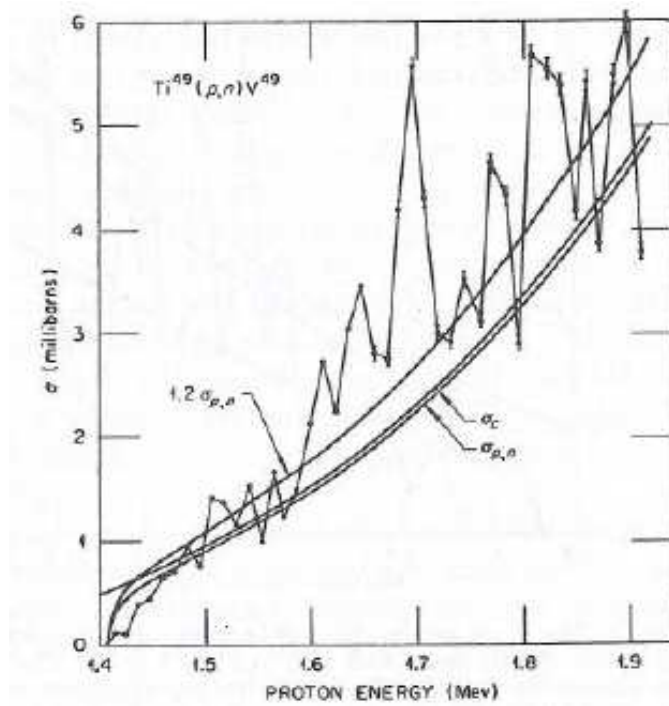
Fig. 29: *Total cross section of ^{49}Ti(p,n) reaction. (Jo57)*

2.3 DISCUSSION ON NEEDED STUDIES

Numerous reactions are already known and have been used for producing monoenergetic neutron fields between a few and few tens of keV, mainly ^{7}Li(p,n) reaction at large angles and ^{45}Sc(p,n) reaction.

2.3.1 FULL CHARACTERISATION OF ^{45}SC(P,N) REACTION

The ^{45}Sc(p,n) reaction is already well-known and has been employed for detector calibration, as well as other scientific use requiring neutron fields. The feasibility of its use has been demonstrated in terms of fluence and quality due its possible use at 0°, *i.e.* in the ion beam direction. In a few words, we know it is largely usable and of sufficient order of magnitude for several neutron applications.

However, the reaction has severe drawbacks limiting its use, and suffers a lack of knowledge. Its absolute cross section has never been accurately measured, as well as its related angular distribution. Presence of resonances in the cross section complicates the experimental setup, and if solutions exist, they have not yet become standard.

The present work focuses on characterising the experimental constraints and quantifying the main quantities defining the reaction. By characterising these properties, possibilities and limits should appear. It should allow using ^{45}Sc(p,n) reaction routinely in a metrological way. A methodology for offering its best use will be defined along the measurements.

Since the neutron yield of ^{45}Sc(p,n) reaction is low, one solution for increasing the neutron fluence rate without degrading the quality is to increase the beam current. This is possible only if the targets are able to sustain those higher currents. It requires irradiation at various currents until reaching limits and monitoring of the target state during and after each irradiation. Bond between reactive layer and backing is of primary importance, different material should be tried out as backing.

Another concern when using (p,n) reactions is the gamma contribution compared to neutron one to the total dose. A too important gamma-neutron ratio is unacceptable for many applications, such as calibrating dosimeters. This should be evaluated through gamma spectrum measurements.

Differential cross sections are needed for taking into account scattered neutrons in the uncertainty estimation through simulation. This is of primary importance at those neutron energies, neutrons being considerably scattered in air and any other materials along their path. Cross section and its angular distribution should be measured at each neutron energy of interest.

Knowledge of the cross section resonances is a prerequisite for cross section absolute measurements. It is first needed for selecting resonances deserving study. In this way excitation function has been already measured, showing the main usable resonances: 8 and 27 keV-resonances are commonly employed. The results are not usable as they are, and do not cover the whole monoenergetic range. Moreover, for estimating cross section independently from other parameters, a description as accurate as possible is needed. New measurements of

excitation function covering the whole monoenergetic range should be performed. These measurements should be completed by time-of-flight measurements, as well thick than thin targets ones.

2.3.2 EXPLORATION OF OTHER REACTIONS

Any other reaction than ^{7}Li(p,n) and ^{45}Sc(p,n) discussed in the previous part presents the same drawback: no one demonstrated their interest for scientific use such as detector calibration. There is no available and usable estimation of their fluence rate at the studied energy range.

In consequence they need first to be compared in term of neutron yield with known reactions. Excitation functions of each reaction should be performed in equivalent experimental setup.

3 <u>EXPERIMENTAL SETUPS</u>

In this chapter are first described the facilities employed: accelerators, detectors and specific experimental setups of each laboratory. In a second part are presented the type of measurements performed at those facilities, i.e. the experimental methods.

3.1 FACILITIES AND DETECTION METHODS

3.1.1 ACCELERATORS

In this part are presented the accelerator types that were used, all DC ones. It is based on the book by Editor R. Hellborg (He05).

3.1.1.1 <u>Principle of direct voltage accelerators</u>

Following Rutherford experiments using radionuclide sources, the goal of continuing investigations of nuclear structure created a demand for beams with higher intensities, well-defined energy and choice in the accelerated particle species.

The first nuclear reaction induced by artificially accelerated particles was achieved by J.D. Cockcroft and E.T.S. Walton in 1932. They won the Nobel Prize in 1951 for producing the $Li(p,\alpha)$ reaction with their 600 kV-proton accelerator:

$$Li + p \rightarrow 2He$$
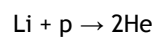
The used technique consists in accelerating particles in one step with an electric potential difference. At the same period than Cockcroft and Walton, R. Van de Graaff developed another method for producing the required high-voltage. Whatever system is preferred, the accelerator usually consists of:

- An ion source
- A vacuum chamber and its guiding setup
- An acceleration system composed of a high-voltage generator and an accelerator tube
- Several instruments of beam measurement and control
- A target or a beam extraction system.

Initially, the ion source is located at the terminal electrode at the end of the acceleration tube. Many kinds of ion source exist; usually the chosen technique consists in ionising the atoms of a gas with electrons. Atoms/ions and electrons are confined in a plasma, from which ions are expelled by an electrode at a few tens of kilovolts.

The high-voltage can be generated by mechanical or electrical systems: this is the difference between Cockcroft-Walton and Van de Graaff accelerators. This issue is discussed in the next part. The accelerator tube is a long hermetic tube under vacuum with successively electrodes and insulators along the axis for controlling the voltage gradient. Thus particles are accelerated uniformly and focused onto the exit slit, without hitting any residual atoms.

Applied acceleration is limited by the increased probability of electric discharge with increase of the high-voltage. This issue can be solved by enclosing all the acceleration system either in a tank under very high vacuum or high pressure. The latter solution with an insulating gas stable at high pressure is preferred for limiting the production of secondary electrons at the surface of the acceleration tube.

Energy of the accelerated particles is usually measured in a uniform magnetic field at the end of the acceleration tube. This measurement is also used for controlling and stabilising the beam energy.

Particle energy of such accelerators is tuneable: particles gain qeU eV, where e is the elementary charge, q the number of charges of the ions and U the high-voltage. The same accelerator can be used to accelerate any charged particle species, depending on the ion source capability. In principle they are made for continuous emission of accelerated particles, but pulsation system can be added. Direct voltage accelerators allow for very good energy resolution, in the order of 10^{-4}.

3.1.1.2 <u>Used accelerators</u>

Depending on the facility employed for this study, Van de Graaff or Cockcroft-Walton, single stage or tandem accelerators are employed. As presented in the previous part, all are based on the same principle but with some differences presented hereafter.

Van de Graaff and Cockcroft-Walton accelerators

In the case of a Van de Graaff accelerator, the high-voltage is produced by charging electrostatically the high-voltage terminal. A mechanical system, i.e. a belt, carries the charges from a DC high-voltage of few tens of kV at one end to the electrode at the other end. Such accelerators are commonly called electrostatic accelerators. The belt is built in a dielectric material, usually cotton or silk with rubber; it is charged and discharged at the extremities using metal combs, respectively by ionisation and corona effect. Van de Graaff accelerators are limited in term of beam current (a few hundred of µA maximum), because of the limited amount of charges which can be transported by the belt. However they are well suited for high voltage and very low energy width. It makes them appreciated tools for nuclear physics.

In some modern versions of electrostatic accelerators, the belt has been replaced by a chain of metallic cylinders, as is the case of Pelletron accelerators. It allows for more robust and better defined charge transport.

In Cockcroft-Walton accelerators there is no mechanical system for charge transportation but a voltage multiplier cascade, also called rectifier- condenser system. This electronic circuit consists of a network of capacitors and diodes which allows rectifying an AC lower voltage to a DC higher voltage. The principle of the multiplier cascade limits the achievable voltage. First the electric potential sustained by each rectifier is limited. This effect combines the decrease of the mean voltage with the augmentation of rectifier-condenser couples: it varies with the number of stages cubed. There is as well a residual alternating voltage increasing the beam energy width. However, important beam current in the mA range are achievable.

Tandem accelerators

Following the development of negative ion sources, Alvarez proposed in 1951 an accelerator structure with two successive acceleration stages using the same high-voltage (Al51). In its proposition, the high-voltage is obtained like in any classical Van de Graaff, but the use of a Cockcroft-Walton system in this geometry is possible and common nowadays. The electrode is set in between the two acceleration tubes, the whole acceleration system enclosed in a tank under pressure.

The ion source is set outside the tank, at ground potential and has to produce negative ions. These negative ions are injected into the first tube, accelerated toward the positive high-voltage and gaining eU eV. A stripper system (gas or metal layer) in the high-voltage terminal converts them again into positive ions. They are repelled into the second acceleration tube, gaining qeU eV. When ions leave the tank at the end of the two acceleration stages, total energy gain is $(1+q)eU$ eV.

3.1.2 DETECTION METHODS

3.1.2.1 Neutron detection

Long counters and Bonner spheres

For the detection of neutrons in the keV energy range, high sensitive thermal detector surrounded by moderator, as long counter or Bonner spheres, are the best suited detectors. Expected neutron yields are very low (see part 3), which prevent the use of proportional counters such as particle recoil detectors: it would require around ten times more irradiation time for obtaining equivalent and sufficient statistics. Neutron energy is determined by other means (see next part on Li glass detector, and part 4.2.1.2.).

For both long counter and Bonner sphere, the detection is carried out in two steps:
- Thermalisation of the neutrons through moderator
- Detection of the thermalised neutrons in a ^{3}He or BF$_3$ counter (respectively (n,p) and (n,α) reactions).

A long counter is composed of a ^{3}He or BF$_3$ tube in a cylindrical moderator composed of polyethylene, polyethylene with boron and cadmium (see Fig. 30). The mean path of a neutron in the moderator before being thermalised enough and detected depends on its initial energy. Low-energy neutrons are mainly detected in the front side, high energy neutrons in a depth depending of its incident energy. The two most important characteristics of a long counter are the relatively flat response between a few eV and the MeV range, and its high detection response R, at least a few cm^{-2} .
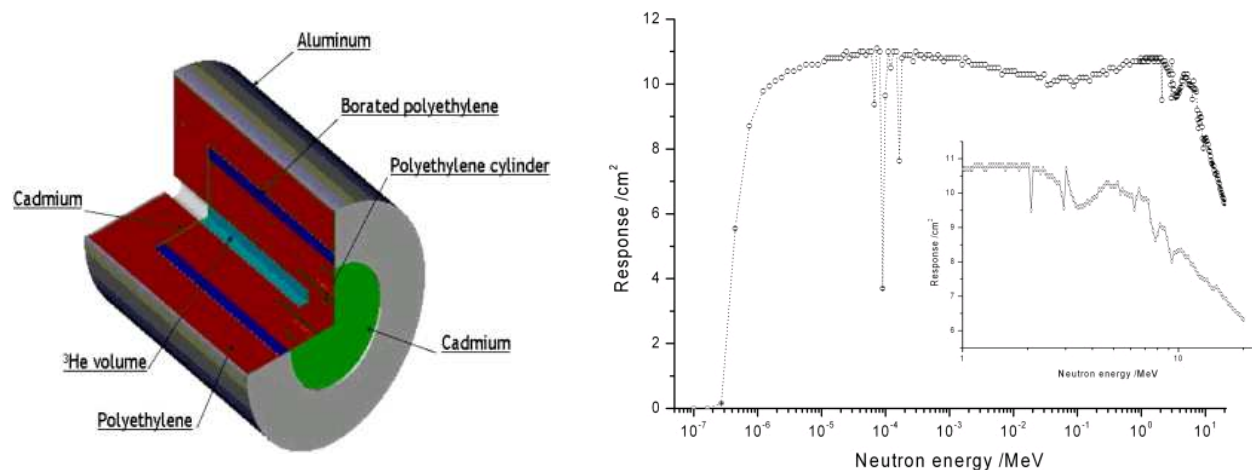
Fig. 30: *On the left, IRSN long counter modelled with MCNPX (La10-1). On the right, the response function of this detector, calculated with MCNPX 2.4.0. The magnification represents the response in the energy range 1-20 MeV, with variations due to the carbon resonances (La10-2).*

A Bonner sphere consists of a cylindrical or spherical, ^{3}He or BF$_3$ detector placed at the centre of a moderator sphere such as polyethylene. It can be employed alone or in set of different diameters. Measurement with one single sphere allows determining the fluence rate, as is the case in the present work. Neutron energy has to be known to use the appropriate moderator size, as well as the detector response at the measured energy.

By comparing neutrons detected by a set of spheres of different sizes, Bonner spheres are also used to perform accurate measurement of neutron energy spectrum. Bonner Sphere Spectroscopy requires simulation and experimental characterisation of each sphere neutron response. The spectrum is obtained using unfolding methods. Thanks to the detector symmetry and efficiency (see Fig. 31), it is well suited for characterisation of neutron environment such as nuclear workplaces.
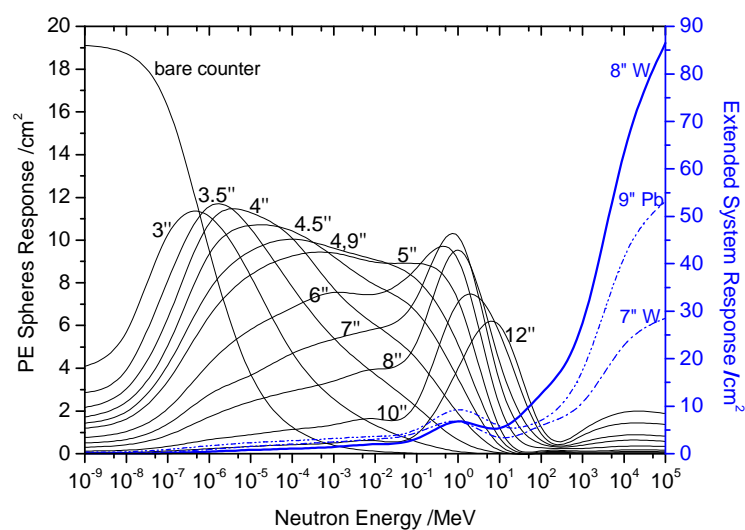
Fig. 31: *Response functions of the IRSN HERMEIS Bonner sphere system and its extension for high neutron energies. (Se09)*

Lithium glass detector

The lithium glass detector is a scintillation detector developed in 1960 by R.J. Ginther (Gi60). Scintillation detection method consists in a conversion of the energy of the charged particles, such as protons, into detectable light. A scintillation detector is composed at least of a scintillating material (a crystal for example), a photomultiplier tube (PMT) and electronic modules for measuring the amplitude of the pulses produced by the PMT. The crystal fluoresces when struck by ionizing radiation. The PMT collects the light from the crystal and generate photo-electrons. Electronic amplifier and equipment allow quantifying the produced signal, and then reconstructing the spectrum using unfolding method.

Lithium glass detector is based on the ^{6}Li(n,α)^{3}He reaction. Neutrons interact with the lithium comprised inside or outside the scintillating surroundings. The so-created α- and ^{3}He- particles ionises the crystal, inducing light emission.

This kind of detector is usable up to a few hundreds of keV, corresponding to the fall of ^{6}Li(n,α) cross section. It has good detection efficiency for low-energy neutrons (see Fig. 32) and is not too sensitive to gammas, but sufficiently for time-of-flight method as explained in part 4.2.1.2.
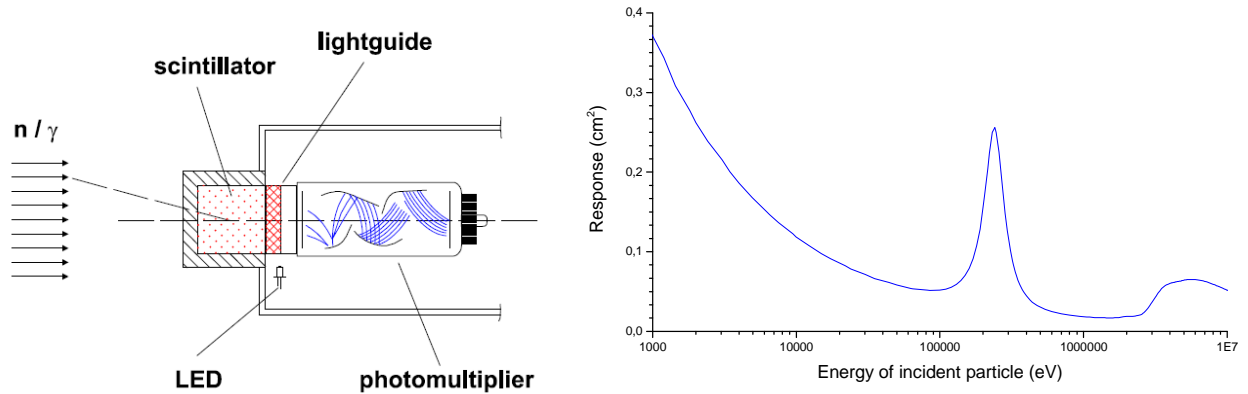
Fig. 32: *Schematic diagram of a liquid scintillator spectrometer (Th10, left) and response function of the PTB Lithium glass detector (38 mm x 3 mm, right).*

3.1.2.2 Photon detection: BGO spectrometer

A BGO spectrometer has been employed in this work for photon component determination in neutron fields. It is a scintillator as the lithium glass detector (see previous part for more details). In the case of BGO spectrometer, the number of photo-electrons, i.e. the height pulse at the exit of the PMT is proportional to the photons of low energy produced by the crystal: it is proportional to the energy deposited by the initial particle. Electronic amplifier and equipment allow quantifying the produced signal, and then reconstructing the spectrum using unfolding method (Ro77-2). The detector is usually calibrated using radionuclide sources and some of their usable peaks.

The used BGO spectrometer (see Fig. 33) is composed of a cylindrical BGO crystal (height and diameter: 2.54 cm) optically coupled to a 3.8 cm diameter photomultiplier. Two different electronic cards are employed simultaneously, one for the low gain and the other one for the high gain (As05).

Fig. 33: *View of a BGO spectrometer.*

3.1.3 FACILITIES

3.1.3.1 The AMANDE facility

AMANDE stands for *Accélérateur pour la Métrologie et les Applications Neutroniques en Dosimétrie Externe*, i.e. accelerator dedicated to metrology and neutron applications in external dosimetry (Gr03). It consists of a 2 MV Tandetron, a Cockcroft-Walton accelerator with tandem geometry. It can produce continuous or ns pulsed beams of protons or deuterons between a few hundreds of keV and 4 MeV.

Accelerated ions go through four different magnets from the ion source to 35 m ahead, the neutron producing target placed at the end of the beamline. The 90° analysing magnet allows for determination of the ion beam with a relative uncertainty of 5.10^{-4}. Depending on different parameters such as the stripping gas pressure, the ion beam energy spread FWHM is between 500 eV and 1 keV.

The AMANDE building comprises:

- A concrete part containing the accelerator room, the control room, offices and several technical rooms
- An experiment area of 20m x 20m x 16m (400 m²), behind a 40-cm-thick concrete wall for radiation protection

Fig. 34: *View of AMANDE experimental hall*.

This experiment hall was designed to reduce as much as possible neutron scattering:

- It is surrounded by mainly light metallic walls (relatively transparent to neutrons), except for the control and accelerator rooms enclosed in concrete walls for radiation protection purposes. Since the facility is at the centre of a 300-m radius excluding area, there is no need to stop the neutrons inside the building.
- The end of the beamline and the target are located 7.2 m above the floor of the experiment hall.
- A floor grating is placed at 6 m above the ground, over the entire hall surface to the exception of a 6-m-radius hole around the target.

Three mobile and motor-driven arms allow automatic, precise and reproducible placement of the detectors and related equipments around the target. The target is air cooled and mounted on a wobbling target holder allowing for a circular scan of the beam spot onto the target. Devices can be placed between 50 cm and 6 m from the target and $\pm150°$ with respect to the ion beam direction (Gr03).

3.1.3.2 NPL facility for neutron metrology

The National Physical Laboratory facility contains a 3.5 MV Van de Graaff accelerator and different beamlines for reference neutron field production in a dedicated experiment room (Ha07). This low scatter cell is approximately 25 m-long by 18 m-wide. It is surrounded by concrete walls which are 1-m thick in most places. The target is at the centre of the cell, 6 m above a concrete floor. The roof is 12 m above the target position and is made of about 15 cm-thick concrete.

Four mobile and motor-driven arms allow automatic, precise and reproducible placement of detectors around the target up to 135° with respect to the ion beam direction. The targets are cooled by a jet of cold dry air to limit scattered neutron production compared to water cooling systems. The beam spot is defocused to cover an area of about 0.5-cm radius and scanned at a rate of 50 Hz in a circle of diameter about 1 cm. The scanning allows for minimising the effect of any thickness inhomogeneity in the target as well as avoiding localised heating of the layer (Ta98).

3.1.3.3 PTB Ion Accelerator Facility (PIAF)

The PTB experimental platform for neutron metrology is constituted by two accelerators and a large experimental hall with five beamlines and dedicated areas. The Van de Graaff accelerator and the energy-variable cyclotron furnish routinely protons, deuterons and α-particles accelerated respectively up to 19, and between 13.5 and 27 MeV.

The Van de Graaff accelerator has a terminal voltage of 3.5 MV. It can be employed either in DC or pulsed mode, with a time resolution between 1 and 3 ns. Accelerated beam is guided onto the target position in the centre of the experimental area dedicated to production of monoenergetic neutrons. The target is placed at large distances from concrete walls, floor and ceiling, allowing low backscattering of neutrons. Equipments can be set on three mobile and motor-driven arms around the target. A 10 kV-high voltage can be set at the end of beam line for fine tuning of the projectile energy. Ion beam current cannot be monitored while using this system.

3.1.3.4 The Van de Graaff accelerator facility at JRC-IRMM

The neutron facility of IRMM is based on a 7-MV vertically mounted Van de Graaff accelerator. Radio-frequency ion source allows production of proton, deuteron or alpha beams, guided to one of the six beamlines and attached setups in the two experimental halls.

Accelerator can be operated in either DC or pulsed mode. Ion beams up to 60 μA can be delivered on targets in continuous mode. In pulsed mode, 2-ns pulse can be produced at frequency between 0.625 and 2.5 MHz; mean target current of 5 μA are achievable.

3.1.3.5 CENBG facility: AIFIRA

AIFIRA stands for "Applications Interdisciplinaires des Faisceaux d'Ions en Région Aquitaine" (Ha06), i.e. Interdisciplinary Applications of ion beam in the Aquitaine Region Platform. This ion beam facility is equipped with a single-stage electrostatic accelerator (HVEE 3.5 MV Singletron) delivering bright beams of light ions (H+, D+, He+) with currents up to 100 μA. Ion beam analysis, material characterisation, irradiation (fast neutrons, charged particles) and imaging techniques are carried out to conduct an interdisciplinary research program in various fields. The building is equipped with concrete radiation shielding for fast neutron experiments.

Five beamlines are available for dedicated applications. For this study, two lines were employed:

- the focused macrobeam allowing material characterisation and imaging at submicron scale through PIXE, RBS, NRA, STIM, etc.
- the physics beamline, employed for all kind of nuclear use.

Fig. 35: *AIFIRA facility. On the left, the 3.5 MV singletron; on the right the target chamber of the micrometric beamline.*

3.2 MEASUREMENT TYPES & ASSOCIATED METHODS

3.2.1 CHARACTERISATION OF NEUTRON FIELDS

3.2.1.1 Fluence measurements

According to ICRU 60, fluence Φ is the quantity defined as the number of particles dN on a sphere of cross sectional area $d\alpha$:

$$\Phi = \frac{dN}{d\alpha} \qquad (20)$$

It is expressed per unit of surface. Fluence rate is the quantity expressed in a time interval dt, i.e. per unit of surface and time. Neutron fluence is therefore the number of neutrons intersecting a unit area. It is usually expressed in cm^{-2} in neutron metrology and thus in this document.

Neutrons produced by a chosen nuclear reaction interact with each element of their environment and contribute to a total neutron field. For each position of space, there is a contribution to the total fluence Φ_{Total} of:

- neutrons produced by the reaction coming directly from the interaction place: direct neutrons with fluence Φ_{direct}
- neutrons produced by the reaction and scattered in the environment: $\Phi_{scatter}$
  - outscatterred neutrons: initially produced in the direction of the detector, but scattered in air or other material before reaching the device
  - inscattered neutrons: initially produced in another direction than the solid angle of detection, but deflected and detected after scattering
- neutrons produced from other reactions between ion beam and various materials on its path, such as the target backing: Φ_{other}
- natural neutron background: Φ_{bg}

Determining neutron fluence of a chosen nuclear reaction consists in carrying several measurements for extracting the specific contribution of direct neutrons from the reaction in this field:

$$\Phi_{direct} = \Phi_{Total} - \Phi_{scattered} - \Phi_{other} - \Phi_{bg}$$
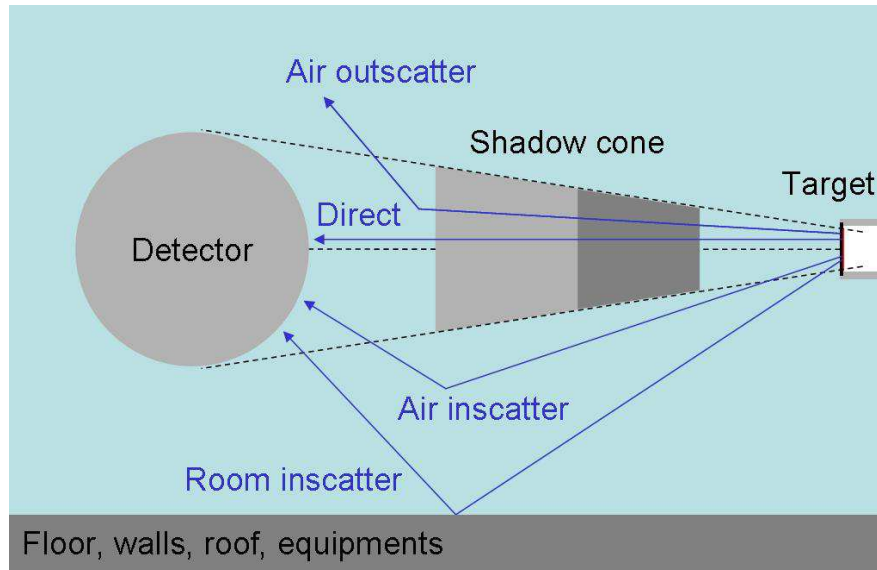
Fig. 36: *Different types of neutron scattering and principle of shadow cone method.*

Detectors

In this work, fluence measurements are carried with Bonner spheres or Long Counters (see part 3.1.2.1). Both kinds of detectors are well suited for such measurement due to their high neutron response in the energy range below 100 keV. Long counters (LC) have the advantage of limiting scattered neutrons contribution due to their directionality.

Shadow cone measurements

One common method for subtracting the main part of scattered neutrons contribution consists in using a shadow cone (Annexe E in ISO 8529-2). The shadow cone is designed for stopping as much as possible neutrons entering by its small section. It is composed of neutron absorbing materials, usually phosphated steel or copper for the front face, and polyethylene or paraffin wax with boron (at least 5 percents) for the back. It is placed in-between the target and the detector as illustrated in the Fig. 36. The measurement is carried with and without the device. This is the only change in the experimental setup: the shadow cone support is present during all the measurements. The result of the measurement with shadow cone is subtracted to the one carried without. The final result is then corrected for the scattered neutrons hitting the detector and coming from the outside of the solid angle subtended by the shadow cone, i.e. the inscattered neutrons.

Monitoring

Neutron production is induced by an accelerated ion beam. Any variation of the ion beam current impacts directly the neutron emission and thus the fluence rate. The fluence rate variation in time is therefore monitored using a

current integrator or a monitor, i.e. a neutron or photon detector at a fixed position during all the measurements. The current integrator measures the current deposed on the target, without background or dead time. It allows verification that the "ratio of emitted neutrons per ion hitting the target" remains constant. In this work, the current integrator is used as monitor to obtain the reaction cross section. This imposes the requirement that the beam is well-centred on the neutron producing target.

Equation of direct neutrons fluence

The neutron fluence from a nuclear reaction is expressed at the measuring point of the used detector (i.e. set angle θ, set distance d) per unit of µC (i.e. number of ions hitting the target). It is determined by combining several measurements and Monte-Carlo simulations.

$$\frac{\Phi_{direct}(\theta,d)}{it} = \frac{C_N \cdot C_{diff}(d,S)}{C_{LC} \cdot R_E^{LC}}\left(\frac{N_{SC}}{i_N \cdot t_N} - \frac{N_{AC}}{i_{N_C} \cdot t_{N_C}}\right) \tag{21}$$
$$= \Phi_i$$

Where:
- N_{SC} and N_{AC} are the corrected numbers of counts in the detector respectively for the measurements without and with shadow cones.
- i_N, t_N and i_{N_C}, t_{N_C} are the mean ion beam intensity and duration of the irradiations for respectively the measurements without and with shadow cones.
- C_N is the detector stability correction.
- $C_{diff}(d,S)$ is the correction for the scattered neutrons present in the solid angle covered by the shadow cone and for the fluence variation over the front surface of the detector.
- R_E^{LC} is the calculated response of the detector.
- C_{LC} is the calibration factor of the calculated response R_E^{LC} (obtained by calibration at reference neutron field traceable to national standards).

Counting direct neutrons

The number of counts in the detector must be corrected for detector dead time. It must also be corrected for counts due to neutron sources other than the reaction studied:
- natural background
- other neutron sources as those produced in the target backing or along the ion beam path.

The influence of natural background is removed by background measurement. Both measurements with and without shadow cone require supplementary measurements with a blank target, i.e. without reactive layer. They can be expressed as (Gr10):

$$N_{SC} = \frac{N}{1 - \frac{N}{t_N} \cdot \tau} - \frac{N_{ba}}{1 - \frac{N_{ba}}{t_{ba}} \cdot \tau} \cdot \frac{i_N}{i_{ba}} \cdot \frac{t_N}{t_{ba}} - \frac{N_{bg}}{1 - \frac{N_{bg}}{t_{bg}} \cdot \tau} \cdot \frac{t_N}{t_{bg}} \cdot \left(1 - \frac{i_N}{i_{ba}}\right) \tag{22}$$

$$N_{AC} = \frac{N_C}{1 - \frac{N_C}{t_{N_C}} \cdot \tau} - \frac{N_{ba}^C}{1 - \frac{N_{ba}^C}{t_{ba}^C} \cdot \tau} \cdot \frac{i_{N_C}}{i_{ba}^C} \cdot \frac{t_{N_C}}{t_{ba}^C} - \frac{N_{bg}}{1 - \frac{N_{bg}}{t_{bg}} \cdot \tau} \cdot \frac{t_{N_C}}{t_{bg}} \cdot \left(1 - \frac{i_{N_C}}{i_{ba}^C}\right) \tag{23}$$

Where:
- N and N_C are the numbers of counts in the detector for the measurements respectively without and with shadow cone. i_N, t_N and i_{N_C}, t_{N_C} correspond to their mean ion beam intensities and durations.
- N_{ba} and N_{ba}^C is the number of counts in the detector for the blank target measurements respectively without and with shadow cone. i_{ba}, t_{ba} and i_{ba}^C, t_{ba}^C correspond to their mean irradiation intensities and durations.
- N_{bg} is the number of counts in the detector for a t_{bg} duration of background measurement without beam.
- τ is the dead time of the detector.

Uncertainties

All the measured and used quantities are independent. Associated uncertainties and final fluence uncertainty for the fluence are estimated using the GUM methodology (JCGM08).

3.2.1.2 Cross section determination through fluence measurements

Cross section is the physical quantity related to the interaction probability between particles for a given reaction. This quantity is derived from the classical picture of point-like projectiles directed to a solid angle comprising a solid target, like the nucleus of an atom. The interaction occurs if the projectile crosses the surface subtended by the target, i.e. the cross section. The interaction probability is then the ratio between the section of the solid, and the total pointed area. Thus cross section is expressed as a surface unit.

Radius of nuclear particles is of the order 10^{-14} m: cross sections for nuclear reactions are expected to be around $\pi r^2 = 10^{-28} m^2 = 10^{-24} cm^2$. This explains the traditional use of the barn unit (b): $1\,b = 10^{-24} cm^2$.

In the case of neutron producing reactions, there are several possible methods for measuring the reaction cross section, as detecting the associated particle emission, measuring the decay of the reaction product, or directly counting emitted neutrons, like for instance fluence measurements.

This latter method was mostly used in this study as all the involved laboratories are specialised in neutron measurements: they have available facility and neutron detectors designed for such activity. It allows also setting the experiment in the same setup than required for detector calibration.

Besides, the studied reactions do not lend themselves to other measurements. Indeed, since the studied reactions are (p,n) and not (p,nγ) reactions, there is no associated gamma emission which the neutron yield can be deduced from. As for measuring the reaction product decay or material activation, it requires measurable decay. This is rarely the case for the considered reactions: due to low energy associated to low emission rate, activation of material is very low. Either there is no specific decay, either it is too low to be detected.

In the next section is detailed only cross section determination through neutron fluence measurements.

Neutron emission

The chosen method consists in directly counting emitted neutrons rate per incident charged particle. The number of emitted neutrons $N(\theta)$ by the target at a given angle θ and per unit of solid angle is described by the relation:

$$N(\theta) = N_p \left(1 - e^{-nX \frac{d\sigma(\theta)}{d\Omega}} \right) \tag{24}$$

Where:

- $\dfrac{d\sigma(\theta)}{d\Omega}$ is the differential cross section at θ angle
- N_p is the number of charged particles hitting the target
- X is the target thickness (cm)
- n is the number of atoms per cm^3 of the crossed material (cm^{-3}).

Since $\dfrac{d\sigma(\theta)}{d\Omega}$ is very small compared to 1, the number of emitted neutrons can be approximated as:

$$N(\theta) \approx N_p \, n \, X \cdot \frac{d\sigma(\theta)}{d\Omega} \tag{25}$$

The needed quantities for cross section determination are obtained through several measurements detailed in the following parts.

Available quantities

- Neutron fluence

When using detectors such as long counters or Bonner spheres (see 3.1.2.1), neutrons are detected at a set detection angle θ in a specific solid angle $\Delta\Omega = S/d^2$, where S is the detection surface and d the distance of the detector to the target. The quantity measured by these detectors is the neutron fluence $\Phi(\theta,d) = N(\theta)/S$ (cm^{-2}), i.e. a number of neutrons crossing a surface at a set distance. The relation is then expressed as:

$$N(\theta) = N_p \, n \, X \cdot \frac{d\sigma(\theta)}{d\Omega} \Delta\Omega$$
$$\Leftrightarrow \quad \Phi(\theta,d) = N_p \, n \, X \cdot \frac{d\sigma(\theta)}{d\Omega} \frac{1}{d^2} \tag{26}$$

The number of incident charged particles N_p is deduced from the total charge deposed on the target and measured with the current integrator during the experiment:

$$N_p = \frac{C}{e} \tag{27}$$

Where $C = it$ is the integrated charge and e the elementary charge. i is the mean beam intensity during irradiation time t.

- Target thickness

The target thickness is determined in µg.cm^{-2} through material analysis measurements described in part 3.2.2:

$$n \, X = \frac{M_{at}}{N_A \, \varepsilon} \tag{28}$$

Where:
- ε is the thickness in µg.cm^{-2} of the reactive layer,
- M_{at} the atomic mass of the target material
- N_A the Avogadro constant.

Differential angular cross section

The final expression in barns per steradian of measured cross section at a set angle is deduced from equations 26 to 28:

$$\frac{d\sigma(\theta)}{d\Omega}\bigg|_{\theta} = \frac{\Phi(\theta,d)}{it} \cdot e \cdot \frac{d^2}{T_{back}T_{air}} \frac{M_{at}}{N_A \varepsilon \cdot 10^{-24}} \tag{29}$$

Where T_{back} and T_{air} are the transmission factors of neutrons through target backing and air before being detected. They are calculated algebraically (T_{back}) or through Monte-Carlo simulation (T_{air}) using experimental cross section data.

Measurements

Using this detection method, neutron fluence is determined at a set angle θ, so is the differential angular cross section. The determination of cross section for each angle in the whole space requires multiple measurements at as many as possible angles.

The chosen method consists in first performing absolute measurements of differential cross section at 0°, i.e. in the ion beam direction. Each component and contribution is estimated and taken into account.

In a second part is carried out the relative measurement of cross section variation angle. The detector is set at various detection angles, from 0° to high angles. The result is corrected only from varying quantities, such as the attenuation factor from target thickness crossed by neutrons.

In the case of supposed isotropic reactions (see 1.2.2.3), this set of measurements is only a verification and therefore do not require extreme precision. Depending on the needed precision, the used detector is set at more or less different angles.

3.2.1.3 Characterisation of the nuclear structure: excitation function

The excitation function of a nuclear reaction is the measured relative variation of the fluence with the energy of the ion beam. It depends on the nuclear structure of the atoms or nuclei in play. The presence of discrete levels in the nuclear structure at the used energies induces resonances (see 1.2.2.2).

In the case of the studied nuclear reactions, the measurement of excitation function consists in varying slightly the ion beam energy and measuring the corresponding neutron yield. Except the beam energy change, this is comparable to a fluence measurement (see 3.2.1.1).

The ion beam energy must be changed step by step almost continuously. For avoiding multiple accelerator setups, a high voltage of a few tens of kV is set at the end of the beam line. The ion beam energy is then tuneable on a few tens of keV range without changing setup, gaining a lot of time and a better energy control as well as reproducibility. This allows also improving precision and reducing step size.

3.2.1.4 Measurement of neutron spectrum: time-of-flight method

Here is detailed the only method used in this work for characterising energy spectrum of the produced neutrons, which is time-of-flight method. The brief description presented here is based on the detailed article of Cognet *et al.* (Co10).

Principle

Time of flight method is commonly employed for characterising neutron spectrum. It consists in measuring the time needed for the neutrons to cross a known distance, usually from their source to the detector. The neutron speed v is indeed related to its energy E_n by the relativistic relation:

$$E_n = m_n c^2 \left(\frac{1}{\sqrt{1 - \beta^2}} - 1 \right) \tag{30}$$

Where:

- $\beta = \dfrac{v}{c} = \dfrac{L}{cT}$

- m_n is the mass of the neutron,

- L is the distance between neutron source and detector and T the neutron time-of-flight.

- c is the speed of the light in the vacuum.

Time-of-flight measurement

Measuring the neutron time-of-flight requires the use of a time reference. It means first that neutrons of same energy must be created at the same time. In this study, neutrons are created by interaction between accelerated ions and a target: this requirement is met by using a pulsed ion beam. A pick-up ring situated before the target gives the start signal for data acquisition ($t = 0$) at each beam pulse.

When ions hit the target, photons and neutrons are created at the same time t_0. They are detected respectively at time t_γ and t_n. As the real interaction time t_0 is not known, neutron time-of-flight cannot be directly measured (see Fig. 37). If the detector has the same response time for both radiations, as is the case for a Lithium glass scintillator, gamma detection can be used as a reference.

Photon time-of-flight is given by: $t_\gamma - t_0 = L/c$. Since neutron time-of-flight corresponds to $T = t_n - t_0$, time-of-flight becomes:

$$T = t_n - t_\gamma + \frac{L}{c} \tag{31}$$
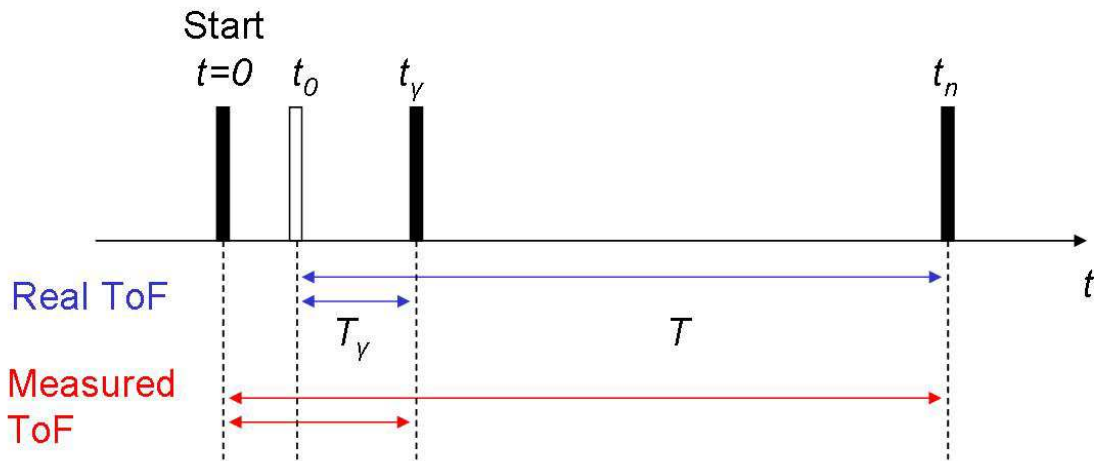
Fig. 37: *Time-of-flight signals, and available time intervals. t=0 corresponds to the start signal for electronic acquisition; time t_0 is the real interaction time when photons and neutrons are created, t_γ and t_n respectively the photon and neutron detection times, T_γ and T_n their time-of-flight.*

Available energy resolution depends on relative distance and time resolution: measurement is more accurate when time-of-flight and/or time resolution are greater. It is thus impacted by any uncertainty on length/time measurements, which are:

- flight distance,
- time calibration factor,
- determination of times t_γ and t_n.

Flight distance can be measured either by a measuring rod or a laser rangefinder, regularly calibrated. Time calibration factor is usually determined by inserting known delays in the electronics with a pulse generator. It can also be calibrated using a specific time calibrator module providing several peaks of known intervals at the same time. Both techniques allow establishing a linear relation between time intervals and associated energy shifts in the spectrum. Times t_γ and t_n are determined by fitting their respective peaks with the suited fitting function like a Gaussian.

Thick and thin target ToF

When charged particles hit the target, they are slowed down depending on the material stopping power. If a thick target is employed, they interact on a wide energy range: they describe the reaction cross section on a selected range depending on target thickness. This method can be employed for describing cross section structure and possible resonances. Relative yield between resonances is also available, with possible cross section determination when all parameters are precisely known.

In the same way, using of a thin target allows to observe the neutron spectrum of a reaction when all projectiles interact at the same energy. In this study it is employed for verifying reaction monoenergeticity.

3.2.2 ION BEAM ANALYSIS OF MATERIALS

3.2.2.1 Rutherford backscattering spectrometry

Principle

Rutherford backscattering consists of an elastic collision between an incident particle and a particle at rest in the target. No energy is lost or gained during the collision.

Rutherford backscattering spectrometry (RBS) is based on the detection of the energy of the scattered particles for a particular angle; it allows for the determination of the mass and thickness of the different nuclei in the sample (target).
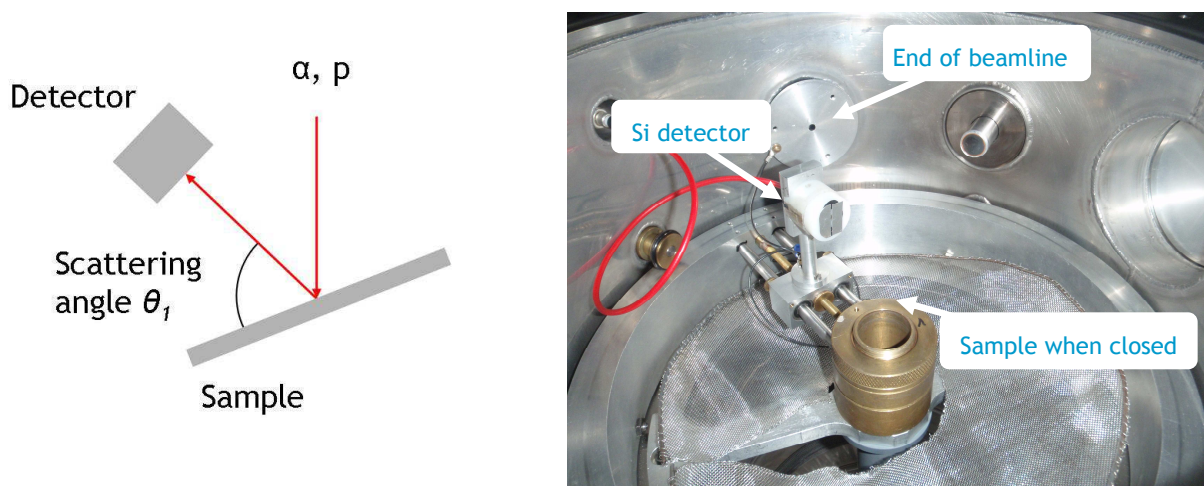
Fig. 38: *RBS principle and experimental setup in a target chamber under vacuum.*

Energy E_1 of the scattered particle 1 is reduced from its initial energy E_0 by a kinematical factor k depending on the mass of the target nucleus 2:

$$E_1 = k \cdot E_0 \qquad (32)$$

where :

$$k = \left(\frac{m_1 \cos\theta_1 \pm \sqrt{m_2^2 - m_1^2 \sin^2\theta_1}}{m_1 + m_2} \right)^2 \qquad (33)$$

and θ_1 is the scattering angle of the projectile in the laboratory frame of reference.

RBS measurements

Energy of the scattered particles directly depends on both the met material and the sample thickness crossed. When energy is calibrated using known samples, it is thus possible to identify the sample composition and respective thicknesses of eventual layers using the obtained energy spectrum (see Fig. 39). Position of the peak front gives the material, whereas peak width depends on the layer thickness. Dedicated software such as SIMNRA (Ma02) is employed for fitting the spectrum by simulating the experiment, and thus obtaining sample composition and structure.
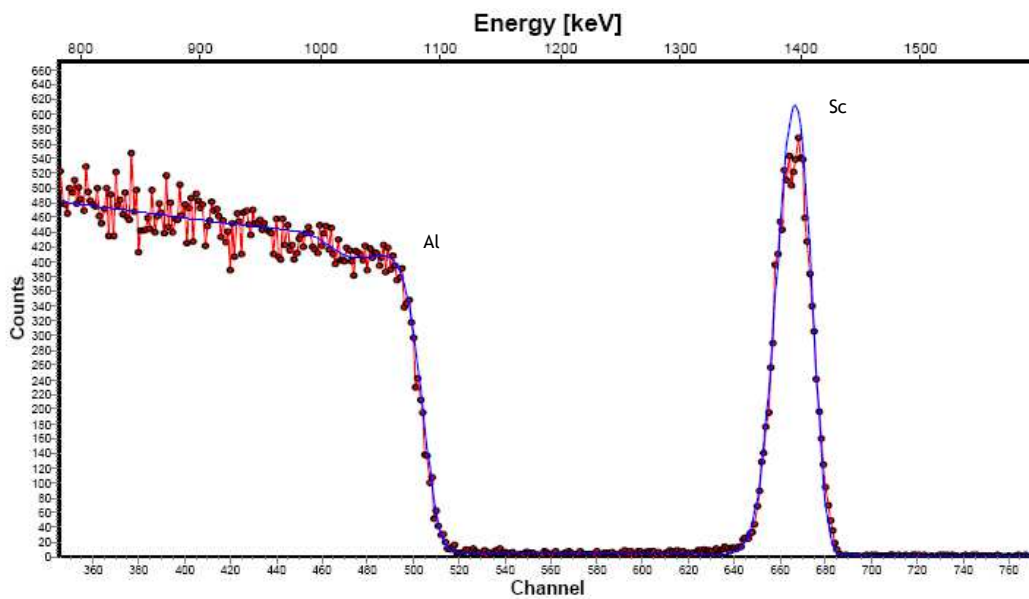
Fig. 39: *RBS spectrum (red) fitted with SIMNRA (blue) of a thin layer of scandium on an aluminium backing.*

When the main material of the sample is heavier than the studied ones, the small peaks of the low contributions appears on an important background. Searched peaks do not sort well and are determined with less accuracy. This is the case of the oxygen peak on aluminium background, compared to the scandium peak.

4 <u>EXPERIMENTAL STUDIES OF POSSIBLE REACTIONS</u>

In chapter 2 of the present document, a few (p,n) reactions were considered and discussed as potential suitable sources of monoenergetic neutron fields in the 1-100 keV range. The need for experiments to explore known and less-known reactions was highlighted, ^{45}Sc(p,n) reaction composing the best candidate.

Thus a full study of this latter reaction was carried out. The first and main part of the present chapter is dedicated to the performed experiments related to the ^{45}Sc(p,n) reaction. The second part details the prospect of alternate reactions and the comparison of their excitation functions with the ^{45}Sc(p,n) one.

4.1 SCANDIUM REACTION

In parts 2.2.2 and 2.3.1 is demonstrated both the interest of the ^{45}Sc(p,n) reaction and the requirements for its use in a metrological way. Following those requirements, the first studies consisted in determining if its main drawbacks, which are its low neutron yield and the unknown but assumed important gamma production *via* competing reactions, could be overcome or lessened.

In the second part are presented several measurements for characterising as accurately as possible the cross section structure of ^{45}Sc(p,n) reaction: in terms of neutron and proton energy, and resonance parameters. Such knowledge is a prerequisite for cross section estimation. It also gives information on nuclear structure and interaction in play.

The third part is dedicated to the determination of angular differential cross sections in whole space for two selected resonances, by fluence measurements.

4.1.1 OVERCOMING ^{45}SC(P,N) REACTION DRAWBACKS

Due to the low cross section of the ^{45}Sc(p,n) reaction (< 3 mb), the neutron fluence and dose equivalent rates per μA of ion beam current are very low. In order to increase the production rate of neutrons, for detector calibration for example, a beam current as high as possible has to be used.

This current increase can be achieved only if scandium targets can withstand high beam power. The two first experiments deal with target behaviour under irradiation. The first one consists in successive irradiation sessions with more and more important beam current on several scandium targets with various backings, looking for neutron emission variation and target alterations. Each one of those targets were characterised by ion beam analysis in-between each irradiation session. These measurements are the object of the second study on target structural changes under irradiation. Those two studies are followed by a brief discussion and conclusion on scandium targets.

4.1.1.1 High beam current irradiations of ^{45}Sc targets with various backings

Previous studies have shown that scandium targets could sustain up to 50 µA during several hours (see 2.2.2.6, and references Br55, Ro77), but this feature depends on the relation between the scandium layer and the backing among others. Scandium targets with several types of backing were therefore tested under irradiation at several tens of µA.

Experimental setup

The targets prepared for this work consisted of a 20-µg.cm^{-2} thick ^{45}Sc deposit on 0.5-mm-thick metallic backings made of Mo, Ag, Al, Ta, W and Pt. The scandium layer and backing have a diameter of 25.4 mm and 44.5 mm, respectively. In order to minimise variance in scandium thickness between samples, the targets were produced simultaneously using the evaporation method. They were manufactured by the CEA Ile-de-France target laboratory.

Irradiations of the ^{45}Sc targets with different metallic backing were conducted at the NPL facility (see 3.1.3). The neutron yields were measured with the NPL long counter (Ro04) set at 150 cm from the target and 0° with respect to the ion beam direction.

Measurements and results

A relative neutron yield measurement as a function of proton energy was carried out increasing the proton energy to a few keV above the neutron threshold at each session in order to observe any change in the ^{45}Sc(p,n) resonance structure.

In a first irradiation campaign, all the targets were irradiated for two hours at 20 µA. Targets with Ag and Mo backings showed a significant neutron background due to the backing compared to the neutrons due to the scandium reaction as shown in Fig. 40. Mechanical and thermal characteristics of aluminium (low fusion temperature combined with its low Young's modulus) make it susceptible to quick deformation under high beam currents as observed in this experiment.

The target with a tungsten backing showed a number of very small (< 1 mm diameter) bubbles (as previously observed at NPL in another study). The degree to which targets 'bubble' with use depends on: backing material, beam current, target cooling, beam-spot size, scanning, and also on the method employed for target production. Targets with platinum backing became blue at the beam irradiation area. No visible change was observed at the surface of the tantalum-backed target.
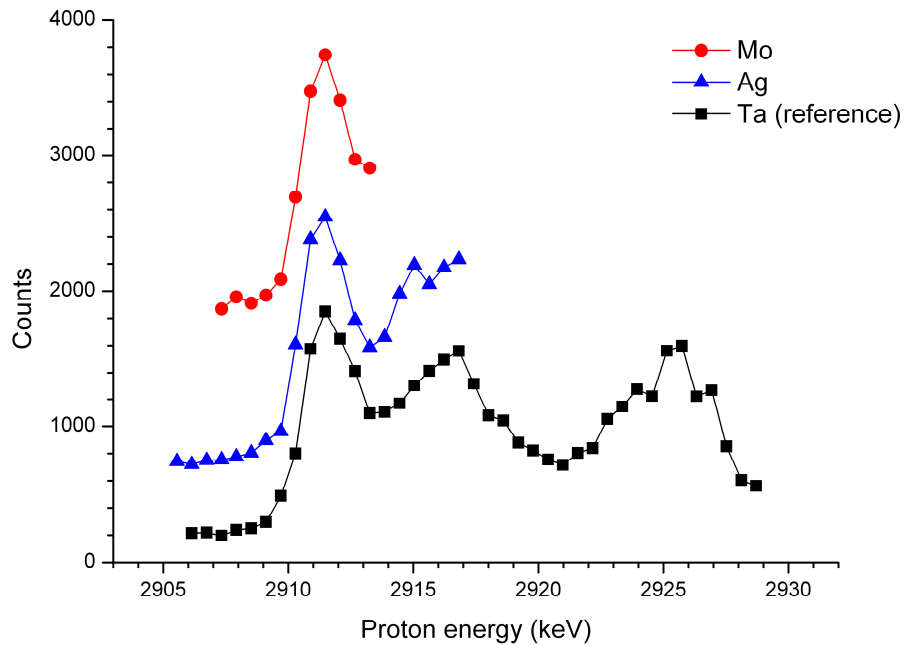
Fig. 40: *Relative neutron yield measurements as a function of proton energy (all points are for the same number of current integrator pulses).*

The three latter targets (with W, Pt and Ta backings) were irradiated in a second campaign at 35 µA for at least one hour. No new phenomena, with the exception of scorch marks, appeared as shown in Fig. 41. The target with tungsten backing displayed a slight increase in the number and size of the bubbles; a new coloured surface appeared on the target with platinum backing at the beam location, but the target with tantalum showed no visible structural changes. Despite visible changes in target structure, no change was observed on the neutron yield measurements.

Fig. 41: *Targets after irradiation at NPL: backings with bubbling as previously observed (left) and presently obtained with W (centre) and Pt backing (right) with colour change.*

4.1.1.2 <u>Study of target structural changes under irradiation</u>

Parallel to irradiation session at NPL facility, target composition, homogeneity and thickness were analysed at the AIFIRA facility (Ha06) by Rutherford Backscattering Spectrometry (RBS), before and after each irradiation. First measurements served to verify target thicknesses and compositions specified by the manufacturer and constitute a zero point of the targets' state. They were then repeated following each irradiation session.

Experimental setup

Experiments were conducted at the micrometric beamline of AIFIRA facility (see 3.1.3 and Fig. 42 and 43). This beamline available at the facility is well-suited for sample characterisation of the scandium targets used. The focused macrobeam allows characterisation and imaging at submicron scale through ion beam analysis methods like PIXE, RBS, NRA, STIM, etc.

Fig. 42: *AIFIRA facility: target chamber of the micrometric beamline.*

Owing to the specificities of the samples (light elements deposited on heavy elements), a 1 MeV H^+-ion beam was selected in order to optimise the separation of the signal from each element and avoid a nuclear reaction with the Sc foil ((p, n) reaction threshold being at 2,908 keV). The scandium target on aluminium backing was also analysed with 2 MeV He^+-ions as the Al and Sc signals are easily distinguishable in these analysis conditions (Fig. 44). A set of collimators were used to shape the ion beam and have a 1-mm beam spot size suitable for a multiple analysis in different parts of the sample. The ion beam current was between 1 and 20 nA, depending on the backing response. The scattered ions were detected in a Si-detector at a backscattering angle of 160° (IBM configuration).
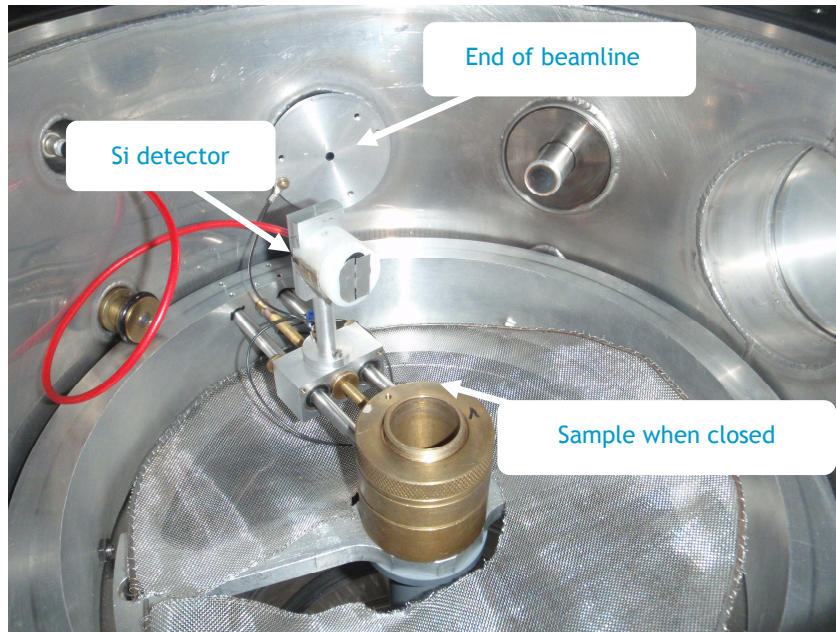
Fig. 43: *RBS experimental setup in the target chamber.*

The data were collected with the MPA3 program which allows for multiple analogous acquisitions. The RBS spectra were then processed with the SIMNRA code (Ma02) in order to simulate the composition and the thickness of the sample.
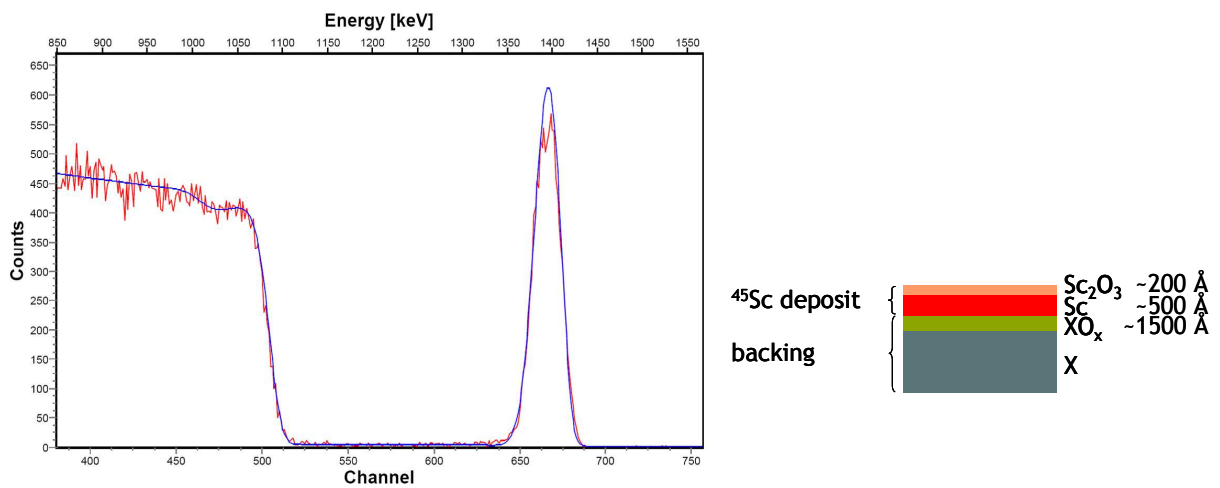
Fig. 44: *Example of a ^{45}Sc target on an Al backing. On the left, RBS spectrum of the target (red) and adjustment with SIMNRA simulation (blue). On the right, target structure with oxidation of both deposit and backing as determined by RBS measurements.*

Results

Results are listed in Table 8. As a first result, the nominal and measured thicknesses were in agreement with the manufacturer within 5%. RBS measurements also gave the initial composition of the targets for further comparison after irradiation.

Calibration with bulk samples (mostly Al, Ta, W and Pt) were used to identify the different signals of the RBS spectra and convert the channels into energy. These signals correspond to the scandium layer (high channels/energy peak), the backing (low channels/energy) and its oxidation (depletion around channel 480). The scandium peak is around 1.4 MeV (channel 665), its width depending on the thickness of the deposit. However, the oxidation of the Sc surface slightly shifts the peak toward lower channels/energy because of the slowing of H^+-ions in the oxidised layer. The oxide composition is non-stoichiometric which reflects the contamination of the Sc foil by the oxygen. The large signal at lower channels represents the backing. The front edge is smoothed owing to the oxidation of the backing surface. The oxide composition is also non-stoichiometric.

Table 8: Summary of the RBS measurements achieved at the CENBG AIFIRA facility.

	Thickness of scandium layer ($\mu g.cm^{-2}$)		
Backing	Before irradiation	After 2h at 20 µA	After 1h at 35 µA
Mo	18.7	18.8	X
Ag	17.9	17.9	X
Al	18.1	18.0	X
Ta	17.5	17.7	-
W	18.1	17.7	17.8
Pt	18.4	18.4	18.2

Since the Q-value of oxygen is higher than the proton energy needed for the $^{45}Sc(p,n)$ reaction, the oxygen does not contribute to neutron production. However, it could be responsible for target phenomenon under irradiation like bubbling by oxygen degassing as well as affecting parameters such as ion beam energy loss and straggling in the target.

Despite the visible changes discussed in the previous part, no evidence of thickness variation or scandium layer composition changes (oxidation) was observed within the accuracy of the RBS analysis method (a few percent). As a result, all observed changes are thought to occur in the backing or the oxidation layer between the backing and the scandium.

4.1.1.3 Conclusion on target study

The goal of this study was to select the most suitable backing for scandium targets in order to sustain high proton beam current to compensate for the low cross section of the ^{45}Sc(p,n) reaction.

Targets with backings made of Mo, Al, W, Ag, Pt and Ta were irradiated for several hours at a few tens of µA at the NPL neutron reference facility. Target thickness and composition were analysed with the RBS method at the AIFIRA facility before and after NPL irradiations.

Thermal properties of all materials have been compared (see Table 9). The visible structural changes (bubbles, colour and scorches), as seen in Fig. 41, do not seem to depend directly on the thermal capacity or diffusivity of the backing material. One of the best materials for target backing—tantalum—has, for example, the lowest thermal diffusivity.

Table 9: Comparison of several thermal properties of the material employed as backings, listed by thermal diffusivity. Respectively best and worse values for each property are bold black and red.

Material	Thermal conductivity (W.m^{-1}.K^{-1})	Specific heat capacity (J.kg^{-1}.K^{-1})	Thermal diffusivity (10^{-5}.m^2.s^{-1})
Silver	**429**	232	**17.6**
Aluminium	237	**900**	9.75
Tungsten	174	130	6.95
Molybdenum	138	250	5.37
Platinum	71.6	**130**	2.61
Tantalum	**57.5**	140	**2.47**

This study shows that, compared to the ^{45}Sc(p,n) neutron emission, silver and molybdenum backings seem to be significant sources of neutrons with a 2.9 MeV proton incident ion beam and are therefore unsuitable for this reaction. The thermal and mechanical characteristics of aluminium are inappropriate, as deformation of the backing is observed under high beam currents. However, because of its low elastic neutron cross section in the keV range, it could be a good candidate for measurements at low beam currents.

Of the platinum, tungsten and tantalum backings only tantalum has shown no structural changes under irradiation. Even if the neutron yield was apparently unaffected by these changes, tantalum seems to be the best choice (in addition to its low production cost).

Following this work, the targets with tantalum backing are chosen for further studies on the ^{45}Sc(p,n) reaction within the framework of the IRMM-IRSN-NPL-PTB scientific cooperation.

4.1.1.4 Photon contribution

The first aim of this measurement is to determine the photon contribution to the total dose equivalent. Indeed, many neutron sensitive devices do not discriminate neutron and photons, such as some kind of passive dosimeters.

It should also allow also a better understanding of the reaction process. By identifying the peaks present in the photon energy distribution, nuclear levels of the compound nucleus participating to the reaction can be identified.

Photons emitted along reaction with scandium

When interacting with scandium, some protons overtake the coulomb and nuclear potential barriers to form excited ^{46}Ti* nuclei.

$$^{45}\text{Sc} + \text{p} \rightarrow \quad ^{46}\text{Ti*}$$
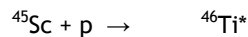
These excited nuclei can decay by various modes, inducing emission of various particles, such as photons or/and neutrons ((p,n) and (p,γ) reactions, see Fig. 45). The results of this study depend on the unknown branching probability of both decay modes.

$$^{46}\text{Ti*} \quad \rightarrow \quad ^{45}\text{Ti} + \text{n}$$
$$^{46}\text{Ti*} \quad \rightarrow \quad ^{46}\text{Ti} + \gamma$$
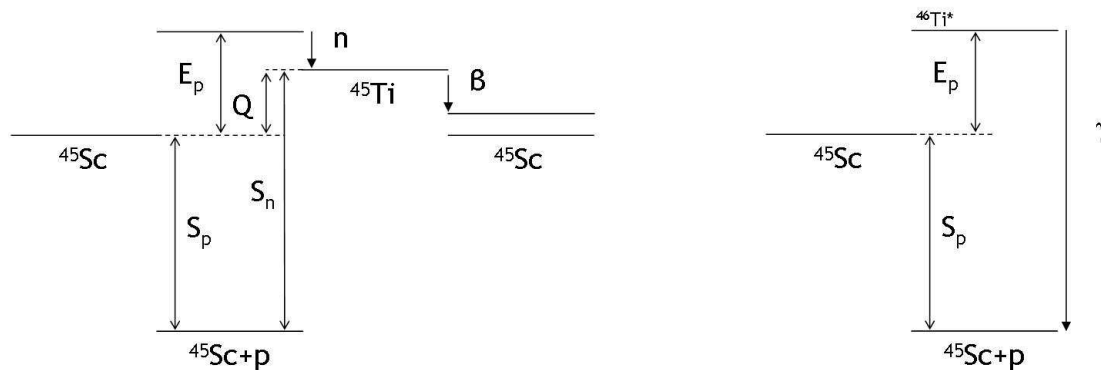
Fig. 45: ^{45}Sc(p,n) and ^{45}Sc(p,γ) reactions, respectively on the left and on the right. ^{46}Ti values of S_n and S_p are respectively 13189.8 8 and 10345.0 7 keV.

If the proton excites the ^{46}Ti* nucleus above the first excitation level of ^{45}Ti, the decay from ^{46}Ti* to ^{45}Ti can happen in two steps ((p,nγ) reaction, see Fig. 46). This is not the case of this study, since the proton energy remains below this threshold energy in our experiment.
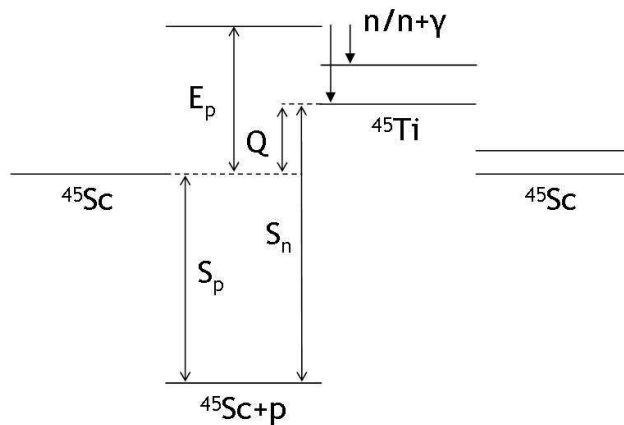
Fig. 46: *$^{45}Sc(p,n\gamma)$ reaction, allowed when ^{46}Ti is excited above the energy of first excitation of ^{45}Ti.*

The formed ^{46}Ti atom is stable, whereas the formed nucleus of ^{45}Ti decays by electron capture and β^+ emission (100 %, $T_{1/2}$=184.8 min 5.0).

$$^{45}Ti \quad \rightarrow \quad ^{45}Sc^* + e^+ + \nu_e$$

Finally the remaining excited scandium rearranges its electron cloud by X-rays or Auger electron emission. This is another source of photon emission.

$$^{45}Sc \quad \rightarrow \quad ^{45}Sc + X$$
$$^{45}Sc \quad \rightarrow \quad ^{45}Sc + e^-$$

Another source of photons can arise in the reactive layer from interactions between produced neutrons and scandium nuclei through (n,γ) reactions.

Reactions list

When hitting the targets, protons can interact with an extensive list of materials in or around the target:
- scandium from the target reactive layer,
- tantalum from the target backing,
- oxygen, since both reactive layer and backing are partially oxidised (see previous part 5.1.1.2),
- iron, and possibly chromium or nickel from the accelerator stainless steel, mainly the target holder.

Depending on reaction thresholds, branching and material setup, all possible interactions described in 1.2.2.7 are more or less likely. The reactive layer is not the only material on the path of the proton beam; interactions within the backing have to be taken into account too. Moreover, since the beam is fully stopped in the backing, their contribution can be paramount if the related (p,γ) cross sections are not negligible. Gamma production can occur as well from (n,γ) reactions in the backing.

In Table 10 are listed the reactions able to produce photons in the neutron field, by order of supposed importance. Since only photon energies above 100 keV are considered, only nuclear reactions are taken into account.

Table 10: List of expected sources of gammas above 100 keV.

Incident nucleus	Reaction type	Nucleus emitting photons	Final nucleus
^{181}Ta	(p,p'γ)	^{181}Ta	^{181}Ta
^{181}Ta	(p,γ)	^{182}W	^{182}W (stable)
^{181}Ta	(p,nγ)	^{182}W* or ^{181}W*	^{181}W
^{181}Ta	(n,n'γ)	^{182}Ta* or ^{181}Ta*	^{181}Ta
^{45}Sc	(p,p'γ)	^{45}Sc*	^{45}Sc
^{45}Sc	(p,γ)	^{46}Ti*	^{46}Ti
^{16}O	(p,γ)	^{17}F*	^{17}F
^{16}O	(p,nγ)	^{17}F* or ^{16}F*	^{16}F

Experimental setup

Measurements were conducted at the IRSN AMANDE facility. For this experiment both neutron detector and gamma spectrometer were used. The IRSN PLC was employed for setting the proton energy on the selected resonances. A measurement of the neutron fluence rate was performed before gammas as a reference, the detector set at 70 cm and 0°. The gamma spectrometry was performed using a BGO spectrometer set at 50 cm in the ion beam direction as illustrated on Fig. 47. The spectrometer was calibrated using four gamma sources having well-defined and usable peaks.
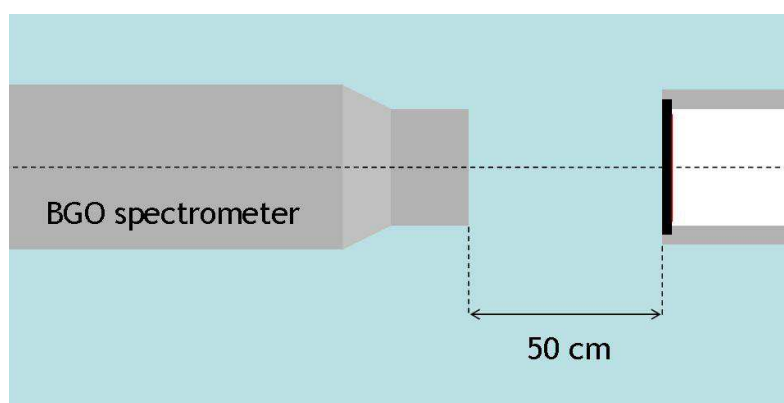
Fig. 47: *Experimental setup using the BGO spectrometer.*

Measurements and results

The measurements have been performed for the two main known resonances of ^{45}Sc(p,n) reaction, i.e. at 8 and 27 keV neutron energies. Three kinds of measurements have been performed:

- background measurements,
- gamma spectrometry with 5- and 20-µg.cm^{-2}-thick scandium targets,
- gamma spectrometry with a backing alone.

In this way, the backing contribution can be identified and eventually subtracted from measurements with scandium targets, before unfolding. Thus the final spectra would represent photon contribution of scandium layer alone or full scandium target. The used unfolding method was developed by Robitaille (Ro77-2).

Whatever neutron energy is considered, it appeared that backing and scandium measurements possessed the same main peaks, as illustrated on Fig. 48 with measurements at the 27 keV-resonance energy.

In the low energy range, i.e. below 3 MeV, photon contribution seems mainly due to interactions in the tantalum backing. Intensities are indeed equivalent on all normalised spectra including backing ones, and thus this background is easily subtracted.
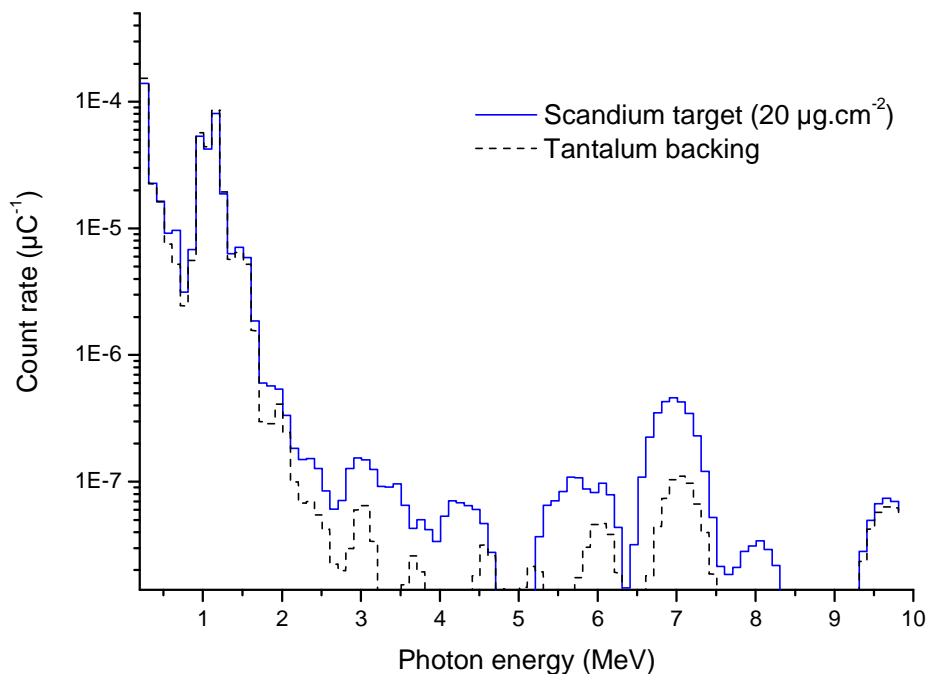
Fig. 48: *Photon spectra of tantalum backing alone and target with scandium layer, normalised to 1 µC, ion beam energy set on 27 keV- resonance.*

However, this cannot be the case of peaks around 6 and 7 MeV, since their intensities change from one target/backing to another (see Fig. 49). They have been identified as (p,γ) reaction on fluorine: targets were contaminated with unpredictable quantities of residuals from lithium fluoride targets. Backings seem less contaminated, which can be explained by a probable contamination during irradiation in the accelerator tube.
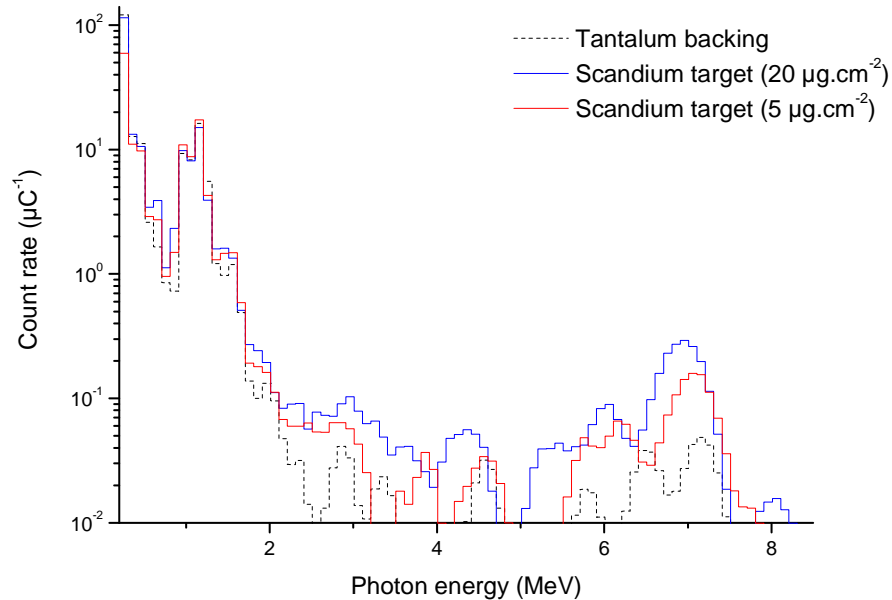
Fig. 49: *Photon spectra of tantalum backing alone and target with scandium layer*

(5 and 20 µg.cm^{-2}), normalised to 1 µC, ion beam energy set on 8 keV-resonance.

Due to this contamination issue, it was difficult to identify other peaks present in the spectra. Following hypothesis of fluorine contamination composing the main part of peaks at 6 and 7 MeV, these were suppressed to calculate the photon dose equivalents (see Fig. 50). Those were calculated each time for two different configurations, with or without subtracting background. In case tantalum is used as a standard backing for scandium layers, its contribution is as important as the scandium one. All results are given in Table 11.
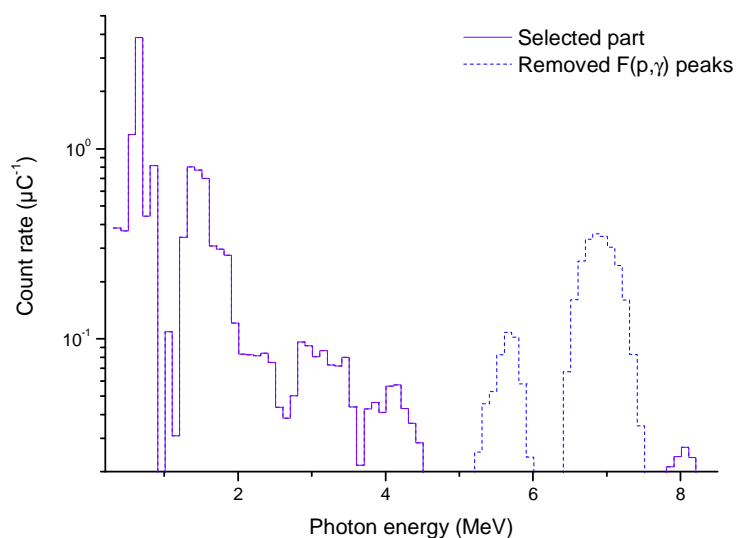
Fig. 50: *Photon spectrum of target with 20 µg.cm^{-2}-thick scandium layer when ion beam energy set on 27 keV-*

^{45}Sc(p,n) resonance. Spectrum is normalised to 1 µC and backing contribution was subtracted.*

Table 11: Compared photon and neutron dose equivalents per µC at 50 cm, and respective contribution to the total dose in percent. Fluence to dose conversion factors are given in (ICRP74).

Resonance			8 keV		27 keV
Target thickness			5 µg.cm^{-2}	20 µg.cm^{-2}	20 µg.cm^{-2}
Photon dose equivalent (Sv.µC^{-1})	Without correction on contamination	With Ta	4.06 x 10^{-11}	4.80 x 10^{-11}	1.54 x 10^{-10}
		Without Ta	4.89 x 10^{-12}	9.55 x 10^{-12}	1.24 x 10^{-11}
	Fluorine contribution subtracted	With Ta	3.79 x 10^{-11}	4.35 x 10^{-11}	1.47 x 10^{-10}
		Without Ta	3.80 x 10^{-12}	5.81 x 10^{-12}	6.96 x 10^{-12}
		% of the total dose	-	0.68 %	0.47 %
Neutron dose equivalent		Fluence at 50 cm (cm^{-2})	-	169.56	146.16
		Dose equivalent (Sv.µC^{-1})	-	8.48 x 10^{-10}	1.46 x 10^{-9}
		% of the total dose	-	99.32 %	99.53 %

Conclusion

Despite contamination issues, photon contribution to the total dose equivalent when using ^{45}Sc(p,n) reaction was proved negligible. Main contribution arises from interaction in tantalum backing. Even in such small quantities, the produced low energy gammas must be considered when irradiating gamma sensitive devices.

Interest of new measurements without lithium fluoride contamination could be justified by a study of the nuclear structure and interactions of ^{45}Sc(p,n) reaction.

4.1.1.5 Conclusion on proof of principle discussion

Ability of scandium targets to withstand beam current of the order of a few tens of µA largely depends on the experimental setup: beam size and scanning system, cooling system… However the presented studies showed that scandium targets were able to withstand easily 20 to 30 µA.

Target study has also shown that some materials such as molybdenum or silver are inappropriate as backing. They indeed induce a neutron background non-negligible in this energy range, especially when used with ^{45}Sc(p,n) reaction. Even if further studies (bibliographical and/or experimental) are needed to fully understand the origin of the bubbling phenomenon, this work allowed selection of an appropriate backing material, i.e. tantalum.

Some lithium and fluorine contamination prevented real estimation of the photon dose equivalent induced by use of ^{45}Sc(p,n) reaction. However, obtained values are still acceptable for calibrating both neutron and gamma sensitive devices using this reaction neutron field.

^{45}Sc(p,n) reaction appears therefore suitable for scientific purpose such as calibration of neutron devices. This leads to full characterisation for allowing real use of it.

4.1.2 IDENTIFICATION OF THE RESONANCES

The ^{45}Sc(p,n) cross section has a resonant structure in our range of interest. This structure has been already qualitatively determined by experiments as presented in part 2.2.2. The aim of these new measurements is gathering the maximum amount of information on these resonances in order to allow simulation of the resonance widths in a specific setup, and determine the resonance parameters.

4.1.2.1 Characterisation of the neutron spectrum

Choice of the time-of-flight method

There are several methods allowing experimental determination of a neutron spectrum. It can be achieved by performing measurements using detectors such as recoil proton telescope or a set of Bonner spheres. In the case of this study, neutrons are generated by an accelerator: the field has an identified emission source and is easily tuneable. If the accelerator present pulsing capabilities, it is possible to employ the time-of-flight method (TOF, see 3.2.1.4), whose precision is mainly limited by distance between particle emission and detection, and related needed irradiation time.

By using a thick target and well-chosen beam energy, it is possible to observe neutrons produced in a wide proton energy range. Being slowed in the target, protons interact at various energies, from initial energy to possibly reaction threshold if target is thick enough. It is thus well suited for observing cross section structure, resonances and associated neutron energies.

Measurements were performed at the PTB facility.

Experimental setup

As presented in part 3.2.1.2 on measurement methods, time-of-flight requires the use of an accelerator in pulsed mode. This mode is obtained on the PTB Van de Graaff using a chopper-buncher system, i.e. with a pick-up ring (Mo04). The pulsed beam is a compromise between beam current and beam quality: increasing beam current deteriorates beam energy spread and time structure. Time distribution has to be composed of a unique and symmetrical peak, ideally with a Gaussian shape. Thus it allows as many protons as possible to reach simultaneously the target.

Ideal accelerator setup was determined using successively accelerator's monitoring tools and TOF detection system by monitoring the time structure of the gamma peak. Since all gamma particles travels at the same speed, their time distribution directly reflects the beam's one. A defective pulsation of the beam induces visible widening as well as the creation of a front or end tail in the gamma time distribution.

Proton energy was set at 2950 keV for covering the whole monoenergetic range between reaction threshold and first excitation level of ^{45}Ti at 37 keV (see 2.2.2). The beam was pulsed at 1.25 MHz. The pulse width for this measurement was around 2 ns for a beam current around 1 µA (accurately monitored).

Experiments were conducted using a Lithium glass detector. This detector is described in the part 3.1.2.1. Its front side was set at 70 cm from the target (i.e. 71.47 cm from target to detector effective centre), in the ion beam direction (0°). A plastic detector was set at 90° around 200 cm from the target for monitoring the shape of the gamma peak (see Fig. 51). Scandium target consists of an (601±5)-µg.cm^{-2} thick deposit on a tantalum backing; it was produced at CEA Ile-de-France and characterised at ARCANE, alike other targets used in this study.
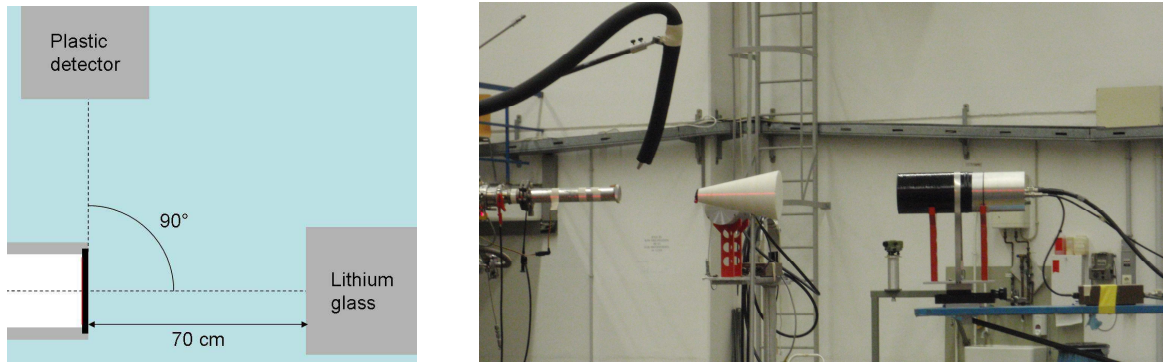
Fig. 51: *Experimental setup: on the left-side outline of the setup, on the right-side picture of the experimental setup with shadow cone (end of the beamline and target on the left, detector on the right).*

Data acquisition system

Data acquisition system is mainly based on the time-to-amplitude converter (TAC). In principle, it computes the time difference between emission (start) and detection of the particle (stop). The start signal is given by the pick-up ring of the accelerator. A constant-fraction discriminator (CFD) directly treats the signal from the detector corresponding to the detection of a particle, being used as a stop. The TAC output is linked to an analogue-to-digital converter (ADC) for data acquisition on a multichannel analyser system and its software (here FAST MPA-3).

In practice, start and stop are inverted for avoiding the TAC to process uselessly during the time of flight, when there is no associated event. The pick-up ring signal is therefore delayed and used as the real stop.

Moreover, pulse height of the detector signal is obtained simultaneously. It can be represented along with neutron TOF on a two-dimensional spectrum using MPA-3 software for imposing new cuts and better selection of the neutron signal (see Fig. 53). This issue is discussed later in this part.

Time calibration

Logically, once the experiment is set up, precision of the measurement mainly depends on two time parameters: achieved time resolution (creation and detection) and time calibration. The data acquisition system was calibrated using two equivalent electronic systems for comparison purpose:

- o a well-suited time calibrator, generating simultaneously pulses separated by a chosen time interval
- o a pulse generator associated to a delay: pulses with various delays, selected manually.
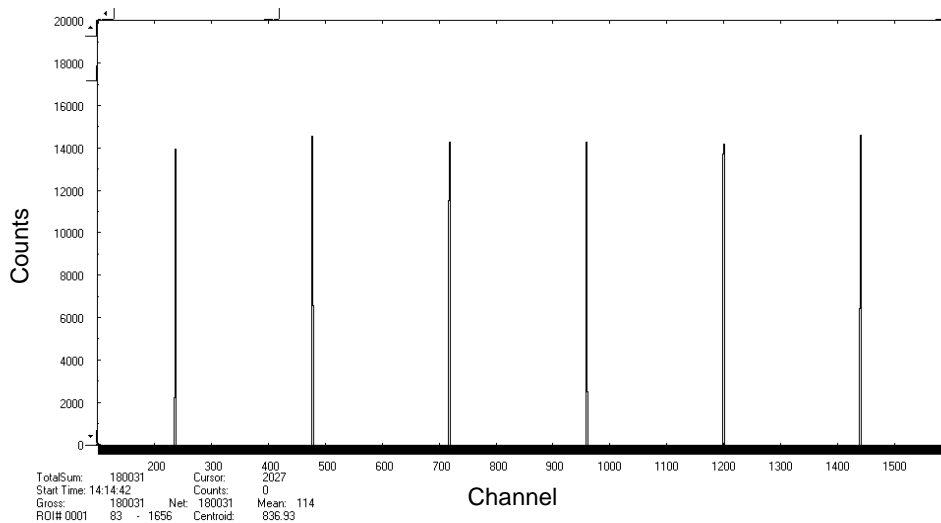
Fig. 52: *TOF spectrum for time calibration using the pulse generator and the delay (here for 700-ns time interval), as represented in MPA-3.*

The signal is treated by the TAC, resulting in a TOF spectrum (see Fig. 52). Knowing the introduced time interval or chosen delays, it gives conversion coefficient from time to TOF channel, i.e. calibration of the TAC. The calibration coefficients for Lithium glass and plastic detectors are given in Table 12. Uncertainty on calibration coefficient of plastic detector was not evaluated.

Table 12: Results of time calibration of employed detectors.

Detector	Calibration coefficient (ns.channel^{-1})
Lithium glass	415.30 ± 0.03
Plastic detector	844.26

Thresholds and study of gamma centroids

As introduced in the previous part on data acquisition, the two-dimensional spectrum representing count rate versus TOF and pulse height (see Fig. 53) can be used for applying new thresholds on the signal. New cuts on pulse height allow better selection of the neutron events:

- o cut on the low range for excluding non-neutron event and tail of the gamma peak
- o cut on the high range for excluding noise and scattered neutrons.
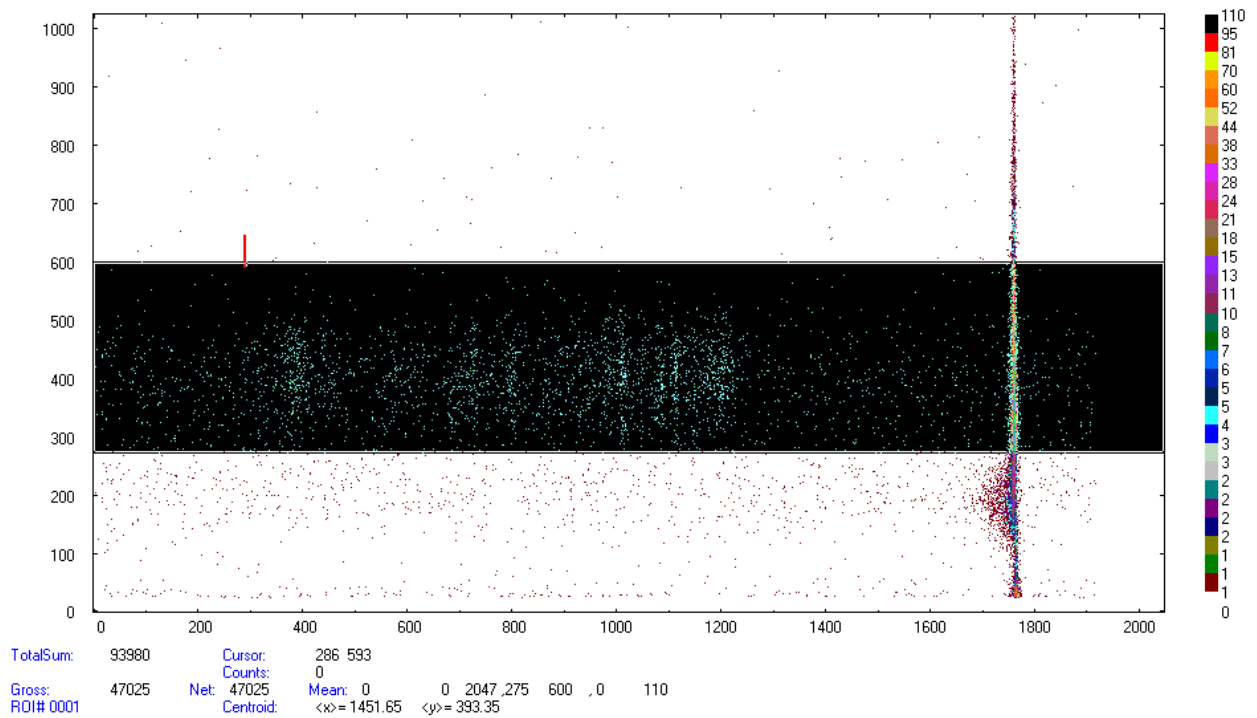
Fig. 53: *Two-dimensional spectrum representing count rate (colours) versus neutron TOF (x-axis) and pulse height (y-axis). The black tint part corresponds to the applied cuts in pulse height.*

However, centroid of the gamma peak may depend on the chosen cut. Since it is the reference for calculating the neutron time of flight, i.e. energy, a study of the influence of the different cuts on gamma centroid and width has been carried out (see Fig. 54). For each upper and lower cut, one tight and one large Gaussian fit have been realised using PTB software WinSpekt (WI06). The influence on gamma centroid position is of 1 channel maximum, i.e. 0.41 ns.
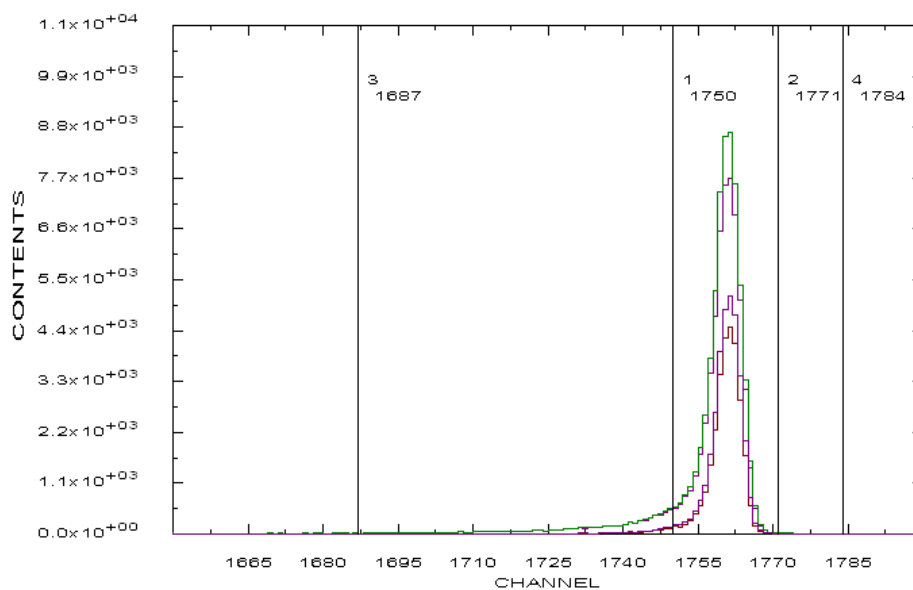
Fig. 54: *Gamma peaks of TOF spectra, corresponding to the same irradiation but with different cuts in pulse height. Vertical bars correspond to boundaries of the two Gaussian fits (as presented in WinSpekt).*

Measurements and results

Irradiations have been carried out in five parts for verifying stability of the pulse width every few hours. Shadow cone measurements have been performed as well for subtracting scattered neutrons. Final cuts have been applied in the same way at each spectrum using MPA-3 software.
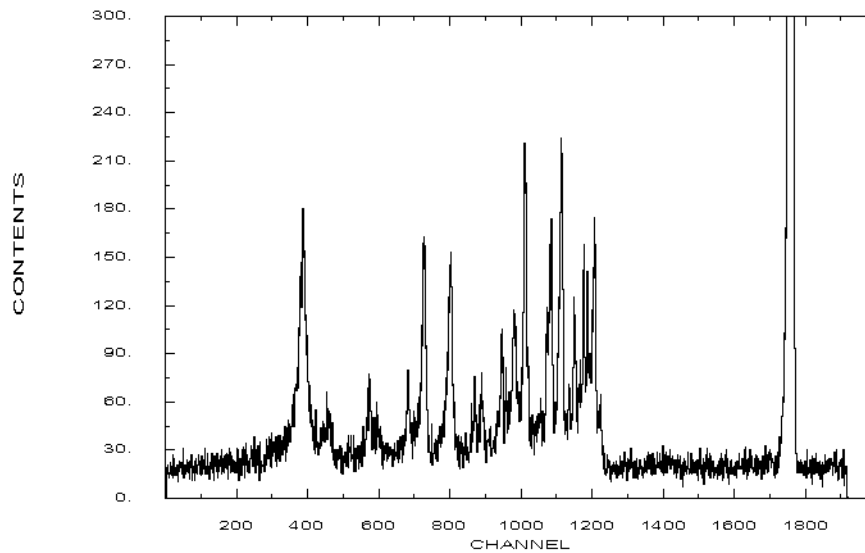
Fig. 55: *Sum of all TOF spectra normalised to 1 µC (WinSpekt data treatment).Since start and stop were switched, gamma peak is on the right-side of the picture, and slowest neutrons on the left side.*

Spectra have been summed and then normalised to 1 µC. Background has been subtracted before unfolding data from the detector efficiency. The whole data treatment and time-to-energy conversion have been realised using the PTB software WinSpekt. It results in a time-of-flight spectrum which has been converted for obtaining the final neutron spectrum presented in

Fig. 56.

As explained in the previous part, gamma peak was adjusted using a Gaussian distribution. This shape is due to the time resolution of the beam, and each resonance is folded with it. Neutron spectrum has been fitted using this Gaussian distribution for finding resonances. Identified resonances are reported on

Fig. 56, and fits results on resonance position are compared with Cosack *et al.* results (Co85) in Table 13. Results are in good agreement; differences can be explained by the uncertainties and the identification method.

Table 13: List of identified resonances during this experiment and by Cosack *et al.*

Resonance #	1	2	3	4	5	6	7	8	9	10	11
This experiment	8.12 ±0.01	9.01 ±0.07	10.85 ±0.05	11.36 ±0.09	13.22 ±0.04	14.32 ±0.02	16.61 ±0.03	19.32 ±0.05	20.08 ±0.06	23.02 ±0.04	25.11 ±0.05
Cosack et al.	8.15	9.1	10.9	-	13.2	14.4	16.7	19.4	20.2	23.3	25.2

Resonance #	12	13	14	15	16	17	18	19	20	21	22
This experiment	27.24 ±0.05	32.39 ±0.08	33.33 ±0.07	35.69 ±0.23	36.45 ±0.10	40.7 ±0.14	41.37 ±0.38	44.6 ±0.10	46.16 ±0.10	48.57 ±0.29	49.61 ±0.25
Cosack et al.	27.4	-	33.4	36.7	-	-	-	-	-	-	-
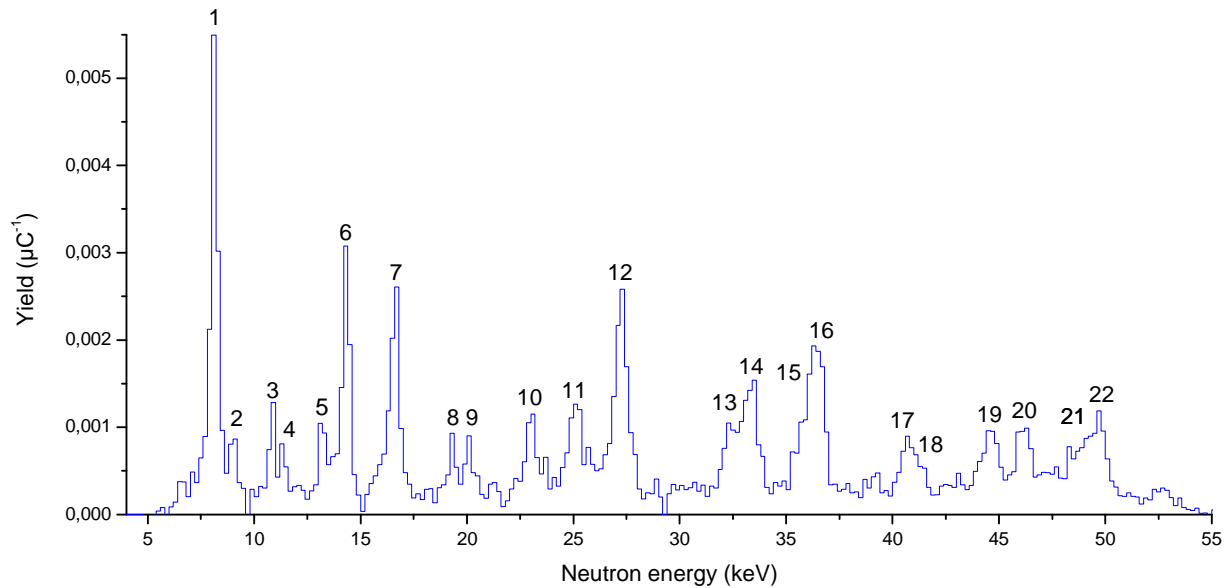
Fig. 56: ^{45}Sc(p,n) neutron spectrum on its whole monoenergetic range.

Source of uncertainties

Treatment method of uncertainties associated with TOF measurements have been fully described by Cognet and Gressier (Co10). The uncertainty budget has not been fully carried out for this experiment due to a lack of time and accuracy on a few minor issues.

Main contributions to the total uncertainty come from time calibration and uncertainty on gamma centroids. The combined influence of both uncertainties is around 0.24 ns, i.e. ±0.01 keV at 8 keV. Uncertainty on the distance crossed by the particles is around 1 mm, i.e. around 10^{-4} compared to the total distance, which is negligible. Uncertainty on beam charge may be taken for null, as well as detector dead time considering the very low neutron fluence rate. The main remaining uncertainty consists in the detector efficiency, which was not estimated here.

Uncertainty on the resonances position (reported in Table 13) is larger as it includes also the uncertainty on the fit results for identifying them.

Conclusion

Performed time-of-flight measurements are in agreement with the previous measurements of Cosack *et al.* for the cross-checking range (Co85): measured resonances are found at the same neutron energy. New resonances are observed, especially at higher energies, still in the monoenergetic range. These latter ones at higher energies do not seem of real interest for competing with ^{7}Li(p,n) reaction in neutron production, their yield being far too low. The already known and supplementary resonances are full of interest for determining resonance parameters and reaction characteristics by simulation. The results need to be refined with the determination of the excitation function, at least for verifying no neutrons from ^{45}Sc(p,n)^{45}Ti* were produced. Such measurement is the object of the next part.

4.1.2.2 Characterisation of cross section resonances: excitation function

The aim of this experiment is to gather as much information as possible on the position (i.e. corresponding proton energy), energy width and relative yield of resonances present in the ^{45}Sc(p,n) cross section. This for several reasons:

- o Select resonances of interest for further characterisation
- o Gather information for calculating the resonances parameters of the reaction.
- o Acquire knowledge for cross section determination: cross section of which resonance(s) is measured.

The employed method for this measurement is briefly described in 3.2.1.3, along other fluence measurements. In order to obtain the best separation between resonances, the experimental setup has been designed for limiting as much as possible the contributions degrading the total energy resolution: beam energy spread and target thickness. Both have been characterised, respectively by study of the aluminium (p,γ) resonances and RBS spectrometry.

Experimental setup

The experiment has been performed at the AIFIRA physics beamline to benefit from the very narrow beam energy spread, expected to a maximum of a few hundred eV. A positive 20-kV high-voltage (Sefelec GKHT920P700) was installed at the end of the beamline for tuning the proton energy without changing the accelerator setup. It is tuned and controlled from the control room *via* a source meter. A small magnet was set closed to the target for repelling possible secondary electrons induced by the reaction in the target.
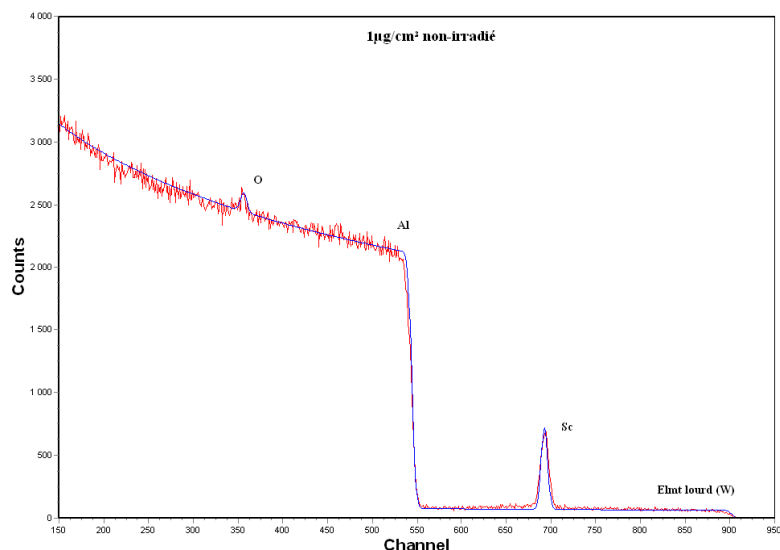
Fig. 57: *RBS spectrum of the thinner scandium target. On the left side, the main edge corresponds to the thick layer of the aluminium backing; on the right side, the well-separated scandium peak. One can observe on the left the small peak corresponding to the presence of oxygen.*

Targets with two different thicknesses of scandium layer were employed for this measurement. They were produced at CEA Ile-de-France on a 0.5-mm thick aluminium backing. The thicker target was 20-µg.cm^{-2} scandium thick. This very common target was employed for notably facilitating the overlapping between the different series. This issue is discussed in the next parts. The thinner targets were made as close as possible to 1 µg.cm^{-2}- thick with the employed evaporation technique, i.e. finally 2.5-µg.cm^{-2} or 180-eV-thick.

As explained in part on RBS measurements, aluminium was chosen for easing the thickness characterisation of the used targets: the scandium peak is well separated from aluminium edge in RBS spectrum (see Fig. 57). Their characterisation was performed by ARCANE, the unit for technologic transfer of CENBG. Results of RBS measurements are presented in Table 14.

Table 14: Summary of targets' thickness measurements performed by ARCANE unit, using RBS technique. Measurements were performed on both irradiated and non-used thinner targets for comparison purpose.

Sample	Scandium thickness (±3; 1e15 at.cm^{-2})	Corresponding scandium thickness (µg.cm^{-2})
Thin target (non-exposed)	32	2.5
Thin target (exposed)	33	2.5
Thick target (exposed)	263	20

Choice of the neutron detector was made according to the use of a target with a very thin scandium layer: it required the use of a detector with a maximum neutron sensibility for compensating for the very low neutron fluence rate.

A 4.9" Bonner sphere of IRSN HERMEIS spectrometer was thus employed (see 3.1.2). The sphere diameter was selected in order to have a maximum and relatively flat response in the energy range of produced neutrons (see Fig. 58). The detector was set closed to the target: at 13.8 cm to detector front, i.e. 20 cm to sphere centre, in the ion beam direction (0°).
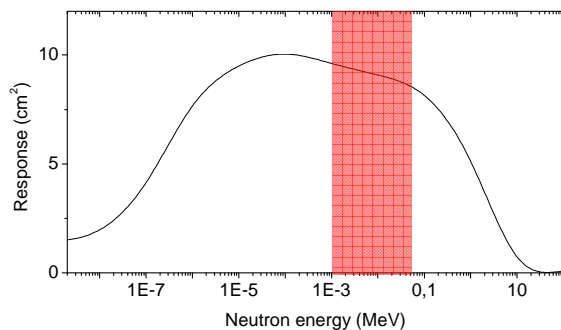
Fig. 58: *On the left-side, response function of the 4.9" IRSN Bonner sphere (Se09); in red, energy range of the neutrons to be detected in this experiment. On the right-side, experimental setup for fluence measurements: Bonner sphere mounted on its base (left), end of the beam line with target, magnet and cable for current measurement (right), and target-cooling system (green).*

Gamma measurements for beam energy spread characterisation have been carried out using the same BGO scintillator (see part 3.1.2.2) than for determining the gamma contribution of ^{45}Sc(p,n) reaction. It was set at 0°, at a few cm from the target. Count rate was low enough for avoiding dead-time and pile-up (see Fig. 59).

Fig. 59: *Experimental setup for gamma measurements: on the left, end of the BGO spectrometer; on the right end of the beam line and target; in green, tube for air-cooling.*

Target-cooling was achieved using a cooled air-jet. Contrary to other experiment setups detailed in this work, no wobbling or scanning system was available for avoiding heating of the target. In order to reduce the risk of excessive target heating and scandium melting and/or evaporation, beam size on target was broaden as much as possible without hitting beyond the scandium deposit and beam current was limited to 5 µA. It was also verified that no excessive heating occurs at various considered beam currents using a temperature probe (see Table 15).

Table 15: Observed target temperature depending on deposited beam current.

Beam current on target (µA)	Target temperature (°C)
1.5	19°
4	20°
5	25°

The adding of a high-voltage at the end of the beam line prevented any monitoring of beam current on target during experiment. However, it was measured regularly prior to each neutron measurement for verification purpose. Considering the *a priori* very good current stability of AIFIRA accelerator, beam current on target was assumed approximately constant during experiment.

Determination of the ⁴⁵Sc(p,n) excitation function

Use of the 20-kV high voltage at the end of the beam line allowed us to limit the number of accelerator setups (see methodology of such measurements in 3.2.1.3). Basically, only three beam energy setups were necessary for covering the whole monoenergetic range of the ^{45}Sc(p,n) reaction: 2925, 2937 and 2952 keV. These energies were chosen for allowing a sufficient range of overlapping at the junction between measurements. Proton energy steps between each points of excitation function were adjusted depending on the importance of structure variation, from 40 to 200 eV.

For each energy setup of the accelerator, two runs were performed successively: one per target, beginning with the thicker one. Indeed, during experiments, runs with the 20-µg.cm^{-2} thick target were used as reference due to their higher fluence rate: it was used for verifying quickly the energy setup and general shape of the excitation function. During analysis, measurements with this target were employed for joining the different parts of the excitation function of measurement with the thin target (see Fig. 60). Excitation functions obtained by Cosack et al. (Co85) are reported on the figure: results are in excellent agreement with previous yield measurements.
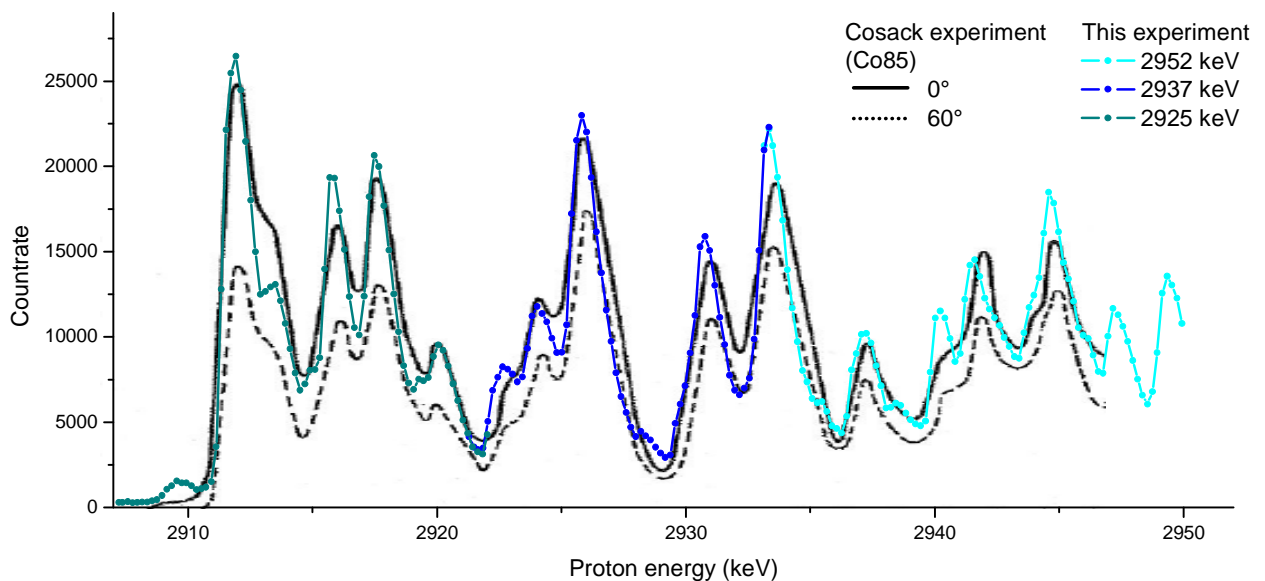
Fig. 60: *In blue, excitation function of ^{45}Sc(p,n) reaction determined using the 20-µg.cm^{-2} thick target. Each colour corresponds to an accelerator setup. In black, ^{45}Sc(p,n) reaction excitation functions obtained by Cosack et al. (Co85).*

No shadow cone measurements were performed for subtracting neutron scattering contribution due to too short distance between target and detector (see 3.2.1.1). However neutron background was subtracted using measurements with blank target, i.e. backing alone. They were carried out after each accelerator setup without the supplementary target voltage, along beam current verifications. In this way neutron contributions arising from unwanted reactions were limited, even at the upper proton energies.

Some variation in the beam current was observed during measurement with the thin target at upper proton energy (2952-keV accelerator setup). A 15% linear decrease was assumed during the acquisition of the first measured points, and data corrected according to this hypothesis. It induces a count rate change and thus supplementary uncertainty on those points.
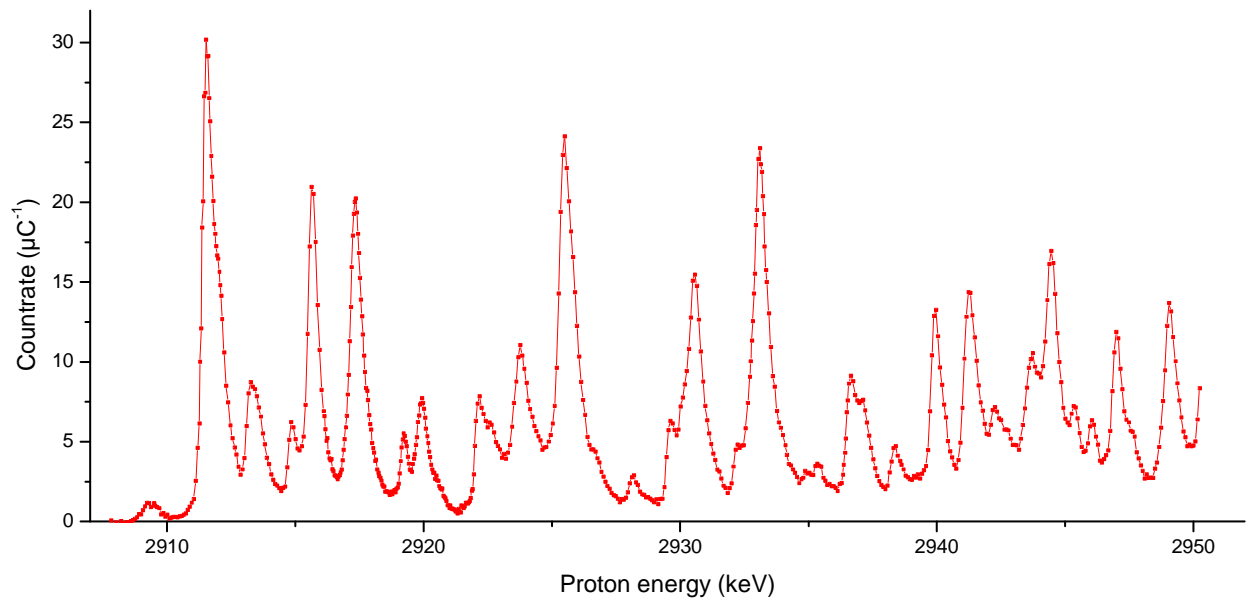
Fig. 61: *Excitation function of ^{45}Sc(p,n) reaction over its full monoenergetic range using AIFIRA facility (203 ± 20 eV energy spread) and an as thin as possible scandium target (2.5 µg.cm^{-2}). Data are not unfolded from beam energy spread and target thickness contributions to the total resonances width.*

Count rate have been normalised to 1 µC, i.e. irradiation time and beam current (see Fig. 61). Then runs corresponding to each accelerator setup were fitted together using the overlapping ranges between them. On Fig. 62 are compared results with 20- and 2.5- µg.cm^{-2} thick targets.
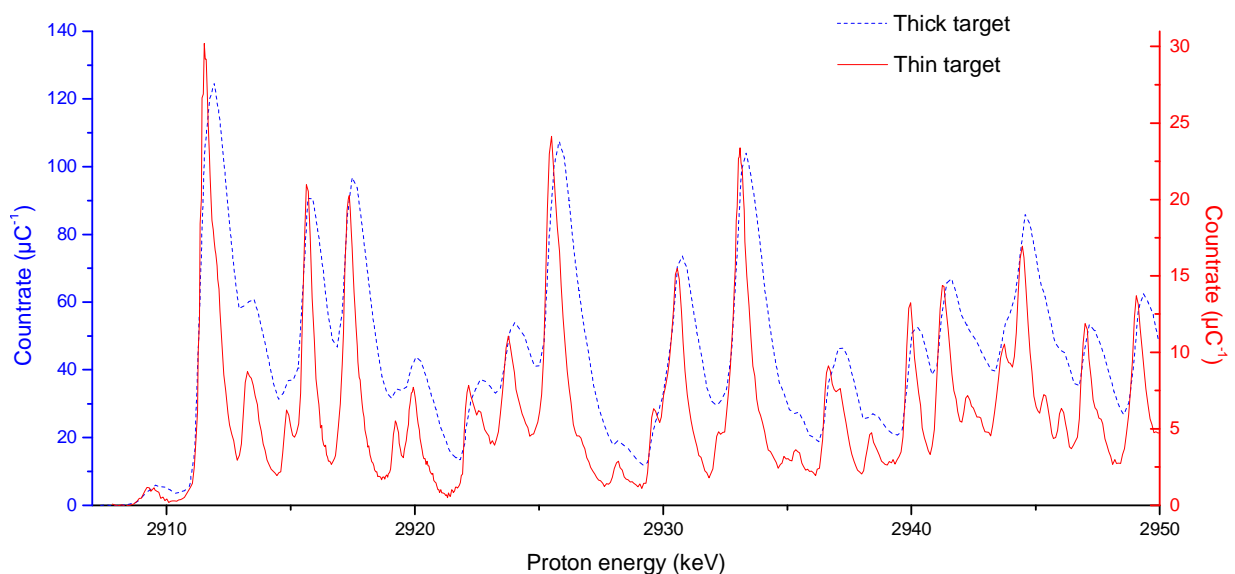
Fig. 62: *Excitation functions of ^{45}Sc(p,n) reaction with thick (20 µg.cm^{-2}) and thin (2.5 µg.cm^{-2}) targets.*

Determination of beam energy spread

Bream energy spread has been determined at three proton energies by using several aluminium (p,γ) resonances according to the methodology described in (Br94). Shape of the 1316.87-keV resonance threshold is represented in Fig. 63, as well as a summary of the obtained values in Table 16.
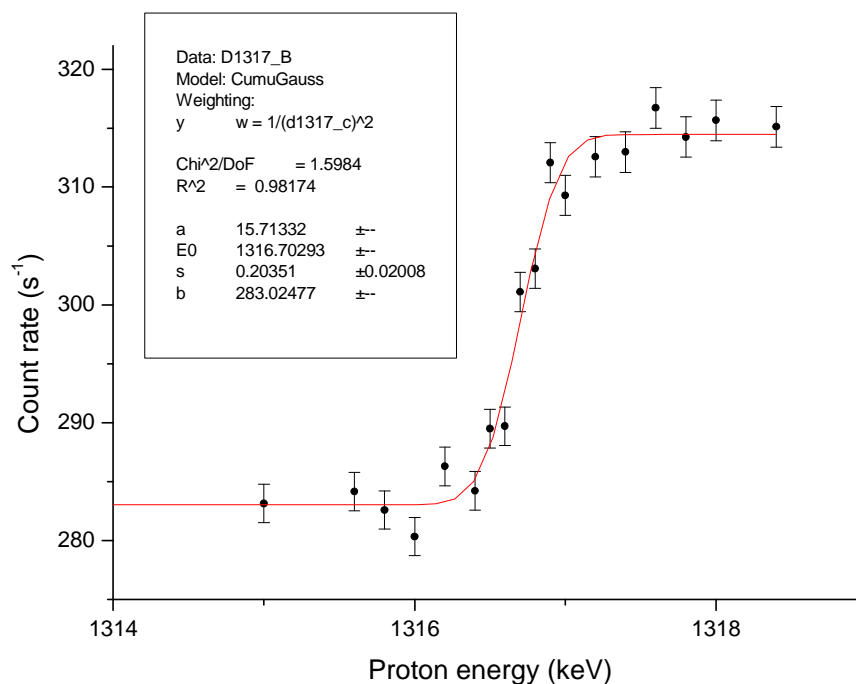
Fig. 63: _1316.87-keV gamma resonance of Al(p,γ) reaction. Data were fitted using a cumulative Gaussian function._

Uncertainty on gamma detection using the BGO scintillator is considered negligible compared to the effect of statistics. The associated uncertainty is given by the fit results. The order of magnitude is retained for identifying the resonances by fitting the excitation function.

Table 16: Measurements of AIFIRA beam energy spread using Al(p,γ) resonances.

Al(p,γ) resonance (keV)	Energy spread (eV)
632.23	478 ± 24
986.9	520 ± 40
1316.87	406 ± 40

Analysis

Following the compound nucleus hypothesis, resonances of ^{45}Sc(p,n) reaction cross section were assumed to be much thinner than Gaussian shaped function resulting from folding of thickness and beam energy spread. In order to extract both number and accurate position of the resonances, the normalised excitation function represented on Fig. 61 was thus fitted by multiple Gaussian functions of about 500-eV wide, part by part. On Fig. 64 is represented the fit result on a limited range, as successively performed on the whole proton energy range of the excitation function.
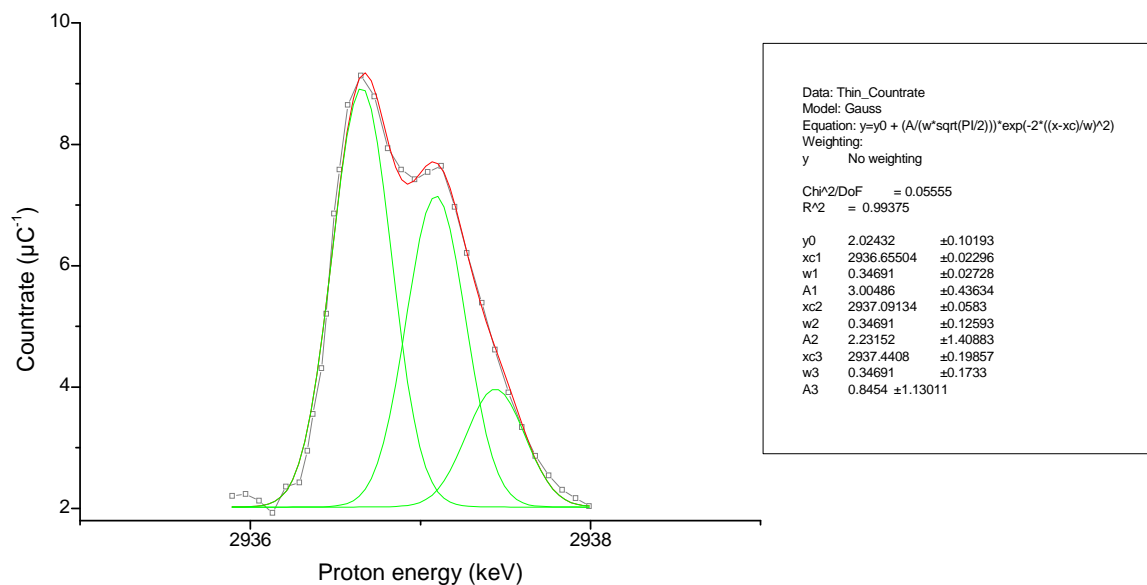
Fig. 64: *Multi-peak fit result using Gaussian shape functions on a selected part of the ^{45}Sc(p,n) reaction excitation function with 1 µg.cm^{-2} thick target. Constraints were imposed on the widths of the Gaussian distribution: same energy widths of about 500 eV for all resonances.*

Only obvious resonances from fit results were selected, other being dismissed. It resulted in a list of resonances. Resonances energy positions were first corrected from the influence of target thickness. Indeed, because of beam energy spread and thickness folding, maximum neutron fluence from a resonance is obtained at a proton energy increased by the half of the target thickness. Resonances positions were thus reduced by 90 eV.

Obtained resonance positions using excitation function measurements depend on the accelerator energy accuracy. In the case of the performed experiment, energy position was measured with more accuracy during time-of-flight measurements. Thus resonance positions obtained from excitation function were converted from proton to neutron energy using reaction kinematics formula (see Equation 4). Each part of the excitation function was adjusted to the time-of-flight results by comparing resonance positions.

Finally the excitation function was corrected from detector efficiency: it required having first corrected data from any energy shift. Data were normalised using the detector efficiency interpolated between 1 and 50 keV (Fig. 65).
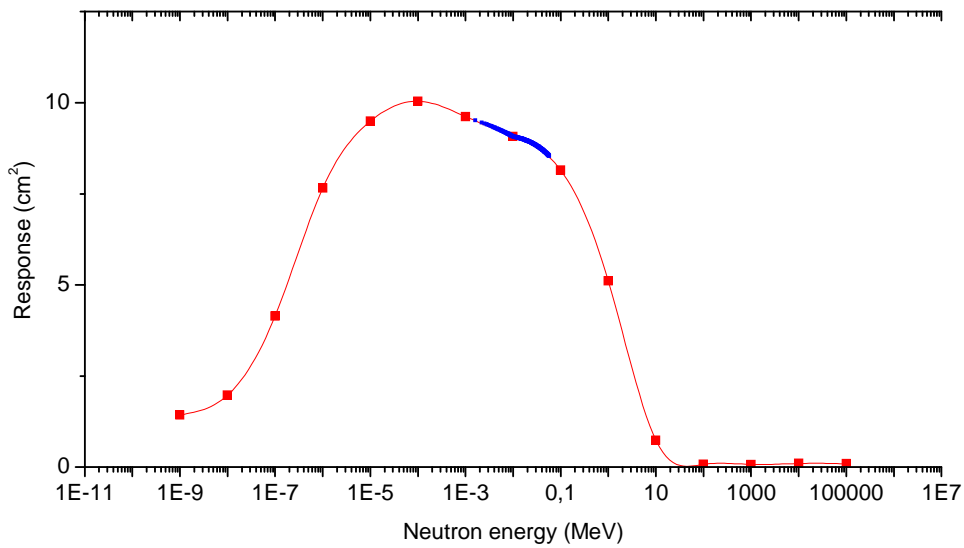
Fig. 65: *In blue, logarithmic interpolation of detector efficiency between 1 and 50 keV (neutron energy).*

The final excitation function of $^{45}Sc(p,n)$ reaction is presented on Fig. 66. The 38 identified resonances are reported on the figure, and are listed in Table 17, as well as the position of the Gaussian fits centroids, and corrected proton and neutron energies of the resonances. Those latter ones are compared with ToF results: for resonances identified in both experiments, some energy differences remain. It is obviously due to measurement uncertainties, but also on errors induced by fitting difficulties.
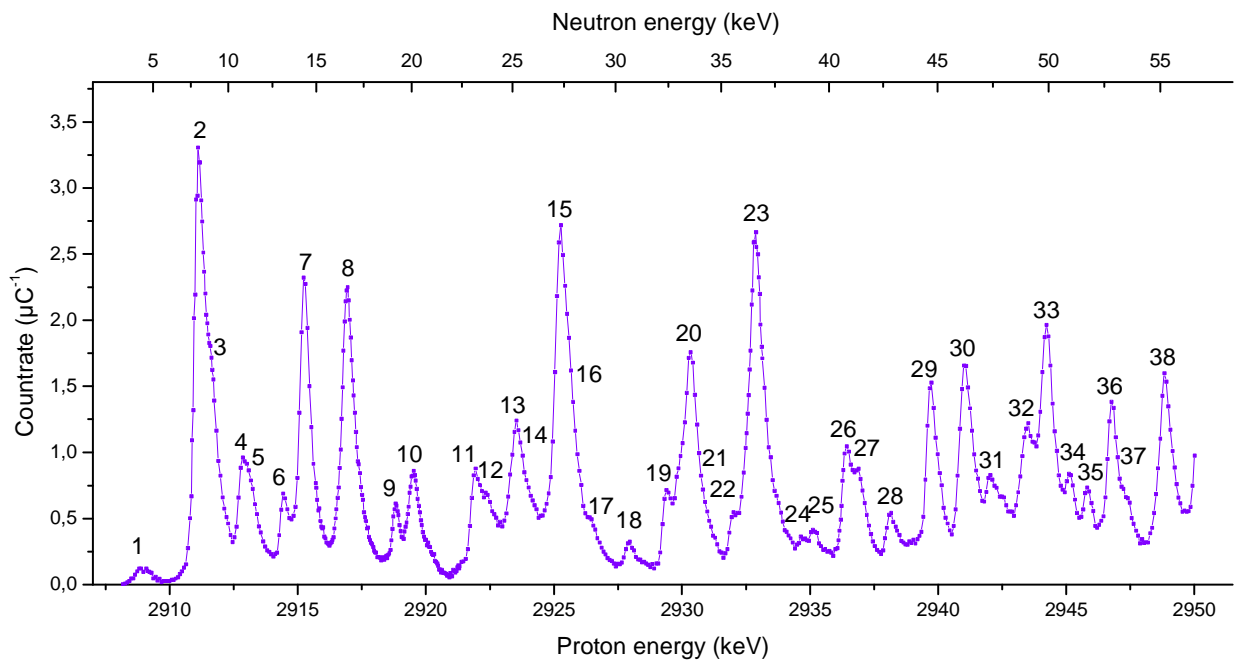
Fig. 66: *Excitation function of $^{45}Sc(p,n)$ reaction, normalised and energy adjusted.*

Table 17: List of the 38 identified resonances in the ⁴⁵Sc(p,n) excitation function.

Resonance number	Excitation function (energies in keV, yield in µC⁻¹)			Time-of-flight results (keV)	
	Gaussian centroid	Proton energy	Neutron energy	This study	Cosack et al.
1	2908.98	2908.89	4.06 *		
2	2911.16	2911.07	8.12	8.12 ± 0.01	8.15
3	2911.70	2911.61	8.99	9.01 ± 0.07	9.1
4	2912.87	2912.78	10.79	10.85 ± 0.05	10.9
5	2913.24	2913.15	11.34	11.36 ± 0.09	
6	2914.51	2914.42	13.17	13.22 ± 0.04	13.2
7	2915.28	2915.19	14.26	14.32 ± 0.02	14.4
8	2916.97	2916.88	16.58	16.61 ± 0.03	16.7
9	2918.85	2918.76	19.08	19.32 ± 0.05	19.4
10	2919.52	2919.43	19.96	20.08 ± 0.06	20.2
11	2921.98	2921.89	23.12	23.02 ± 0.04	23.3
12	2922.52	2922.43	23.81		
13	2923.53	2923.44	25.08	25.11 ± 0.05	25.2
14	2924.19	2924.10	25.91		
15	2925.26	2925.17	27.24	27.24 ± 0.05	27.4
16	2925.75	2925.66	27.85		
17	2926.41	2926.32	28.66		
18	2927.96	2927.87	30.56		
19	2929.43	2929.34	32.35	32.39 ± 0.08	
20	2929.94	2929.85	32.96	33.33 ± 0.07	33.4
21	2930.37	2930.28	33.48		
22	2932.05	2931.96	35.50	35.69 ± 0.23	36.7
23	2932.86	2932.77	36.47	36.45 ± 0.10	
24	2934.68	2934.59	38.63		
25	2935.15	2935.06	39.19		
26	2936.43	2936.34	40.70	40.70 ± 0.14	
27	2936.86	2936.77	41.21	41.37 ± 0.38	
28	2938.19	2938.10	42.77		
29	2939.70	2939.61	44.54	44.6 ± 0.10	
30	2941.04	2940.95	46.10	46.16 ± 0.10	
31	2942.04	2941.95	47.26		
32	2943.49	2943.40	48.94	48.57 ± 0.29	
33	2944.25	2944.16	49.81	49.61 ± 0.25	
34	2945.12	2945.03	50.82		
35	2945.82	2945.73	51.62		
36	2946.79	2946.70	*		
37	2947.37	2947.28	*		
38	2948.89	2948.80	*		

Non monoenergetic range: below backward threshold of ⁴⁵Sc(p,n)⁴⁵Ti reaction, or above threshold of ⁴⁵Sc(p,n)⁴⁵Ti* reaction (first excited level of ⁴⁵Ti at 37 keV).

Conclusion

For this excitation function measurement, combined impact of beam energy spread and target thickness on resolving power has been limited as much as possible. It results in the most detailed excitation function of the ^{45}Sc(p,n) reaction, in very good agreement with previous studies.

38 resonances were identified, whereof 34 in the 37-keV (proton) monoenergetic energy range, in terms of energy (proton and neutron) and relative yield. It corresponds to a density of less than one resonance per keV, which is surely underestimated due to experimental energy resolution and limits of the fit method. Resonances width seems very small compared to beam energy spread and target thickness, as it did not seem to contribute to the total observed width when fitting. It tends to confirm the hypothesis of a compound nucleus formation.

It should still be possible to improve the measurement by improving even more the resolving power. Another way for better discrimination of the resonances consists in applying an unfolding method with a fixed Gaussian distribution on the results. It should allow better precision on the resonances position, and possible determination of the resonances shape and width.

4.1.2.3 Verification of monoenergeticity on selected resonances

The aim of this study was to verify monoenergeticity of 8- and 27-keV scandium resonances using time-of-flight method. It requires setting the beam energy just above the resonance and using a thin target. Produced neutrons all come from interaction in a narrow beam energy range. Thus it is of good use for noticing unexpected neutron energies in the spectrum.

Experimental setup

This experiment has been conducted during the same irradiation campaign as the time-of-flight measurements described in part 4.1.2.1. Same setup was employed, except the thin scandium target about 5 µg.cm^{-2}-thick and the Li-glass detector front set at 30 cm from target. PTB long counter was employed for setting up beam energy.

Measurements and results

First proton beam energy was set just above energy corresponding to the 8-keV resonance. Then time-of-flight measurements were performed, without shadow cone method since searched result was only qualitative. Experiment was aborted due to technical issues, thus statistics is low. Experiment on the 27-keV resonance could not be conducted.

Time-of-flight spectrum was unfolded using PTB WinSpekt software. Determined neutron spectrum is presented in Fig. 67. Although statistics is low, main peak of the 8-keV resonances is distinguishable at 8.1 keV. A second peak seems appearing around 9.1 keV, which is also in good agreement with measurements detailed in the previous parts. No other and more exotic neutron energies were observed.
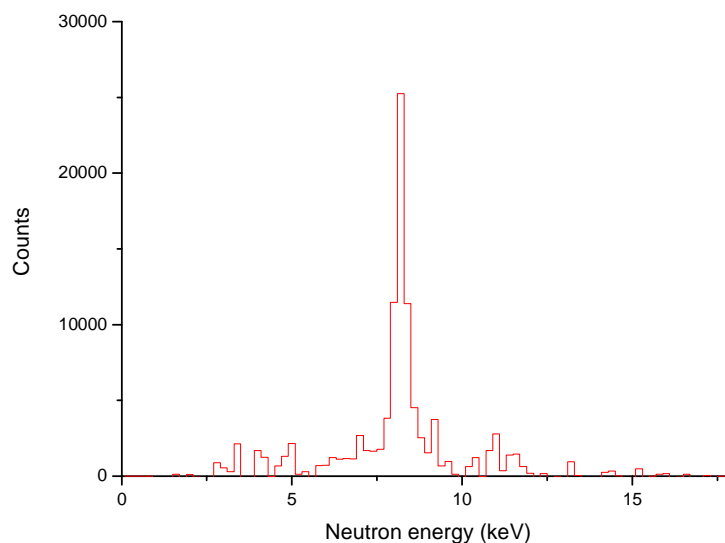
Fig. 67: *Neutron spectrum of ^{45}Sc(p,n) reaction when about 2911-keV incident protons.*

Conclusion

No other reactions emitting neutron at different energies are produced when using 8-keV scandium resonance: despite low statistics, 8-keV resonance can be considered monoenergetic.

Since 27-keV resonance is a good candidate for replacing 24-keV from ^{7}Li(p,n) reaction in international key comparison, cancelled measurement could be interesting to repeat.

4.1.2.4 Conclusion on resonances identification

The use of two measurements methods allowed us to gather maximum information on resonances parameters and add up results. Resonances were characterised in terms of energy, width, spacing and density all over the monoenergetic range of ^{45}Sc(p,n)^{45}Ti reaction.

All results are in good agreement with previous studies, qualitatively for the excitation function on its own, as well as quantitatively when combined to time-of-flight results for resonances position.

With the employed experimental setups, excitation function measurements gave the most detailed data on the resonant structure. Time-of-flight method allowed better accuracy for setting energy of the resonances (incident proton or emitted neutron energies being equivalent using kinematics) and thus positioning the obtained excitation function.

Despite experimental failure preventing same measurement for 27-keV resonance, monoenergeticity has been verified using the 8-keV resonance, within the limits of beam time resolution. Moreover, all resonances identified by time-of-flight method were confirmed by excitation function measurements. Both observations tend to confirm there are no competing reactions and little interference effects between resonances: reaction is monoenergetic in this energy range. Resonances are numerous and narrow, which tends to validate compound nucleus hypothesis.

Experiments confirm the interest of 8- and 27-keV resonances, and possibly 36-keV one as well, for producing quality monoenergetic neutron fields. As yield and quality of emitted neutrons using alternate ^{7}Li(p,n) reaction increase with energy, scandium resonances at higher energies seem less interesting.

Determination of accurate resonance parameters and related nuclear structure could be achieved by using unfolding methods, or even combine data with simulation using theoretical models (reaction matrix). Measurements could be as well repeated at specific angles for discriminating interaction processes (energy levels in play) and modes (compound nucleus, direct reaction).

These experiments gave also precious information for cross section measurements by characterising the multi-resonance composition of the observed peaks, as well as hint of reaction isotropy in its centre of mass.

4.1.3 DETERMINATION OF CROSS SECTION FOR THE SELECTED RESONANCES

All over its available monoenergetic range, two resonances of the ^{45}Sc(p,n) reaction present important yield at their low energies: 8- and 27-keV resonances. This work will therefore focus on these two resonances. As stated in part 2.3.1, differential angular cross sections are needed for estimating neutron scattering *via* Monte-Carlo simulations. Determination of the neutron emission cross section in whole space of both selected resonances is the aim of the measurements presented hereafter, performed in two steps:

- o the first step consists in measuring absolute cross section at one specific angle, 0° in this study,
- o then the angular variation of the cross section is determined by placing successively the detector at various emission angles, from 0° to high angles.

4.1.3.1 Determination of absolute reaction cross section in the ion beam direction

Depending on the cross section structure and experimental constraints, results of cross section measurements do not describe the same quantity (see part 1.2.2.2 on resonance structure). If the cross section structure consists in a monotonic function composed of the interaction of many undistinguishable levels, only a cross section averaged over an energy range is available. This is the case of the ^{7}Li(p,n) reaction cross section. In our case, there are distinguishable and well-separated resonances. It is thus possible to directly measure the cross section of one or nearly one resonance alone, if using a thin enough target coupled to a low enough ion beam spread.

Measuring cross section of specific resonances implies that the beam energy has to be tuned at the resonance energy and be very stable during all the measurement, i.e. several hours. Once found, this was basically a fluence measurement as described in part 3.2.1.1.

Experimental setup

Measurements have been performed at AMANDE facility (see part 3.1.3.1). A fully integrated 10-kV high voltage at the end of the beam line was used for this measurement. It is designed for allowing simultaneous use of high voltage and beam current monitoring. The knowledge of target thickness is of primary importance for determining the cross section. Beam current was thus kept below 10 µA for avoiding any possible and unexpected damage of the scandium target.

The IRSN long counter (PLC, see 3.1.2.1) was employed for its flat and important neutron response, with its 1-atm ^{3}He central counter. The PLC is set as close as possible from the target for resonance selection, and at a reasonably large distance allowing the use of shadow cone: d=300 cm from target to detector front. Neutron monitors were employed during experiment. Since their statistic is low, they are less precise than current integrator which was thus preferred for fluence estimation.

The used target consisted of an 18.9-μg.cm^{-2} thick scandium layer on a 0.5-mm thick tantalum backing. It was characterised using ion beam analysis methods at ARCANE laboratory. Another measurement with a thinner target was planned for comparison purpose. It was however cancelled due to technical issues discussed in the next part.
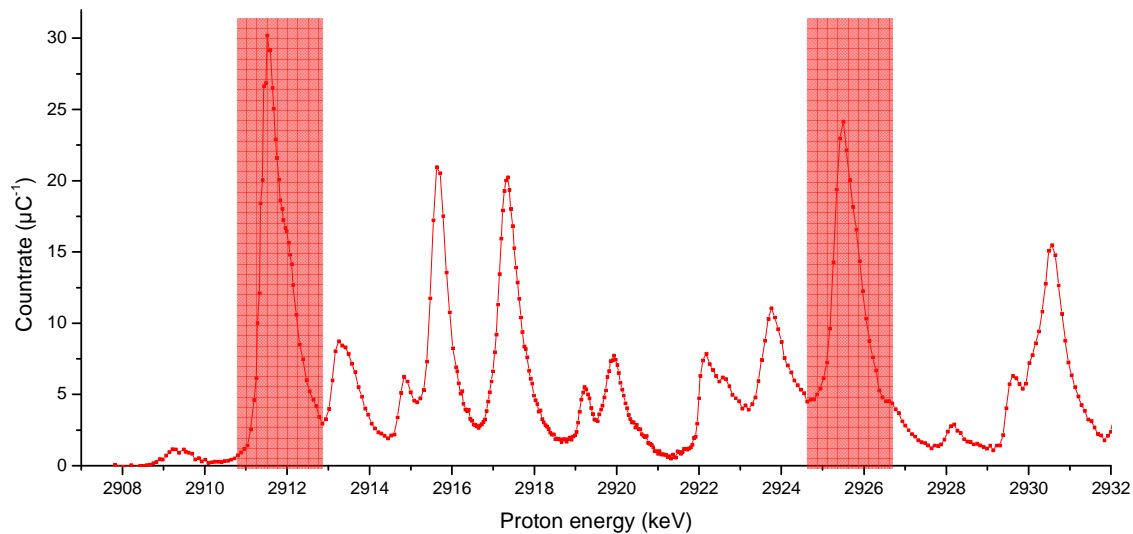
Fig. 68: *Plotting of the proton range theoretically covered by the ion beam profile (beam resolution and target thickness: Gaussian FWHM ~ 2 keV) on the excitation function of the $^{45}Sc(p,n)$ reaction, for both the 8-keV and 27-keV resonances.*

Measurements

For each resonance, proton beam energy was set a few keV above the resonance energy. The positive target voltage was then employed for scanning cross section and selecting the resonance. As described in fluence measurements methodology, four different measurements were performed:

- o   Using scandium target with and without shadow cone
- o   Using blank target (i.e. tantalum backing alone) with and without shadow cone.

Measurement with blank target seemed to produce largely more neutrons than usually observed in pure tantalum background. Some tests were performed to identify the source of these neutrons: it was identified as lithium-7 contamination of both backing and scandium targets, but at different level. Neutron background was therefore determined by measurement using the scandium target just below the $^{45}Sc(p,n)$ reaction threshold.

Results

Complete methodology of measurements of differential angular cross section is given in part 3.2.1.2. As described in this latter part, calculations were performed in two steps. First, fluence rate $\Phi_i(\theta, d)$ was estimated at the measuring point by composing the results of each specific measurement: counts and beam current, with target or backing alone, with or without shadow cone.

Once this quantity calculated, differential cross section $d\sigma(0°)/d\Omega$ was calculated using equation 29. It frees the new quantity from distance, target thickness and the associated contribution of neutrons through materials (air and target).

$$\left.\frac{d\sigma(\theta)}{d\Omega}\right|_{\theta} = \Phi_i(\theta, d) \cdot e \cdot \frac{d^2}{T_{back}T_{air}} \frac{M_{at}}{N_A \varepsilon \cdot 10^{-24}}$$

Source of uncertainties were evaluated applying the GUM methodology (JCGM08) on the equations. The unwanted [7]Li contribution, and its related uncertainty, was treated like a supplementary background. Results of the measurements are detailed in Table 18. Calculations details are presented in Annex.

Table 18: Results of cross section estimation by fluence measurements at the AMANDE facility

Neutron energy of the [45]Sc(p,n) resonance (keV)	Fluence in the ion beam direction, at 300 cm (cm^{-2}.µC^{-1})	Differential cross section in the ion beam direction (mb)
8.12	4.71 ± 0.09	3.39 ± 0.08
27.24	4.06 ± 0.09	2.93 ± 0.07

Conclusion

Results are of the expected order of magnitude, with relatively low uncertainty considering the unexpected lithium-7 contamination. It could be interesting to repeat this measurement with thinner target and no lithium contamination for verification purpose.

Measurements have been performed with relatively thick target compared to the resonance width: based on previous part, composition of one main and one smaller resonance was covered for each measurement. Results could be unfolded from excitation function results for determining contribution of each resonance in the measured cross section.

4.1.3.2 Determination of differential angular cross section

Several studies on ^{45}Sc(p,n) reaction have mentioned that neutron emission is isotropic in the centre of mass (Br55, Ro77, Co85, Ta07). This assumption is based on the theory of formation of a compound nucleus and decay, which is the most probable process at these energies.

Experimental setup

Irradiations were conducted at the NPL facility. The neutron yields were measured with both NPL long counter (Ro04) and a DePangher long counter (see Fig. 69). They were set on different detection angles and used simultaneously. Their fronts were set at 150 cm from the target. The DePangher long counter was used for scanning angles from 0° to 135° with respect to the ion beam direction, whereas the NPL long counter was geometrically limited to 100°. This simultaneous use allows for direct observation of measurement reproducibility and a possible reduction of uncertainties.

Three different slab detectors as well as a current integrator were employed as monitors. The excitation function of the ^{45}Sc(p,n) reaction was scanned from below reaction threshold until finding the desired resonance. The beam current was about 30 µA for all experiments.

The target used for this work consisted of a 20-µg.cm^{-2} thick ^{45}Sc deposit on 0.5-mm-thick Ta backings. The scandium layer and backing diameters are respectively of 25.4 mm and 44.5 mm. They were produced at CEA Ile-de-France simultaneously with the targets employed for the target study (see part 4.1.1)
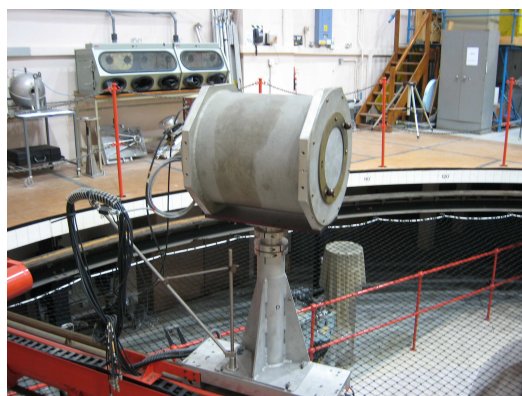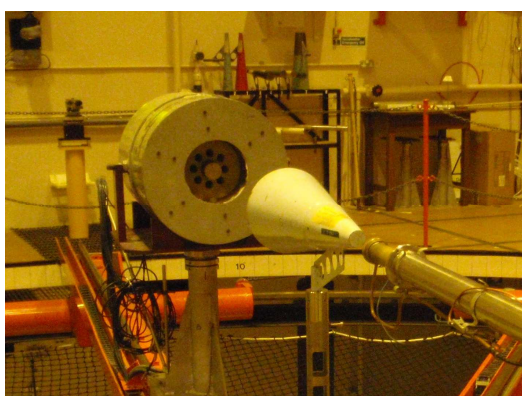
Fig. 69: *NPL neutron detectors employed for measurement of the ^{45}Sc(p,n) angular distribution: NPL long counter (left) and DePangher long counter (right).*

Experimental results

The relative variation of fluence with detection angle was measured for the 8.15 and 27.4 keV resonances of $^{45}Sc(p,n)$ reaction. Background, shadow cone and backing measurements were also conducted.

Fig. 70 presents the results of this experiment. The obtained curves must still be corrected from the attenuation factor through the target holder, the position of the effective centres and the efficiencies of the detectors. These correction factors are currently estimated through MCNP calculations. However a good agreement is observed between experimental data and theory in the case of an isotropic emission in reaction centre of mass. Variations around 90° should be caused by the neutron attenuation in the target slice and target holder. It should also increase the scattered neutrons amount, explaining the slight bumps at larger angles.
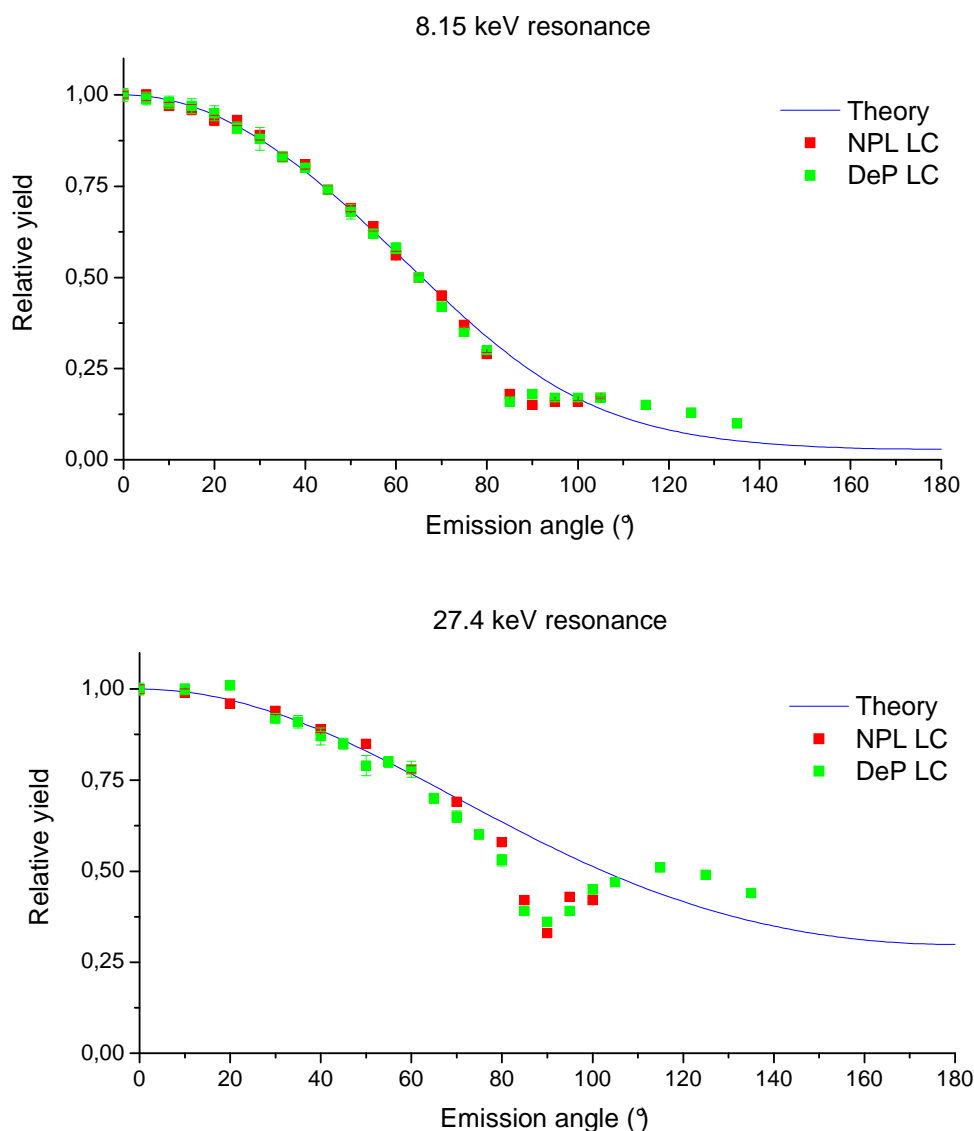
Fig. 70: *Variation of the neutron fluence with angle in the laboratory frame of reference, for the 8.15 and 27.4 keV resonances of the $^{45}Sc(p,n)$ reaction. The curve in blue represents the theoretical variation predicted by kinematics calculation (Ma68). Red and green points represent the experimental data obtained with both long counters. Variations around 90° are due to the neutron attenuation in the target holder.*

Conclusion

These preliminary results can already confirm, with a high degree of confidence, the hypothesis of the neutron emission isotropy in the centre of mass of ^{45}Sc(p,n) at both resonance energies, and consequently the hypothesis of a nuclear reaction through the formation of a compound nucleus.

It should be noted that no target degradation (except scorches) and no yield decrease were observed during the whole experiment with one only target, confirming that scandium targets on tantalum backing can sustain without alteration 30 µA beam current at 3 MeV (i.e. ~90 W) during several hours.

4.1.3.3 Conclusion on cross section measurements

By combining results of both experiments detailed in this study, absolute differential angular cross section of $^{45}Sc(p,n)^{45}Ti$ reaction was characterised in the whole space for two main resonances, i.e. 8.15- and 27.24-keV ones.

As expected, the final values are low, even at 0°: respectively 3.39 ± 0.08 and 2.93 ± 0.07 mb.sr^{-1}. However, the reaction is confirmed isotropic, which allows applications to get the advantage from the medium-weight of scandium for better fluence homogeneity on irradiated devices.

Because of contamination issues, only measurement with the thicker target could be performed. Yet using this target produced neutrons come from several and undistinguishable resonances. Experiment could be repeated with a thinner target for covering one resonance alone at a time, and separate influence of lithium-7 contamination. Another way for determining cross section of the main resonance of the peak could be unfolding results with the resonance parameters determined in previous experiment.

However, and since beam parameters and target composition corresponds to usual setup for calibration purpose, obtained results are sufficient for the daily use of neutron fields produced by the $^{45}Sc(p,n)$ reaction.

The logical continuation of these results is their implementation in the simulation codes. In this way, metrological calculation of neutron scattering contribution and fluence homogeneity at the surface of the irradiated device using $^{45}Sc(p,n)$ reaction will be available.

4.2 EXPERIMENTAL PROSPECT OF OTHER POSSIBLE REACTIONS

This part of the study focuses on the investigation and experimental comparison of several reactions, in terms of achievable fluence rates at neutron energies below 50 keV. Relative variations of their yields with the incident proton energy have been measured at the IRSN AMANDE facility.

4.2.1 SELECTION OF THE NUCLEAR REACTIONS

The selection of reactions was based on kinematics calculations and previous studies (see 2.2). If data were available, cross sections and/or neutron and gamma yields were taken into account. The selected reactions for a first measurement campaign were ^{45}Sc(p,n), ^{65}Cu(p,n), ^{51}V(p,n), ^{57}Fe(p,n) and ^{37}Cl(p,n). In a second campaign were studied ^{53}Cr(p,n), ^{49}Ti(p,n), ^{77}Se(p,n) and ^{59}Co(p,n) reactions. All selected reactions are detailed in Table 19.

Table 19: List of the nuclear reactions studied in this work, with their neutron threshold energy $E_{p,th}$, the ion beam energy at which the neutrons become monoenergetic at 0° (backward threshold) $E_{p,m}$, the minimum neutron energy at 0° at the backward threshold, and the target thickness expressed as ion beam energy loss for the targets studied.

Reaction	Energy of the reaction Q (keV)	Proton energy $E_{p,th}$ / $E_{p,m}$ (keV)	Lowest $E_{neutron}$ (keV)	Target thickness (keV) / (µg.cm^{-2})
^{45}Sc(p,n)	-2,844.4	2,908.2 / 2,909.6	5.6	1.5 / 20.0
^{65}Cu(p,n)	-2,134.4	2,167.5 / 2,168.1	2.0	1.5 / 20.0
^{51}V(p,n)	-1,534.9	1,565.5 / 1,565.9	2.4	2.3 / 20.0
^{57}Fe(p,n)	-1,618.3	1,647.0 / 1,647.4	2.0	2.0 / 20.0
^{37}Cl(p,n)	-1,596.2	1,639.3 / 1,640.5	4.6	2.5 / 20.0
^{53}Cr(p,n)	-1,379.2	1,405.4 / 1,406.0	2.0	1.5 / 13.6
^{49}Ti(p,n)	-1,384.2	1,412.7 / 1,413.3	2.3	1.5 / 13.5
^{77}Se(p,n)	-2,147.0	2,175.2 / 2,175.5	1.5	1.5 / 20.8
^{59}Co(p,n)	-1,855.1	1,886.8 / 1,887.4	2.1	1.5 / 17.5

This list is non-exhaustive and other reactions, such as ^{12}C(d,n) and other suggested in part 2.2.5, could be studied in further experiments.

4.2.2 EXPERIMENTAL SETUP

4.2.2.1 <u>Target production</u>

Scandium targets were produced by the commonly-used evaporation method. Other targets were made by implantation at the SIDONIE facility (CSNSM, France) (Al70, Ca70). In this small accelerator, isotopes are separated electromagnetically with an analysis magnet. The selected element can be focused and decelerated to form a homogeneous deposit onto a small surface. This allows for direct production of an isotopic deposit and the consumption of much less material. The targets consisted of a 13 to 20 µg.cm^{-2} thick deposit on 0.5-mm-thick aluminium backings. Deposit and backing have a diameter of 18 mm and 25 mm, respectively.

Fig. 71: *SIDONIE facility. On the left, in blue, the ion source; in the middle the analysis magnet; on the right, the target chamber.*

Because of the gaseous state of ^{37}Cl in standard conditions for temperature and pressure, two different methods were tested for the production of the ^{37}Cl solid target:
- ^{37}Cl deposit protected by two very thin layers of Ta and Au corresponding both to a few atomic layers only,
- Implantation of the ^{37}Cl directly into the surface layer of the backing used as occlusion matrix.

Target thickness and composition were verified at the AIFIRA facility (CENBG, France) using the RBS method as described in 3.2.2.

4.2.2.2 <u>Experimental setup of the facility</u>

Irradiations were all conducted at the IRSN AMANDE facility. The neutron yields were measured with the IRSN long counter at 0° with respect to the ion beam direction. It was employed with 10- and 1-atm ^{3}He central detector with the effective centre set at 66 cm and 41 cm from target, respectively for the first and second irradiation campaigns. Two De Pangher long counters set at 20° and 100°, as well as a current integrator, were employed as monitors. A specific high voltage was employed at the end of the beamline to vary the energy, in steps of 250 or 500 eV without changing the accelerator setup. The beam current was about between 5 and 10 µA for all experiments.

4.2.3 EXPERIMENTAL RESULTS

The obtained results are first discussed separately for each reaction and then compared together. Excitation functions of ^{45}Sc(p,n), ^{65}Cu(p,n), ^{51}V(p,n), ^{57}Fe(p,n) and ^{37}Cl(p,n) reactions were obtained during the first session. Excitation functions are normalised with distance and energy dependent detector response (see detailed methodology in 4.1.2.2). Neutron energy corresponding to ion beam energy was calculated using kinematics equation and is indicated as a secondary axis.

Neutron production from ^{59}Co(p,n) and ^{77}Se(p,n) reactions was considered at first glance negligible and erratic. In the end, it led us to a global and more or less important contamination of targets with lithium fluoride.

4.2.3.1 ^{45}Sc(p,n) reaction

For comparison purpose, the excitation function of the ^{45}Sc(p,n) reaction was determined in the same setup as was used for the other reactions, from threshold to 2,935 keV proton energy, approximately 40-keV neutrons. The results are in excellent agreement with previous yield measurements (Co85), as can be seen in Fig. 72. The main resonances are clearly identified, such as those corresponding to 8.15 keV (E_p= 2911 keV) and 27.4 keV (E_p= 2925 keV) neutron energy.
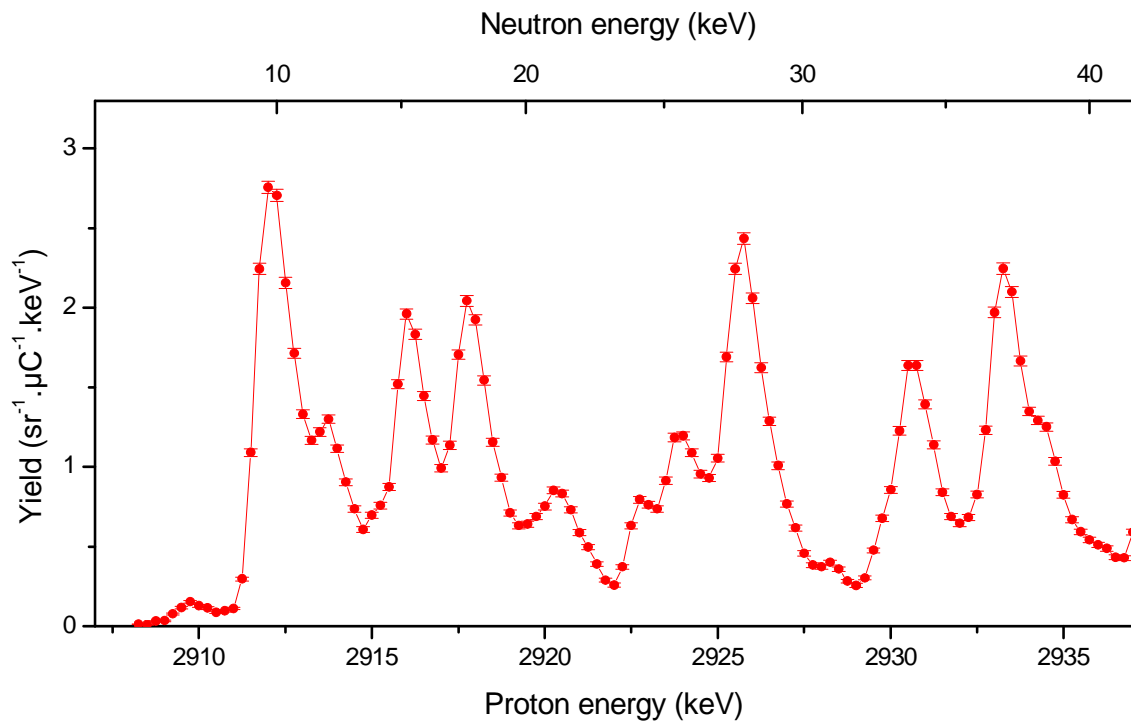
Fig. 72: *^{45}Sc(p,n) reaction excitation function from reaction threshold, determined at the AMANDE facility.*

4.2.3.2 ^{65}Cu(p,n) reaction

The excitation function of ^{65}Cu(p,n) reaction was determined from threshold to 2,210 keV proton energy, approximately 50 keV neutrons. The 1.17 keV peak, previously measured using the time-of-flight technique by (Sc89), is the most prominent resonance (see Fig. 73). Two others at roughly 12 and 30 keV could be used, but with a neutron emission rate nearly 2 times lower. The first resonance at 1.17 keV corresponds to a proton energy below the monoenergetic threshold. As a consequence, a second neutron group (0.116 keV-neutron energy) is produced at 0° with a fluence production corresponding to about 9% relative to the 1.17 keV-resonance (Bö89). In addition, the long counter count rate is less than 1 $\mu C^{-1}.keV^{-1}$ in this peak (i.e. 17 times less than for the 8 keV-scandium resonance).
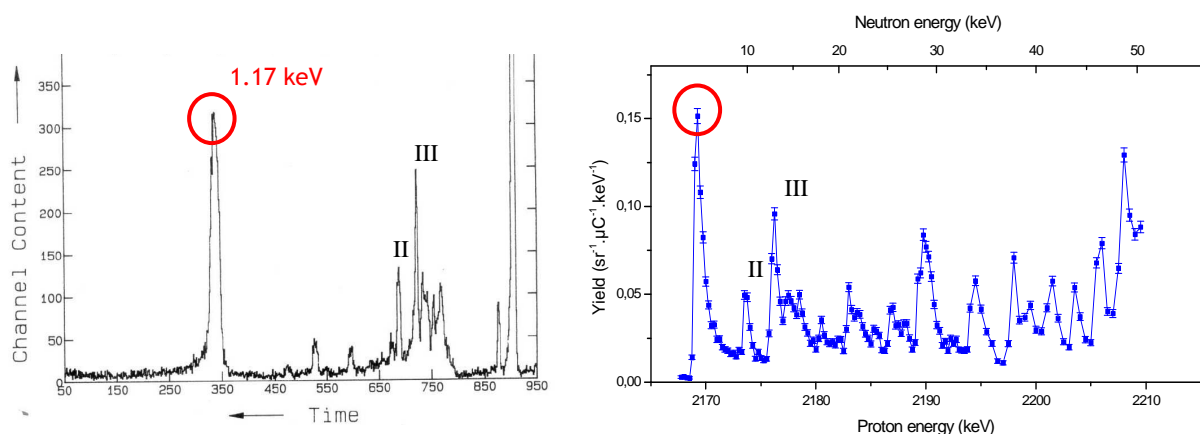
Fig. 73: *Neutron spectrum of the ^{65}Cu(p,n) reaction obtained by Schölermann and Böttger using TOF technique (Sc89) and excitation function determined at the AMANDE facility. According to kinematics, the first and main peak on the right-hand side graph corresponds to the 1.17 keV resonance observed by (Sc89).*

4.2.3.3 <u>^{51}V(p,n) reaction</u>

The excitation function of ^{51}V(p,n) reaction was determined from threshold to 1 607 keV proton energy, i.e. approximately 50 keV neutrons. The results are in excellent agreement with previous studies (Gi65) (see

Fig. 74). The first main resonance at 6.64 keV, as determined using the time-of-flight method (Sc89), is clearly visible. In the energy range studied (below 50 keV), two other resonances (not measured in this study) are also of interest at respectively 40 and 50 keV neutron energy with up to a factor 2 higher neutron yield.
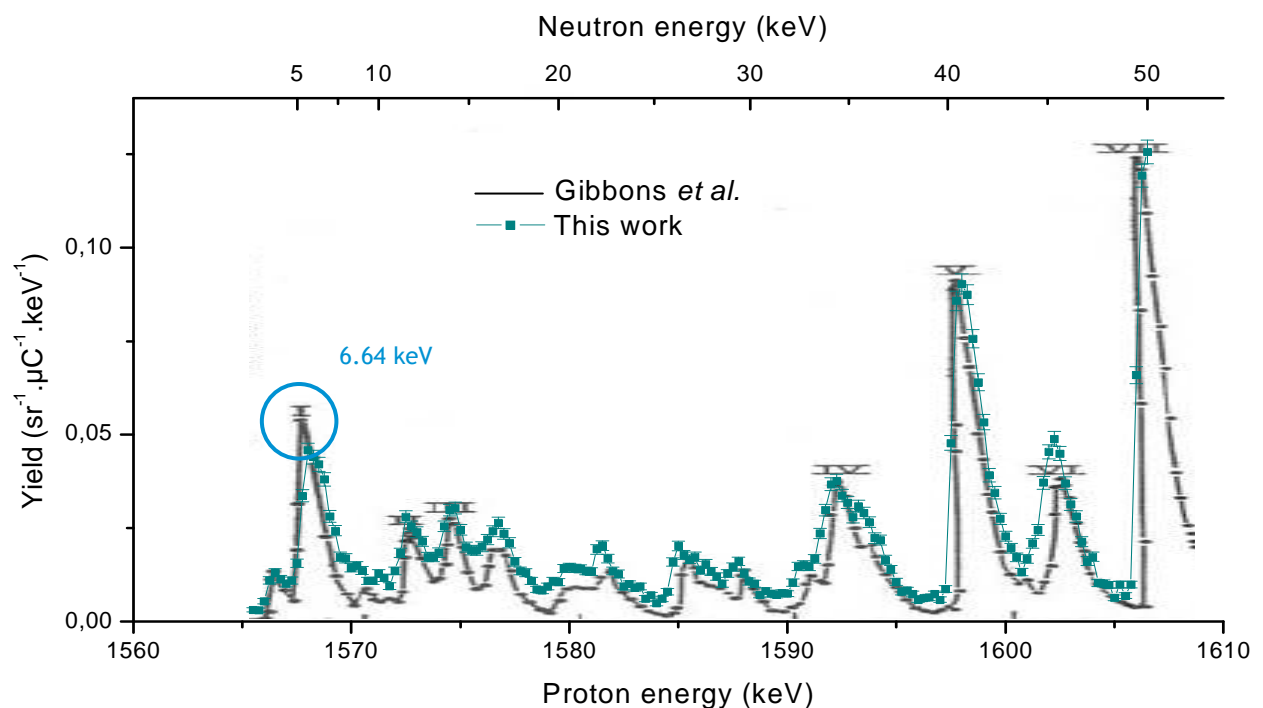
Fig. 74: *Comparison of the ^{51}V(p,n) reaction excitation functions determined by Gibbons et al. (Gi55, black)) and at the AMANDE facility (green). The energy of the second resonance noted I is about 6.64 keV.*

4.2.3.4 ^{57}Fe(p,n) reaction

The excitation function of the ^{57}Fe(p,n) reaction was determined from threshold to 1,695 keV proton energy, approximately 56 keV neutrons (see Fig. 75). The reaction is usually employed for higher energies (Ut83). A resonance structure was observed just above the reaction threshold. A well resolved peak of low energy (FWHM<1 keV) was identified, corresponding to a calculated 6.5 ± 1.0 keV neutron energy.
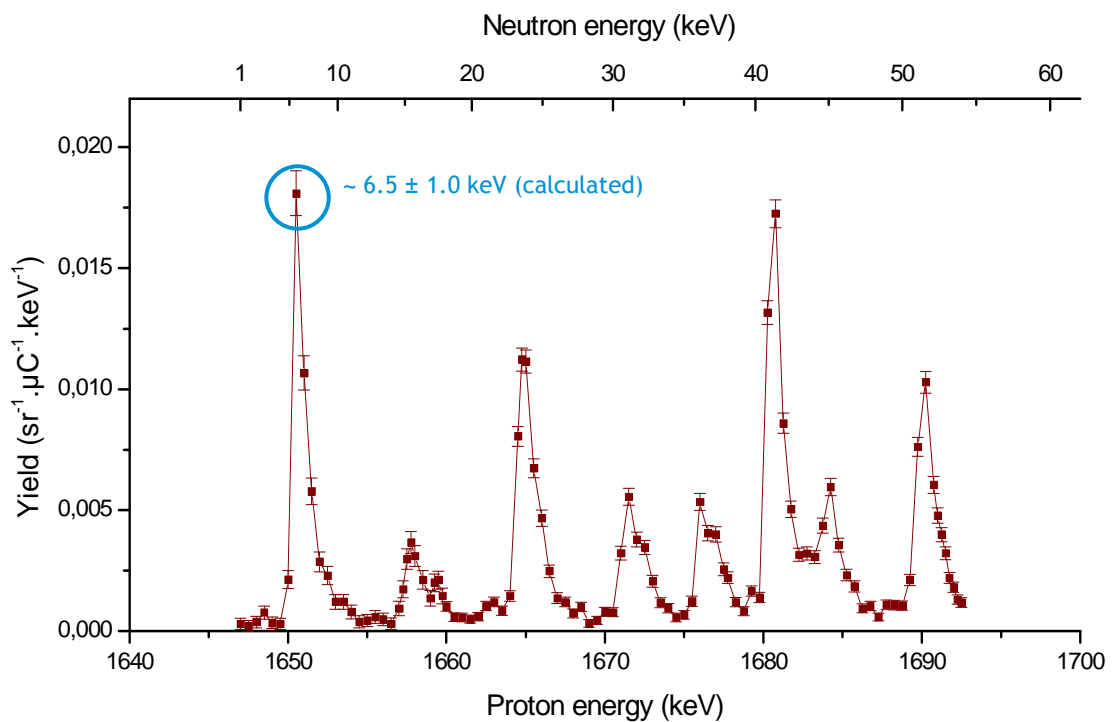
Fig. 75: *Excitation function of the ^{57}Fe(p,n) reaction from reaction threshold, determined at the AMANDE facility.*

4.2.3.5 ^{49}Ti(p,n) reaction

The excitation function of ^{49}Ti(p,n) reaction was determined from threshold to 1,438 keV proton energy, approximately 32-keV neutrons (see Fig. 76). The reaction cross section describes many resonances; the first and main one at lowest energies corresponds to a calculated energy of 0.9 ± 1.2 keV. However, it is situated below the monoenergetic threshold and thus non monoenergetic *stricto sensu*.
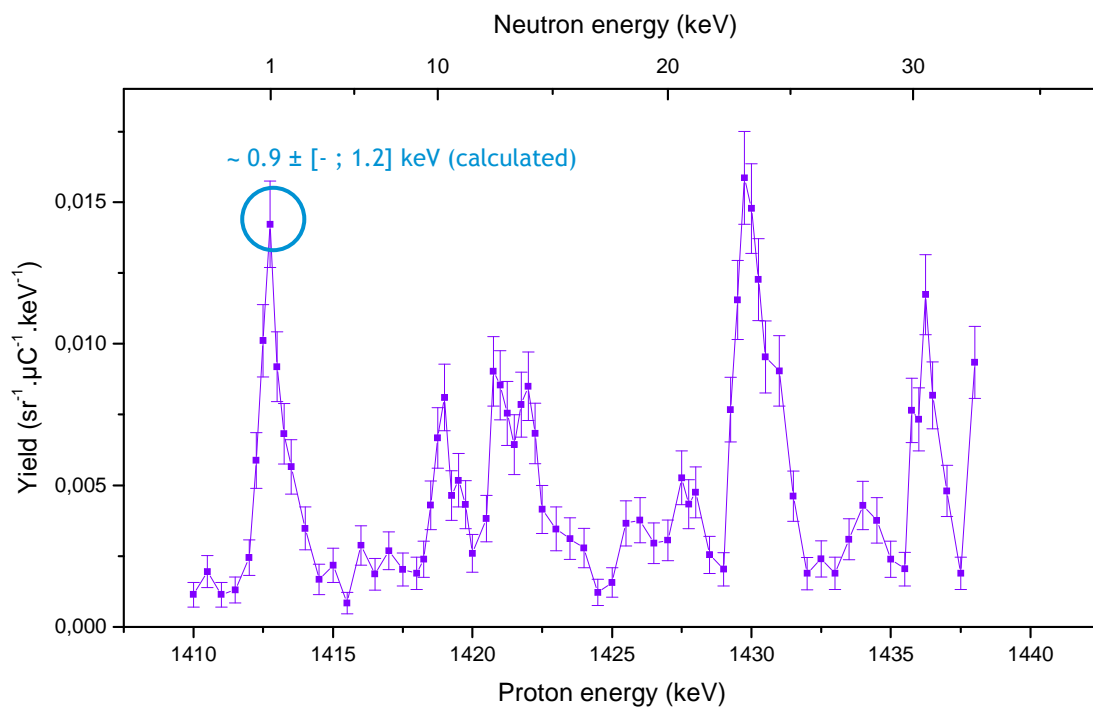
Fig. 76: *Excitation function of the ^{49}Ti(p,n) reaction from reaction threshold, determined at the AMANDE facility.*

4.2.3.6 ^{53}Cr(p,n) reaction

The excitation function of ^{53}Cr(p,n) reaction was determined from threshold to 1,430 keV proton energy, approximately 31-keV neutrons (see Fig. 77). The reaction shows two resonances of low neutron energy, respectively corresponding to calculated neutron energies of 6.2 ± 0.7 keV and 14.3 ± 0.9 keV.
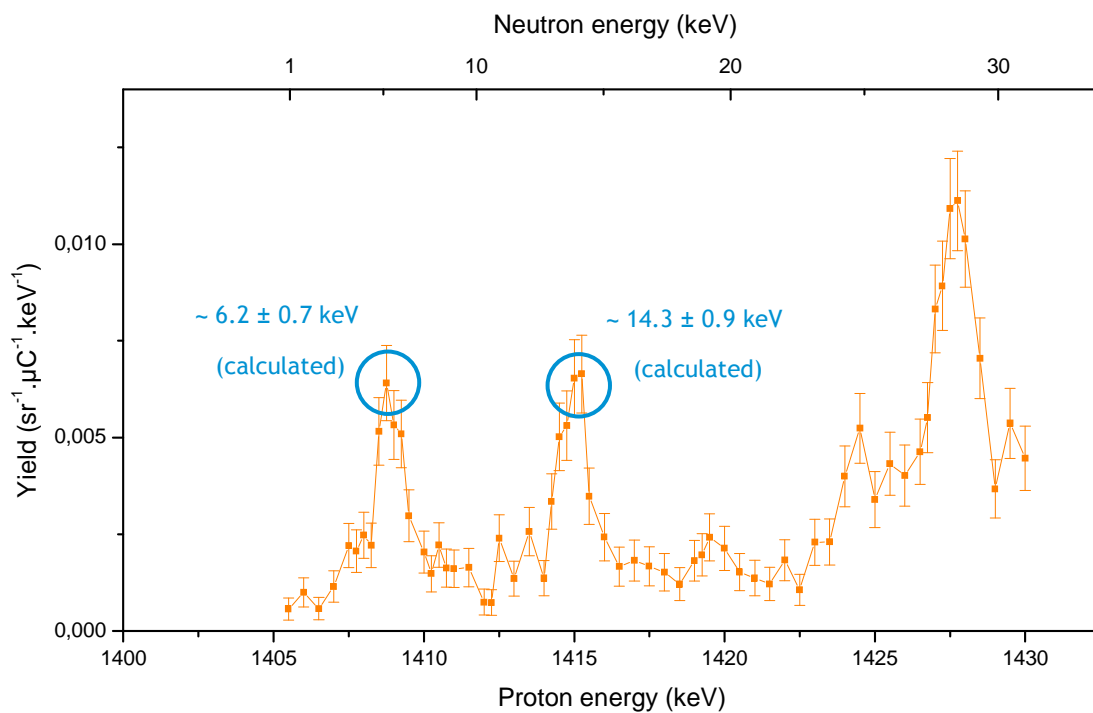
Fig. 77: *Excitation function of the ^{53}Cr(p,n) reaction from reaction threshold, determined at the AMANDE facility.*

4.2.3.7 ³⁷Cl(p,n) reaction

The excitation function of ^{37}Cl(p,n) reaction was determined from threshold to 1,668 keV proton energy, approximately 40 keV neutrons (see Fig. 78). The reaction shows a few peaks of low neutron energy, the first one corresponding to a calculated energy of 8.0 ± 1.5 keV. The main result of these measurements is the feasibility of using targets with gaseous isotopes for further studies.
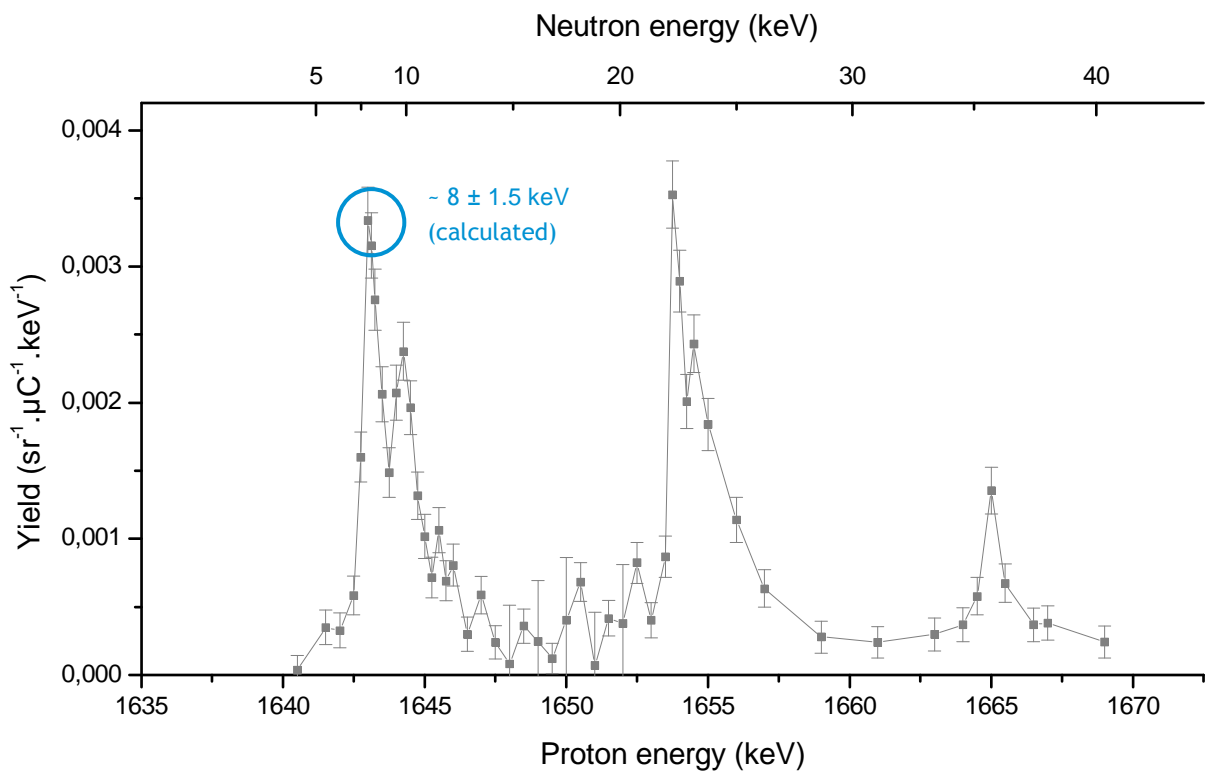
Fig. 78: *Excitation function of the ^{37}Cl(p,n) reaction from reaction threshold, determined at the AMANDE facility.*

4.2.3.8 <u>Reaction comparison</u>

All the (p,n) reactions studied exhibit resonance structures as a function of the proton beam energy as shown in Fig. 79. The results presented in Fig. 79 and 80 are normalised for yield comparison. Neutron yield of the ^{45}Sc(p,n) reaction is at least one order of magnitude greater than those of the other compared reactions, two in the case of ^{37}Cl(p,n) reaction. Despite its low yield, the ^{65}Cu(p,n) reaction is interesting for its 1.17 keV resonance. Even if this neutron energy is achievable with the ^{45}Sc(p,n) reaction, it is at the expense of backward angle measurements (around 100° using 8.15 keV resonance).
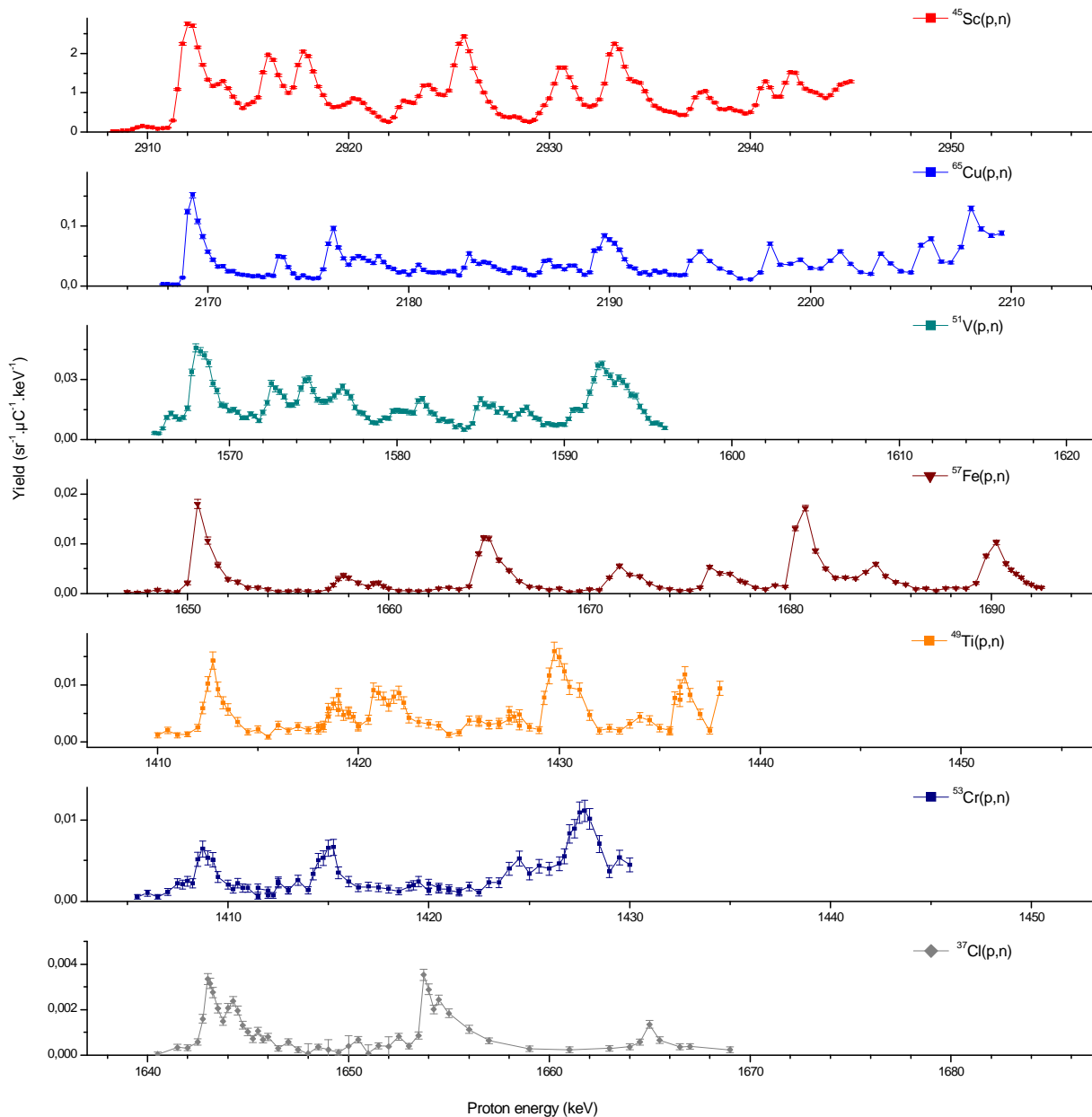
Fig. 79: *Count rate, normalised for 1 keV ion beam energy loss in the target, determined with the 10 atm IRSN long counter placed at 0° and 66 cm from the target for ^{45}Sc(p,n), ^{65}Cu(p,n), ^{51}V(p,n), ^{57}Fe(p,n), ^{37}Cl(p,n) reactions, respectively, as a function of the proton beam energy.*

The ^{51}V(p,n), ^{57}Fe(p,n) and ^{37}Cl(p,n) reactions have very low neutron yields that are not suitable for any practical calibration of neutron measuring devices. The achievable neutron energies with those reactions do not justify a use with more constraints on the yield.

The neutron yields available at the main resonances of the studied reactions are compared in Fig. 80 to the achievable yield with ^{7}Li(p,n). To be interesting alternatives, scandium and copper-65 targets have to be used with high beam currents (see 4.1.1) while avoiding if possible the use of water cooling, which tends to produce too much scattering in this neutron energy range.
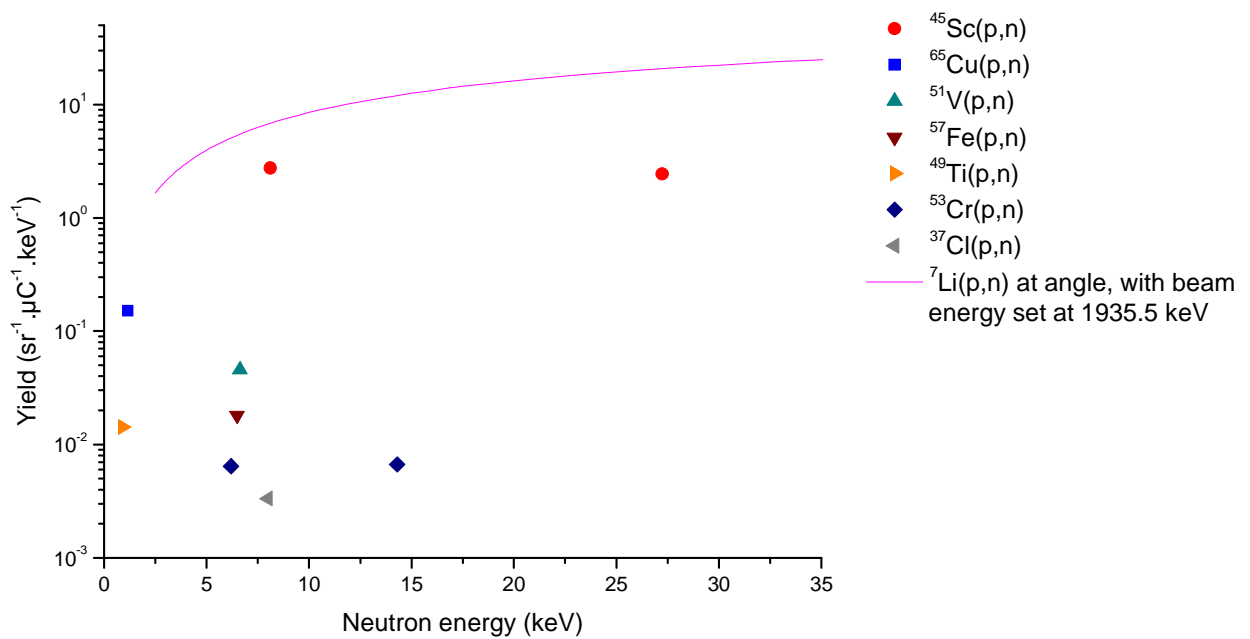
Fig. 80: *Yield comparison of the main resonances of the studied reactions with simulated yield of ^{7}Li(p,n) reaction using Drosg2000 (for 1 keV ion beam energy loss in the target).*

4.2.4 CONCLUSION ON REACTION COMPARISON

The purpose of this study was to investigate reactions for producing monoenergetic neutron fields with energies below 50 keV. Comparisons of the results with previous measurements validated the experimental setup. Variations of the neutron yields of ^{45}Sc(p,n), ^{65}Cu(p,n), ^{51}V(p,n), ^{57}Fe(p,n), ^{49}Ti(p,n), ^{53}Cr(p,n) and ^{37}Cl(p,n) reactions for neutron energies below 50 keV have been studied at the AMANDE facility. All the studied reactions have a cross section with resonant structure, which is advantageous for fine neutron energy resolution. The ^{45}Sc(p,n) reaction remains the best candidate for the production of low-energy neutrons at 0°, especially at the 8 and 27 keV-resonances, as it presents the highest yield of the studied reactions. The ^{65}Cu(p,n) reaction is interesting because of a well-defined resonance at a very low neutron energy of 1.17 keV, even though the corresponding neutron field is not purely monoenergetic. The neutron yield of the other studied reactions is too low to be further considered for neutron calibration.

Another result of this study is the validation of a production method for solid targets with gaseous elements like in the case of the ^{37}Cl(p,n) reaction.

5 <u>USE OF KEV MONOENERGETIC NEUTRON FIELDS</u>

Following the experimental studies on monoenergetic neutron fields in the keV range, several direct applications have or would have been interesting to conduct.

5.1 IMPLEMENTATION OF EXPERIMENTAL RESULTS IN SIMULATION CODES

This work would have consisted in implementing the quantities which have been experimentally determined in several simulation codes employed at the laboratories of the IRMM-IRSN-NPL-PTB scientific cooperation.

PTB *TARGET* and IRMM *NeuSDesc* codes allow simulating the neutron fluence in more or less detailed geometry and setup. By including new differential cross sections in the simulation codes, it would have been interesting to compare their results for neutrons in the keV-energy range, with another and possibly with some MCNP/Geant4 simulation.

Another study could have consisted in simulating excitation function of ^{45}Sc(p,n) or any other studied (p,n) reaction. Using Monte-Carlo methods and new knowledge on resonances energies and relative yield, effective shape of the excitation function could have been reconstructed in any experimental setup. In the end, this simulation could be employed for avoiding simultaneous use of several resonances during irradiation campaigns, which deteriorates the neutron field monoenergeticity.

5.2 CALIBRATION OF SURVEY METERS IN THE 1-100 KEV RANGE

The over response of survey meters and dosimeters in the 1-100 keV range was already demonstrated in previous simulations and measurements (Al94, Kl97). This issue justifies CEI and ISO recommendations for calibrating neutron sensitive devices with sources delivering neutrons in this energy range.

Since this is one of the important reasons for studying low-energy monoenergetic neutron fields, some proof of principle measurements were conducted at the IRSN and NPL reference facilities (Gr03, Ha07), using three survey meters.

Experimental setup

Both the NPL and IRSN AMANDE facilities were used for these measurements. The experimental setups were identical, consisting in setting the survey meters at 0° with respect to the ion beam and a known distance from the target. The reference fluence was determined with long counters (Ro04, La10-1). The scattered neutron background was deduced using the shadow cone method. The irradiated survey meters were: Harwell N91, Wendi FHT-762 and two Berthold LB6411 (one for each institute).

Table 20: Details on irradiation performed at the AMANDE facility.

	Distance d to the target (cm)	Irradiation duration (without/with shadow cone) (min)	
		8.15 keV	27 keV
Harwell N91	107.5	66/20	50/16
Wendi FHT-762	162.0	40/15	50/16
Berthold LB6411	106.6	60/20	60/20

Results and conclusion

The responses of the survey meters were normalised by a calibration with a ^{252}Cf source. Measurement performed at 8 and 27 keV using a ^{45}Sc(p,n) reaction at NPL and IRSN facilities show an over response for all the instruments, up to a factor ten for the Harwell N91 at 8 keV.

These results confirm the over response for the three survey meters used with 8 and 27 keV monoenergetic neutron fields produced by the ^{45}Sc(p,n) reaction, as shown in Fig. 81. It also confirms the possible use of ^{45}Sc(p,n) as a calibration source, already discussed in (Hu85).
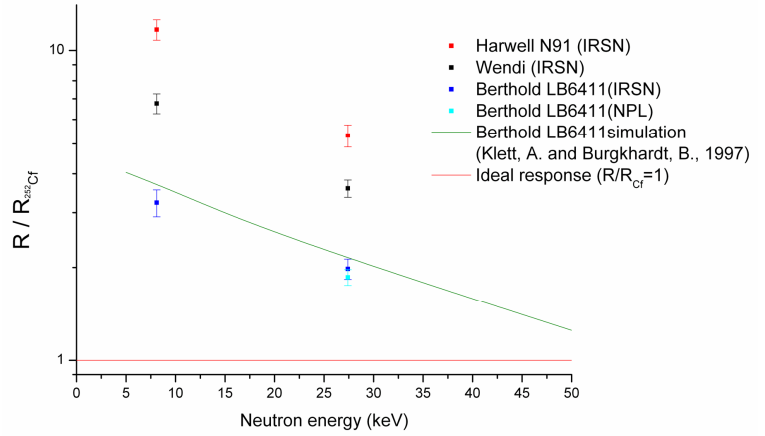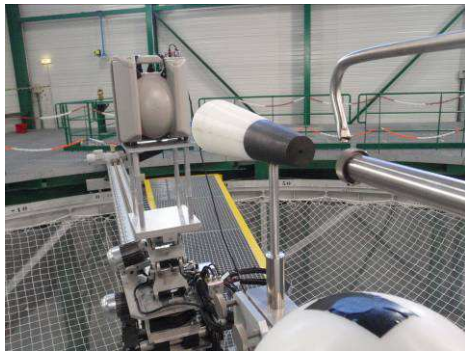
Fig. 81: *On the left, setup for shadow cone measurements with Harwell N91 survey meter. On the right, experimental responses at 8 and 27 keV of three survey meters, determined at IRSN and NPL neutron reference facilities using ^{45}Sc(p,n) reaction.*

CONCLUSION AND ANALYSES

The response of a neutron detector varies with neutron energy. This response function is usually calculated using Monte-Carlo codes and determined through experiments at facilities producing monoenergetic neutron fields. The importance of low-energy calibration can be illustrated by the over response of survey meters and dosimeters in the 10^{-5}-10^2 keV range.

Different methods are available for producing keV- monoenergetic or quasi-monoenergetic neutrons. Radionuclide sources producing neutrons in that energy range are hardly available and of short half-lives. Nuclear reactors could be powerful tools but were not considered due to their very limited availability in the world for detector calibration. Therefore neutron sources based on nuclear reactions between accelerated ions and targets were studied in this work: the aim was to investigate nuclear reactions capable of producing low-energy monoenergetic neutron fields suitable for the calibration of neutron detectors.

Several nuclear reactions are already commonly employed below 100 keV, such as ^{7}Li(p,n) at emission angle and in a lower extent ^{45}Sc(p,n). The use of the well characterised ^{7}Li(p,n) reaction for keV neutron energy range has several physical drawbacks, mainly about energy and fluence homogeneities. Despite its numerous qualities, the use of the ^{45}Sc(p,n) reaction was limited by a low yield and some gaps in knowledge, especially regarding differential cross section for simulation of scattered neutrons.

Experiments performed in this work confirmed the interest of the ^{45}Sc(p,n) reaction for detector calibration. It has been shown that the low yield problem can be compensated for by increasing the beam current up to several tens of μA without deteriorating target deposited on tantalum backing.

Combined thick target time-of-flight and accurate excitation function measurements were performed for detailing the cross section resonant structure. Numerous and new resonances were characterised on the whole monoenergetic range of the reaction in terms of neutron/proton energy and relative yield. These results are in excellent agreement with previous studies. They could still be refined, notably for extracting resonance parameters such as effective widths and interaction modes. Unfolding methods or simulation by using theoretical models could be employed. Time-of-flight measurement allowed also verification of monoenergeticity for 8-keV resonance.

Differential (p,n) cross section was determined for the two most usable resonances, in the whole space, i.e. for any emission angle. Differential cross sections of 8- and 27-keV resonances are respectively of 3.39 ± 0.8 and 2.93 ± 0.7 mb.sr^{-1} in the ion beam direction. Isotropy in the reaction centre-of-mass has been *a priori* verified. Full uncertainty budget was carried out, and uncertainties consequently reduced by accurate target characterisation and resonance selection. The obtained values have to be compared to those of ^{7}Li(p,n) reaction when used at angles, which are respectively 8.3 and 25.4 mb.sr^{-1} at the same neutron energies (ion beam energy set at 1936 keV).

Combined with cross section study, the conducted target study demonstrates that neutron fluence rates such as those of the ^{7}Li(p,n) reaction are achievable in adapted experimental setup. Some measurements of the photon contribution to the total dose equivalent were performed. Contamination issues prevented study of nuclear structure to be achieved along this measurement. However it concludes on an acceptable ratio between neutron and gamma dose equivalents for applications such as detector calibration.

The study of other reactions mainly resulted in dismissing possibilities. It essentially served to validate methods (target production for example) and reactions already known. Despite its very low yield, 65-copper could be an interesting option for developing monoenergetic neutron reference field at about 1 keV.

In conclusion, ^{45}Sc(p,n) reaction has already proved to be a more-than worthy candidate for low-energy monoenergetic neutron production, as an alternative to the ^{7}Li(p,n) reaction, especially at 8 keV neutron energy. This reaction is now available for being a routinely employed reaction allowing calibration of neutron instrument and will be part of the next international key comparison of neutron fluence organised by BIPM. It can be employed for developing instrumentation for reference measurements at this unusual energy range as proton recoil telescope based on particle trace study or on neutron/gamma discrimination.

An outcome of these measurements and studies is the possibility to implement the obtained data in Monte-Carlo codes (*TARGET* or/and *NeuSDesc*) and in various simulations for reproducing experimental data (convolution of energy spread and target thickness, for example). Cross sections and resonance parameters are to be added to nuclear databases.

In parallel to studies of reactions for lowering the achievable neutron energy while maintaining usable yield, efforts could be concentrated on prospecting reactions producing neutrons in the 50 keV-100 keV range at 0° such as ^{11}B(p,n) reaction. New production methods could be considered such as filtered reactions for finding a new compromise between field quality and important neutron yield.

BIBLIOGRAPHY

Al51   Alvarez, L.W., 1951. Energy doubling in DC accelerators. Rev. Sci. Instr. 22, 705.

Al70   Alexandre, K., Camplan, J., Ligonniere, M., Meunier, R., Sarrouy, J.L., Smith, H.J., Vassent, B., 1970. SIDONIE, the new electromagnetic isotope separator at Orsay. Part 2: performances. Nucl. Inst. and Meth. 84, 45.

Al94   Alberts, W.G., Dietz, E., Guldbakke, S. Kluge, H., 1994. Response of an electronic personal neutron dosemeter. Rad. Prot. Dosim. 51, 207-210.

As05   Asselineau, B., 2005. BGO as soft gamma-ray detector in mixed field. IRSN internal report.

Be04   Bertulani, C.A., Danielewicz, P. 2004. Introduction to nuclear reactions. Institute of Physics Publishing.

BerkeleyLab online database   http://ie.lbl.gov/education/isotopes.htm, The Berkeley Laboratory Isotopes Project'.

Bö89   Böttger, R., Guldbakke, S., Klein, H., Schölermann H., Schumacher, H., Strzelczyk, H., 1989. Problems associated with the production of monoenergetic neutrons. Nucl. Instrum. Meths Phys. Res. A282, 358–367.

Br94   Brindhabana, S.A., Barker, P.H., Keeling, M.J., Wood, W.B., 1993. Accelerator beam energy calibration with the ^{27}Al(p, n) and ^{27}Al(p, γ) reactions. Nucl. Instrum. Meths Phys. Res. A340-3, 436–441.

Br55   Brugger, R.M., Bonner, T.W., Marion, J.B., 1955. Study of the nuclear reactions ^{45}Sc(p,n)^{45}Ti, ^{63}Cu(p,n)^{63}Zn, ^{65}Cu(p,n)^{65}Zn and Zn(p,n)Ga. Phys. Rev. 100, 1, 84-90.

Ca70   Camplan, J., Meunier, R., Sarrouy, J.L., 1970. SIDONIE, the new electromagnetic isotope separator at Orsay. Part 1: design and construction. Nucl. Inst. and Meth. 84, 37.

Co10   Cognet M.-A., Gressier V., 2010. Development of a measurement reference standard for neutron energies between 1 MeV and 20 MeV using time of flight method at the AMANDE facility. Metrologia 47, 4, 377-386.

Co85   Cosack, M., Lesiecki, H., Hunt, J.B., 1985. Monoenergetic neutrons of energies from 0.5 keV to 40 keV via the reaction ^{45}Sc(p,n)^{45}Ti. Proc. of 5th symposium on neutron dosimetry, EUR-9762 (CEC Luxembourg), I, 597-606.

Cr54   Crasemann, B., 1954. An isomeric state of ^{65}Ga. Phys. Rev. 93, 1034. And Crasemann, B., 1953. Decay of ^{64}Ga and ^{65}Ga. Phys. Rev. 90, 995-996.

De69   Deconninck, G., Royen, J., 1969. La Réaction ^{51}V(p,n)^{51}Cr comme source de neutrons monoénergétiques. Nucl. Instrum. Meths. 75, 266-270.

Dr90   Drosg, M., 1990. Sources of variable energy monoenergetic neutrons for fusion-related applications. Nuclear Sci. & Eng. 106, 279-295.

Dr99   Drosg, M., 1999. Monoenergetic neutron production by two-body reactions in the energy range from 0.0001 to 500 MeV. An overview. TCM-Meeting of IAEA, Debrecen, Hungary, October 1999.

Dr00   Drosg2000 code, Drosg, M., 2000. Version 2.21 IAEA.

Gi55   Gibbons, J.H., Macklin, R.L., Schmitt H.W., 1955. ^{51}V(p,n)^{51}Cr reaction as a 5- to 120-keV neutron source. Phys. Rev. 100, 167-168.

Gi59   Gibbons, J.H., Macklin, R.L., 1959. Total neutron yields from light elements under proton and alpha bombardement. Phys. Rev. 114, 579.

Gi60   Gibbons, J.H., Newson, H.W., 1960. The ^{7}Li(p,n)^{7}Be reaction, in: Marion, J.B., Fowler, J.L. (Eds.), Fast neutron physics, Part I: Techniques. Interscience Publishers, Inc., New York, 133-176.

Gi65   Gibbons, J.H., Macklin, R.L., 1965. ^{51}V(p,n)^{51}Cr cross section from threshold to 2,25 MeV. Nucl. Instrum. Meths. 37, 330.

Gr03 Gressier, V., Pelcot, G., Pochat, J.L., Bolognese-Milstajn, T., 2003. New IRSN facilities for neutron production. Nucl. Instrum. Meths Phys. Res. A505, 370–373.

Gr10 Gressier, V., 2010. Valeurs de référence et corrections pour la détermination de la fluence neutronique sur AMANDE. IRSN internal report DRPH/SDE/2010-08.

Ha06 Haas, B., 2006. The Bordeaux Nuclear Research Center. Nuclear Physics News 16, 3, 5-11.

Ha07 Hawkes, N.P. Bennett, A., Cheema, S.S., Horwood, N.A., Jones, L.N., Kolkowski, P., Roberts, N.J., Taylor, G.C., Thomas, D.J., 2007. Progress in providing neutron standards at the UK National Physical Laboratory. Nucl. Instrum. Meths Phys. Res. A 580, 183–185.

Ha10 Harano, H., Matsumoto, T., Tanimura, Y., Shikaze, Y., Baba, M., Nakamura, T., 2009. Monoenergetic and quasi-monoenergetic neutron reference fields in Japan. Proceedings of the 11th symposium on neutron and ion, Rad. Meas. 45, 10, 1076-1082.

Ha40 Haxby, R.O., Shoupp, W.E., Stephens, W.E., Wells, W.H., 1940. Thresholds for the proton-neutron reactions of lithium, beryllium, boron and carbon. Phys. Rev. 58, 1035-1042.

Ha65 Harris, K.K., Grench, H.A., Johnson, R.G., Vaughn, F.J., 1965. The $^{51}V(p,n)^{51}Cr$ reaction as a neutron source of known intensity. Nucl. Instrum. Meths. 33, 257-260.

He05 Hellborg, R. (Editor), 2005. Electrostatic accelerators: fundamentals and applications. Berlin, Springer.

Hu85 Hunt, J.B., Cosack, M., Lesiecki, H., 1985. Calibration of neutron survey meters over the energy range from 1 to 30 keV with accelerator produced monoenergetic neutrons. Proc. of 5th symposium on neutron dosimetry, EUR-9762 (CEC Luxembourg) I, 597.

ICRP74 ICRP Publication 74, 1997. Conversion coefficients for use in radiological protection against external radiation. Annals of the International Commission on Radiological Protection vol. 26/3.

ICRU 60 ICRU Report No. 60, 1998. Fundamental quantities and units for ionizing radiations. International Commission on Radiation Units & Measurements.

IEC 61005, 2003. Radiation protection instrumentation - Neutron ambient dose equivalent (rate) meters. International Electrotechnical Commission.

IEC 61526, 2005. Radiation protection instrumentation - Measurement of personal dose equivalents Hp(10) and Hp(0,07) for X, gamma, neutron and beta radiations - Direct reading personal dose equivalent meters and monitors. International Electrotechnical Commission.

ISO 8529-1, 2001. International Organization for Standardization. Reference neutron radiations – Part 1: Characteristics and methods of production. International Standard ISO 8529-1.

ISO 8529-2, 2000. International Organization for Standardization. Reference neutron radiations – Part 2: Calibration fundamentals of radiation protection devices related to the basic quantities characterizing the radiation field. International Standard ISO 8529-2.

JCGM08 Evaluation of measurement data – Guide to the expression of uncertainty in measurement, BIPM, JCGM 100:2008.

Jo54 Jones, K.W., Douglas, R.A., McEllistrem, M.T., Richards, H.T., 1954. Comparison of nuclear and gamma-ray energy scales. Phys. Rev. 94, p 947.

Jo57 Johnson, C.H. et al., 1958. Proton strength functions from (p,n) cross sections. Phys. Rev. 109, 1243.

Kinematics Institute for Reference Materials and Measurements, European Community, 2008.

Kl97 Klett, A., Burgkhardt, B., 1997. The New remcounter LB6411: measurement of neutron ambient dose equivalent H*(10) according to ICRP60 with high sensitivity, IEEE Trans. Nucl. Sc. 44, 3, 757-759.

La10-1 Lacoste, V., 2010. Design of a new long counter for the determination of the neutron fluence reference values at the IRSN AMANDE facility. Proceedings of the 11th symposium on neutron and ion, Rad. Meas. 45, 10, 1250-1253.

La10-2 Lacoste, V., Gressier, V., 2010. Experimental characterization of the IRSN long counter for the determination of the neutron fluence reference values at the AMANDE facility. Proceedings of the 11th symposium on neutron and ion, Rad. Meas. 45, 10, 1254-1257.

Ma02 Mayer, M., 2002. Ion beam analysis of rough thin films. Nucl. Inst. and Meth. B194, 177-186.

Ma60 Marion, J.B., Fowler, J.L., 1960. Fast Neutron Physics, Part I. Interscience Publishers, Inc.

Ma68 Marion, J.B., Young, F.C., 1968. Nuclear reaction analysis, Graphs and tables. North-Holland Publishing Company-AMSTERDAM.

Mo03 Moszynski, M., 2003. Inorganic scintillation detectors in g-ray spectrometry. Nucl. Instrum. Meths Phys. Res. A505, 101-110.

Mo04 Mous, D.J.W., Visser, J., Haitsma, R.G., 2004. A nanosecond pulsing system for MeV light ions using a 2 MV Tandetron[TM]. Nucl. Instrum. Meths Phys. Res. B219-220, 490-493.

Mo09 Mosconi, M., Heil, M., Käppeler, F., Plag, R. Mengoni, A., Nolte, R., 2009. Monoenergetic neutrons for stellar applications. Publications of the Astronomical Society of Australia 26, 232–236.

NE08 NeuSDesc, 2008, Institute for Reference Materials and Measurements, European Community.

QC03 Q-value calculator, http://www.nndc.bnl.gov/qcalc/. National Nuclear Data Center.

Ro04 Roberts, N.J., Tagziria, H., Thomas, D.J., 2004. Determination of the effective centres of the NPL long counters. NPL Report DQL-RN 004.

Ro55 Robley, D., E., 1955. The Atomic nucleus. PhD, McGraw-Hill Book Company, Inc.

Ro77 Rogers, D.W.O., 1977. The ^{45}Sc(p,n) reaction as a source of monoenergetic 10-50 keV neutrons. Nucl. Inst. Meth. 142, 475-478.

Ro77-2 Robitaille, H.A., 1977. Rapid, on-line matrix unfolding of fast neutron spectroscopic data from organic scintillators. Proc. 3rd Symp. on Neutron Dosimetry in Biology and Medicine, 425-442.

Sc05 D. Schlegel, 2005. Target user's manual. Physikalisch-Technische Bundesanstalt laboratory report PTB-6.42-05-2.

Sc85 Schölermann, H., Siebert, B.R.L., 1985. Calibration of a Van de Graaf accelerator and determination of the threshold of the reaction 45Sc(p,n)45Ti using a covariance analysis. Nucl. Instrum. Meths Phys. Res. A 236, 225.

Sc89 Schölermann H., Böttger R., 1989. Q-values for (p,n) reactions on ^{65}Cu and ^{51}V. Nucl. Phys. A501, 86-94.

Se09 Serre, S., Castellani-Coulié, K., Paul, D., Lacoste, V., 2009. Optimization using Monte Carlo calculations of a Bonner sphere spectrometer extended to high energies for the neutron environments characterization. IEEE Transactions on Nuclear Science 56, 3582-3590.

Ta07 Tanimura, Y., Saegusa, J., Shikaze, Y., Tsutsumi, M., Shimizu, S., Yoshizawa, M., 2007. Construction of monoenergetic neutron calibration fields using ^{45}Sc(p,n)^{45}Ti reaction at JAEA. Rad. Prot. Dosim. 126, 8-12.

Ta48 Taschek, R., Hemmendinger, A., 1948. Reaction constants for ^{7}Li(p,n)^{7}Be. Phys. Rev. 74, 373.

Ta98 Tagziria, H., Thomas, D.J., 1998. Re-calibration and Monte Carlo modelling of the NPL long counters. NPL report, CIRM 19.

Th10 Thomas D.J., 2010. Neutron spectrometry. Rad. Meas. 45, 1178-1185.

Th10-2 Thomas D.J., Lewis V.E., Klein H., Allisy-Roberts P.J., 2010. International key comparison of 24 keV neutron fluence measurements (1993-2009): CCRI(III)-K1. Metrologia 47, Tech. Suppl. 06014.

Ut83   Uttley, C.A., 1983. Sources of monoenergetic neutrons, in: Cierjacks, S. (Eds.), Neutron sources for basic physics and applications. Pergamon Press, Oxford, 19-55.

Va57   Van Patter, D.M., Whaling, W., 1957. Nuclear disintegration energies. II. Rev. Modern Phys. 29, 757.

WI06   G. Dietze *et al.*, 2006. WinSpekt 2006 code. Physikalisch-Technische Bundesanstalt.

Wi85   Wilson, J.C., Hewitt, J.S., 1985. Evaluation of a new Monte Carlo code (PEP-C) for predicting the efficiency of a small bismuth germanate detector to photons at energies to 10 MeV, IEEE Trans. Nuc. Sci. 32, 397-401.

This work has been already published in two articles:

Lamirand, V., Gressier, V., Martin, A., Thomas, D.J., 2010. Comparison of nuclear reactions for the production of monoenergetic neutron fields with energies below 100 keV. Proceedings of the 11th symposium on neutron and ion, Rad. Meas. 45, 10, 1112-1115.

Lamirand, V., Thomas, D.J., Gressier, V., Sorieul, S., Liatard, E., 2010. Study of scandium targets for production of monoenergetic neutron fields with energies below 100 keV. Proceedings of the 11th symposium on neutron and ion, Rad. Meas. 45, 10, 1112-1115.

APPENDIX

A. Reaction thresholds

In the case of endothermic (p,n) reactions, kinematics induce several steps before reaching monoenergetic range of the considered reaction.

a. **Reaction threshold:** two groups of neutrons are emitted in a forward cone. Their energy is the same at exact threshold, and then diverges.

$V_{CM} >> V_n(CM)$

$V_1 (lab) \sim V_2(lab)$

V_{CM}

$\theta_{max} \sim 0$
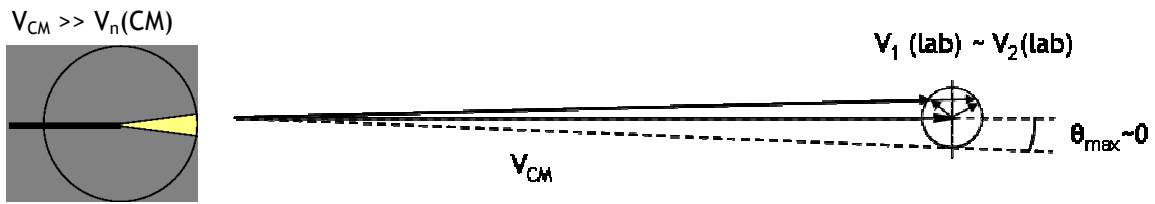
b. **Raising forward cone:** the emission solid angle covered in the laboratory reference of frame grows. For each laboratory angle, two neutron groups of different energies are emitted.

$V_{CM} > V_n(CM)$

$V_1 (lab)$

$V_2(lab)$

$V_n(CM)$

T_2

T_1

θ

θ_{max}

V_{CM}
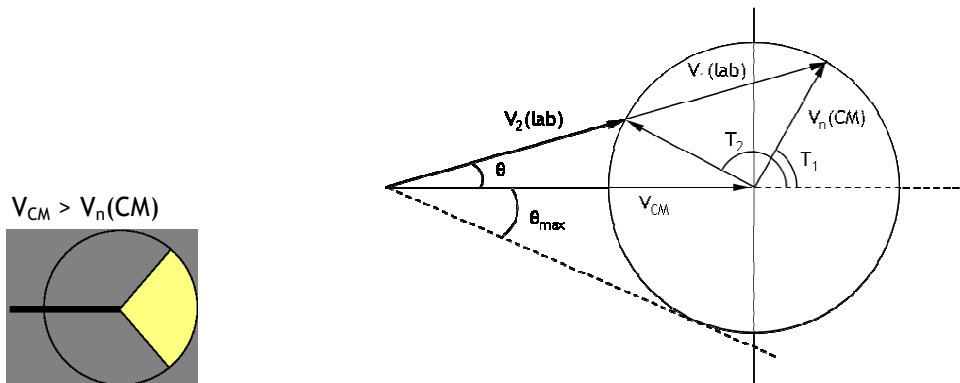
c. **Monoenergetic threshold:** each laboratory emission angle corresponds to unique neutron energy. The emission cone raises 90° degrees before covering the whole space.

$V_{CM} = V_n(CM)$

$V_n (lab)$

$V_n(CM)$

T

θ

V_{CM}

θ_{max}
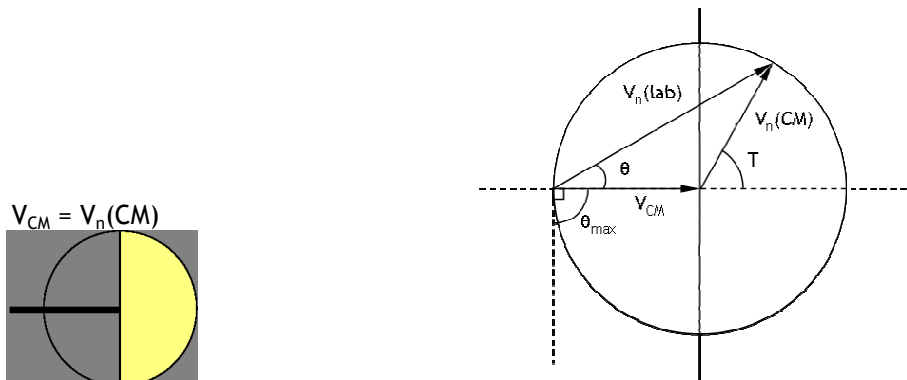
d. **Above monoenergetic threshold:** neutrons are emitted in every direction of the laboratory, constituting a monoenergetic neutron field.

$V_{CM} < V_n(CM)$
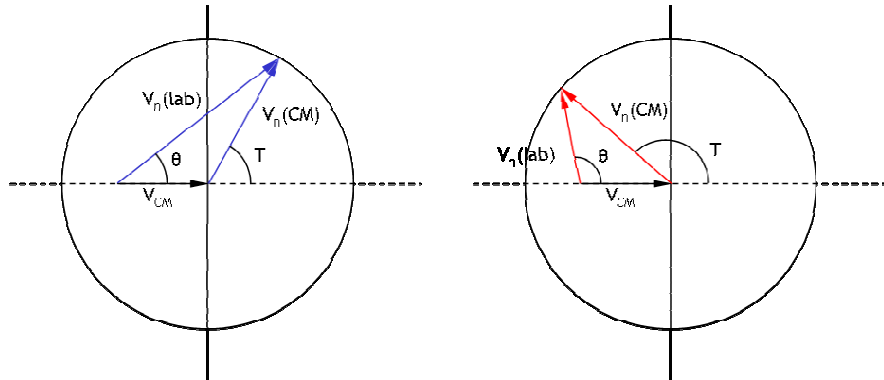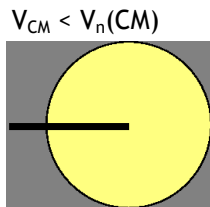
B. French abstract

Introduction
Champs neutroniques monoénergétiques
dédiés à l'étalonnage de détecteurs

La réponse d'un détecteur de neutrons varie avec l'énergie du neutron incident. Cette variation, appelée fonction de réponse, est généralement calculée au moyen de codes Monte-Carlo et déterminée expérimentalement sur des installations délivrant des champs neutroniques monoénergétiques.

Ces champs neutroniques peuvent être produits par des sources radioactives, des réacteurs nucléaires ou des accélérateurs (Ma60). Des sources radioactives telles que l'antimoine-béryllium peuvent être employées. Les neutrons sont produits par réaction (γ,n) entre les gammas à 1691 et 2091 keV de l'antimoine 124 et le beryllium. Le groupe neutron principal possède une énergie de 22,8 ± 1,3 keV. Cette source produisant aussi un groupe de plus haute énergie (378 keV, 3 % de la contribution principale), elle ne peut être considérée seulement comme quasi-monoénergétique. Sa demi-vie est de 60 jours, l'antimoine 124 est donc généralement produit juste auparavant la session de mesures (Th10-2).

L'utilisation d'un réacteur consiste à filtrer le faisceau de neutrons extrait du réacteur au moyen de divers matériaux (Sc, Fe, Al, Si), de façon à obtenir une source quasi-monoénergétiques entre le domaine thermique et 144 keV (ISO 8529). Leur emploi est principalement limité par le besoin et les contraintes d'un réacteur nucléaire.

La production de neutrons par accélérateur, par le biais de réactions à deux corps, est une façon commode de produire des champs neutroniques monoénergétiques. Les neutrons sont obtenus par réaction nucléaire entre les particules chargées accélérées (telles que protons ou deutons) et des cibles de matériaux sélectionnés. Le produit de la collision est l'émission de neutrons dans toutes les directions, formant ainsi un champ neutronique. A chaque énergie de projectile et angle d'émission correspond une seule énergie de neutron ; c'est pourquoi ce sont des sources de neutrons monoénergétiques. Cela permet diverses utilisations telles que l'étalonnage de détecteurs et autres usages scientifiques.

Table 21: *Réactions nucléaires communément employées pour la production de champ neutroniques monoénergétiques. Sont indiqués les domaines en énergie neutron accessibles dans la direction du faisceau incident (0°), ainsi que les domaines en énergie du projectile correspondant. Le domaine en énergie accessible pour un projectile entre 100 keV et 4 MeV est indiqué entre parenthèses.*

Réaction	Domaine en énergie du projectile (MeV)		Domaine en énergie des neutrons produits (à 0°, MeV)	
$^7Li(p,n)^7Be$	1,92	2,37	0,12	0,65
$^3H(p,n)^3He$	1,15	8,35	0,29	7,58 (3,2)
$^2H(d,n)^3He$	0	4,45	2,45 (2,85)	7,71 (7,26)
$^3H(d,n)^4He$	0	3,71	14,1 (14,7)	20,5

Protons et deutons accélérés jusqu'à 3.5 MeV et dirigés sur des cibles appropriées, peuvent produire des neutrons entre 120 keV et 19 MeV dans la direction du faisceau incident (0°), par les réactions nucléaires indiquées dans le Tableau 1. Ces dernières réactions nucléaires ne peuvent produire de neutrons en-dessous de 120 keV dans la direction du faisceau incident. Différentes solutions sont employées pour pallier cette limitation.

Pour atteindre des énergies inférieures, il est possible d'augmenter l'angle du point de mesure par rapport à la direction du faisceau d'ions en utilisant la réaction $^7Li(p,n)$ (Gi60). Cependant, cette méthode présente des problèmes d'homogénéité en énergie et en fluence des neutrons à la surface du détecteur, ainsi qu'une augmentation de la proportion de neutrons diffusés (Ro77).

Une approche originale a été développée par le NMIJ pour produire des neutrons de 24 keV. Elle consiste à filtrer au moyen d'une résonance du fer les neutrons produits avec une cible épaisse de lithium par réaction $^7Li(p, n)^7Be$ sous le seuil monoénergétique (Ha10).

L'utilisation d'autres réactions nucléaires capables de produire des champs neutroniques monoénergétiques de basse énergie à 0° constitue une autre alternative. La principale difficulté de ces champs neutroniques est leur faible rendement par comparaison avec celui de la réaction $^7Li(p,n)$. La réaction $^{45}Sc(p,n)$ semble être un candidat favorable, capable d'étendre le domaine en énergie des neutrons jusqu'à 8 keV à 0°, avec un rendement neutron suffisant pour l'étalonnage d'instruments de radioprotection.
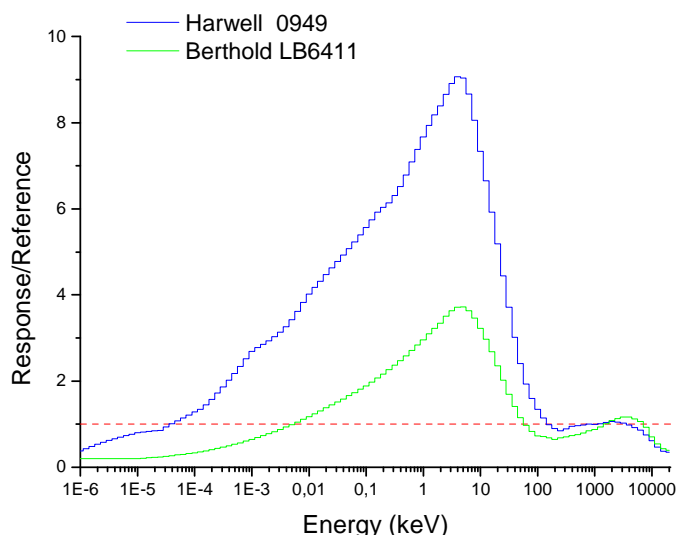
Fig. 82: *Fonctions de réponse simulées (normalisées avec une source de ^{252}Cf) de débitmètres Harwell et Berthold.*

L'importance de l'étalonnage à basse énergie peut être illustrée par :

- La sur-réponse des débitmètres et dosimètres entre 10^{-5}-10^2 keV, comme cela a déjà été montré par des simulations et mesures (cf. Fig. 1, Al94, Kl97 et aussi 5.2)

- Les standards développés par l'IEC (International Electrotechnical Commission) recommandent un point de mesure en dessous de 100 keV et un autre entre 1 et 50 keV pour respectivement l'étalonnage d'instruments de mesures de dose personnelle (IEC 61526) et d'instruments de mesures d'ambiance (IEC 61005). Le standard ISO 8529 (ISO 8529-1) recommande l'emploi des réactions ^{7}Li(p,n) et ^{45}Sc(p,n) pour ce domaine en énergie.

Cette étude est menée dans le cadre d'une coopération scientifique européenne entre l'IRMM (Institute for Reference Materials and Measurements, CE), le NPL (National Physical Laboratory, Royaume-Uni), le PTB (Physikalisch-Technische Bundesanstalt, Allemagne) et l'IRSN (Institut de Radioprotection et de Sûreté Nucléaire, France).

1 REACTIONS NUCLEAIRES EMETTRICES DE NEUTRONS..........6

Lorsqu'une particule pénètre la matière, elle peut interagir de nombreuses façons selon son énergie et la nature des particules en jeu. A basse énergie, c'est l'interaction avec le nuage électronique qui prévaut. Lorsque des particules de plus hautes énergies, provenant d'un accélérateur, d'une source radioactive ou de rayons cosmiques percutent la matière, elles peuvent réussir à interagir avec les noyaux du matériau, entraînant une réaction nucléaire.

Une réaction nucléaire à deux corps est un processus d'interaction entre un projectile et un noyau. Les transformations résultent de la mise en jeu de forces nucléaires. Elle sont conventionnellement écrite X(a,b)Y, où a est le projectile, X le noyau cible, b le produit léger et Y le noyau résultant ou produit lourd.

Les réactions nucléaires employées pour produire des champs neutroniques monoénergétiques sont induites par l'interaction entre des ions accélérés et les noyaux d'une cible. De nombreuses réactions sont alors possibles, selon les spécifications de l'accélérateur (nature et énergie des ions, intensité du faisceau) et la cible sélectionnée. Pour la production de champs neutroniques monoénergétiques, une des conditions est que le produit lourd Y soit dans son état fondamental. Si le noyau est dans un état excité Y*, il émet de nouvelles particules en se désexcitant, et la monoénergéticité peut être perdue.

Dans une première partie sont décrites les principales interactions qui ont lieu lorsqu'une particule approche le noyau d'un atome, ainsi que les mécanismes d'interaction possibles. Sont ensuite présentées les lois de conservation décrivant ces interactions. Une description complète de ces phénomènes peut être obtenue dans la référence (Be04), le but de ces parties étant l'introduction des concepts nécessaires à l'étude présentée dans ce document.

La production de neutrons par réaction nucléaire dépend de nombreux paramètres interdépendants, tels que l'énergie de la réaction, l'énergie du faisceau incident ou la section efficace. Certaines quantités telles que l'énergie de la réaction, les éventuels seuils ou l'énergie des neutrons produits, peuvent être calculés en utilisant les lois de la cinématique. Dans une dernière partie sont discutées plusieurs propriétés importantes des champs neutroniques monoénergétiques produits par accélérateur : notion de monoénergéticité, dispersion en énergie, rendement et caractéristiques des cibles.

Certaines caractéristiques importantes des réactions nucléaires peuvent être calculées a priori, limitant le domaine de prospection de nouvelles réactions. Cela permet la sélection de réaction produisant des neutrons dans le domaine en énergie souhaité, ainsi que l'évaluation d'autres caractéristiques telle que la variation en fluence et en énergie des neutrons en fonction de l'angle. Ces spécifications doivent être complétées par des expériences pour déterminer par la mesure celles inaccessibles ou difficilement accessibles au calcul, comme l'intensité neutronique accessible, basée sur des mesures de section efficace et de tenue des cibles sous irradiation.

2 <u>SELECTION DES REACTIONS</u>......................................

Comme mentionné dans l'introduction de ce document, il existe plusieurs méthodes bien connues pour produire des neutrons monoénergétiques. La production de neutrons de l'ordre du keV est habituellement réalisée par des réactions nucléaires induites par accélérateur.

Dans ce chapitre sont tout d'abord brièvement listées les conditions nécessaires pour qu'une réaction soit une source acceptable de neutrons monoénergétiques aux alentours du keV. Sont aussi discutées les propriétés de plusieurs réactions connues, à partir de la littérature et de calculs réalisés avec les programmes *Drosg2000* (Dr00) et *TARGET* (Sc05).

Trois critères principaux sont considérés : faisabilité, énergie et intensité des neutrons. L'énergie des projectiles nécessaire à la réalisation de la réaction doit être accessible à de petits accélérateurs à tension continue de quelques MV, et les cibles doivent être suffisamment faciles à produire et manipuler. Bien sûr, les neutrons produits doivent avoir l'énergie souhaitée dans le domaine monoénergétique de la réaction. Enfin la fluence neutron accessible doit être suffisante pour l'étalonnage de détecteurs : section efficace acceptable, et bonne tenue de la cible sous des courants de faisceau de quelques µA.

Dans la mesure du possible, la contribution d'autres réactions concurrentes (provenant de la couche réactive de la cible ou d'ailleurs) doit être limitée. Les rayonnements gammas pouvant être détectés par de nombreux instruments dédiés à la détection des neutrons, leur production doit être aussi restreinte que possible.

Plusieurs réactions présentent ces caractéristiques, et sont couramment ou ont été précédemment employées. La réaction ^{7}Li(p,n) est connue depuis des décennies (Ha40) et est toujours employée du fait de ses nombreuses qualités : rendement neutronique important, énergie minimale à 0° de 120 keV. C'est la source de champs neutroniques monoénergétiques la plus commune en dessous de 650 keV. Elle peut aussi être utilisée pour produire des neutrons de plus basse énergie en augmentant l'angle du point de mesure. Elle a alors plusieurs avantages : rendement suffisant même aux angles arrière, préparation et manipulation relativement simple des cibles, structure monotone de la section efficace facilitant le réglage de l'accélérateur. Cependant, son utilisation est limitée par d'importants inconvénients : faible qualité du spectre neutron à ces angles (contribution des neutrons diffusés importante, inhomogénéité en fluence et en énergie des neutrons), faible résistance de la cible au fort courant.

Ces inconvénients sont majoritairement dus à l'utilisation des angles supérieurs, et limitent l'usage de la réaction ^{7}Li(p,n) pour les basses énergies. C'est pourquoi sont recherchées des réactions alternatives utilisables à 0°.

La réaction ^{45}Sc(p,n) est employée pour l'étalonnage de détecteurs depuis de nombreuses années (Hu85, Ta07). Cette réaction permet la production de neutrons d'énergie entre 5,6 et et 53 keV dans la direction du faisceau incident. Plusieurs expériences ont été déjà menées pour caractériser avec plus ou moins de précision son seuil de réaction, sa fonction d'excitation et le spectre neutron produit. Sa section efficace résonante peut être

considérée comme un inconvénient, mais aussi un avantage : elle permet alors la réduction de l'incertitude sur l'énergie des neutrons émis. La difficulté de sélection des résonances est grandement réduite par l'utilisation d'une haute tension en bout de ligne de faisceau. Son principal désavantage est son faible rendement. Il peut être compensé par l'application d'un fort courant sur la cible, rendu possible par la capacité des cibles de scandium à les supporter. La masse atomique élevée du scandium comparativement au lithium ou d'autres éléments légers est un atout pour l'obtention d'une homogénéité en fluence et énergie dans l'angle solide considéré, ce qui permet aussi de rapprocher le détecteur de la cible. Une connaissance exhaustive de sa section efficace différentielle (à 0° et sa variation angulaire), la tenue des cibles à fort courant et le reste de ses caractéristiques font de cette réaction une alternative valable à la réaction ^{7}Li(p,n) (Br55, Ro77).

La réaction ^{51}V(p,n) a été utilisée pour diverses applications au long des dernières décennies (Hu85). Elle peut être employée sur un large domaine en énergie sans réaction concurrente, de quelques keV (résonance à 6,44 keV) au MeV dans la direction du faisceau incident, et est principalement utilisée pour les mesures sur 4π. Cependant, son rendement semble faible et pourrait être insuffisant pour l'étalonnage d'instruments dédiés à la radioprotection.

La réaction ^{65}Cu(p,n) a été largement étudiée par Schölermann et Böttger (Sc89). Elle est un bon candidat pour la production de champs mono- ou quasi-monoénergétiques autour de 1 keV (premier pic à 1,17 keV, sous le seuil monoénergétique). Les cibles de cuivre semblent capables de supporter des courants d'ions importants de quelques dizaines de µA. Cependant, son utilisation pourrait être restreinte par son faible rendement et la contamination d'autres groupes de neutrons aux énergies pertinentes (le champ neutronique n'est pas réellement monoénergétique).

D'autres réactions nucléaires ont été envisagées et/ou partiellement étudiées (Jo57), cependant peu d'informations sont disponibles dans la littérature : ^{57}Fe(p,n), ^{37}Cl(p,n), ^{12}C(d,n)… Ces réactions doivent être sélectionnées *a priori* sur des critères cinématiques, mais seules de nouvelles expérimentations permettront une démonstration de principe.

3 <u>DISPOSITIFS EXPERIMENTAUX</u>.................................60

Dans ce chapitre sont d'abord décrites les installations utilisées : accélérateurs, détecteurs et dispositifs expérimentaux spécifiques à chaque laboratoire. Dans une seconde partie sont présentées les types de mesures réalisées sur ces installations, soit les méthodes expérimentales.

Selon l'installation dans laquelle s'est déroulée l'étude, un accélérateur à tension continue de type Van de Graaff ou Cockcroft-Walton, simple étage ou tandem a été employé. Tous sont basés sur le même principe, à quelques variations près. Un tel accélérateur consiste grossièrement en une source d'ions ; un système d'accélération composé d'un générateur de haute tension et d'une colonne accélératrice ; plusieurs instruments de mesures et contrôle du faisceau ; une cible ou un système d'extraction du faisceau. Dans le cas d'un accélérateur Van de Graaff, la haute-tension est produite par le transport de charges au moyen d'une courroie. Dans un accélérateur Cockcroft-Walton, cette mécanique est remplacée par une série de pont de diodes permettant le redressement du courant alternatif en courant continu.

Pour les neutrons d'énergie dans le domaine du keV, les détecteurs les plus adaptés consistent en un détecteur de neutrons thermiques très efficace, enveloppé d'un modérateur, comme c'est le cas des longs compteurs ou des systèmes à sphères de Bonner. Les rendements neutroniques attendus des réactions sélectionnées sont très faibles, ce qui empêche l'emploi de détecteurs proportionnels tels que les télescopes à protons de recul. Pour les mesures de temps de vol, les détecteurs les plus adaptés sont à les scintillateurs à verre au lithium.

Un long compteur est composé d'un tube de ^{3}He ou BF$_3$ dans un modérateur cylindrique composé de polyéthylène, polyéthylène borée et de cadmium. Dus à sa géométrie spécifique, les deux principales caractéristiques d'un long compteur sont sa réponse relativement plate entre quelques eV et plusieurs MeV, et son importante réponse R, d'au moins quelques cm^2.

Un détecteur à verre au lithium est basé sur la réaction ^{6}Li(n,α)^{3}He. Les neutrons interagissent avec le lithium compris à l'intérieur ou à l'extérieur du matériau scintillant. Les particules α et ^{3}He ainsi créées ionisent le cristal, induisant l'émission de lumière qui sera collectée pour générer des photo-électrons.

Chacune des installations des instituts partenaires ont été employées, ainsi que l'installation AIFIRA du CENBG. Elles consistent en un accélérateur (Van de Graaff ou Cockcroft-Walton) et un hall expérimental plus ou moins grand et équipé : 1 à 5 lignes de faisceau, murs éloignés pour éviter la diffusion des neutrons dans les installations de métrologie, bras motorisés pour le placement des instruments.

Les sections efficaces et leur distribution ont été caractérisée au moyen de deux méthodes principales : par mesure de fluence et par temps de vol. Selon l'ICRU 60, la fluence Φ est l'observable définie par le nombre de particules dN dans une sphère de surface de section efficace $d\alpha$:

$$\Phi = \frac{dN}{d\alpha}$$

Elle s'exprime donc par unité de surface. La fluence neutron est donc le nombre de neutrons traversant une surface unitaire. Elle s'exprime en m^{-2} ou cm^{-2}.

Les neutrons produits par une réaction nucléaire sélectionnée interagissent avec chacun des éléments de leur environnement et contribuent au champ neutronique total. Pour tout point de l'espace, il y a une contribution à la fluence totale : des neutrons directs, produits par la réaction induite et directement détectés ; des neutrons diffusés ; des neutrons produits par d'autres réactions ; du bruit de fond. Déterminer la fluence d'une réaction nucléaire choisie consiste donc à réaliser plusieurs mesures pour extraire la contribution spécifique des neutrons directs du champ mesuré.

La méthode du temps de vol est couramment employée pour caractériser la distribution en énergie des neutrons. Elle consiste à mesurer le temps nécessaire aux neutrons pour parcourir une distance connue, généralement de leur source d'émission au détecteur, puisque leur vitesse est en effet reliée à leur énergie cinétique.

4 <u>ETUDES EXPERIMENTALES DES REACTIONS CANDIDATES</u>....81

Dans le chapitre 2 du document présent, plusieurs réactions (p,n) ont été discutées comme potentielles sources de champs neutroniques monoénergétiques dans le domaine en énergie 1-100 keV. Le besoin d'expériences pour explorer les réactions a été souligné, la réaction ^{45}Sc(p,n) constituant le meilleur candidat.

Une étude complète de cette dernière réaction a été menée ; c'est l'objet de la première et principale partie de ce chapitre. La seconde partie détaille l'investigation de réactions alternatives et la comparaison de leurs fonctions d'excitation mesurées avec celle de la réaction ^{45}Sc(p,n).

<u>Démonstration de principe</u>

Du fait de sa faible section efficace, la réaction ^{45}Sc(p,n) ne permet d'atteindre que de faibles débits de fluence et d'équivalent de dose neutronique. Afin d'augmenter le taux de production des neutrons, pour l'étalonnage de détecteurs par exemple, il convient d'utiliser un courant de faisceau aussi élevé que possible. Cependant, cette augmentation ne peut être réalisée que si les cibles supportent ces forts courants d'ions. Ainsi la première étude a consisté à comparer sous irradiation le comportement de cibles déposées sur différents supports métalliques.

La capacité des cibles de scandium à supporter des courants de quelques dizaines de µA dépend largement des conditions expérimentales : taille du faisceau, système de refroidissement… Le résultat de cette étude est la démonstration de la capacité des cibles de scandium à supporter sans problème des courants de 20 à 30 µA si le faisceau est suffisamment large. Elle a aussi permis de sélectionner le tantale comme support de cible idéal pour les cibles de scandium.

Les mesures des photons produits dans les champs neutroniques ont conclu à une faible contribution de ceux-ci à l'équivalent de dose total. La réaction ^{45}Sc(p,n) peut donc être utilisée pour étalonner des instruments de détection de neutrons également sensibles au gammas.

<u>Identification des résonances</u>

La section efficace de réaction ^{45}Sc(p,n) possède une structure résonante dans le domaine d'intérêt. Cette structure a déjà été observée lors d'expériences précédentes comme présenté dans le chapitre 2. Le but de ces nouvelles mesures est de caractériser les résonances pour permettre la simulation de leurs largeurs dans un dispositif spécifié, et de déterminer les paramètres de ces résonances dans une première étape de détermination de sections efficaces différentielles.

L'emploi de deux méthodes de mesure, temps de vol et fonction d'excitation, a permis de rassembler un maximum d'information par l'utilisation conjointe des résultats. Les résonances ont été caractérisées en termes d'énergie, largeur, espacement et densité sur l'intégralité du domaine monoénergétique de la réaction.

Tous les résultats obtenus sont en bon accord avec les études précédentes, qualitativement pour l'excitation de fonction considérée seule, mais aussi quantitativement lorsque combinée aux résultats du temps de vol pour la position des résonances.

Grâce aux dispositifs expérimentaux employés, la mesure de la fonction d'excitation est celle qui a permis la collecte du plus grand nombre d'information sur la structure résonante. La méthode du temps de vol a permis une plus grande précision quant à la position des résonances (énergies du proton incident ou du neutron émis étant équivalentes par le calcul de la cinématique), et ainsi le positionnement global de la fonction d'excitation obtenue.

Malgré des problèmes expérimentaux ayant rendu impossible la répétition de la mesure sur la résonance à 27 keV, la monoénergéticité a pu être vérifiée sur la résonance à 8 keV, dans les limites de la résolution du faisceau. De plus, toutes les résonances identifiées par la méthode du temps de vol ont été confirmée par la fonction d'excitation. Chacune des observations tend à démontrer qu'il n'y a pas de réactions concurrentes et très peu d'interférences entre résonances : la réaction est monoénergétique dans ce domaine en énergie. Les résonances sont nombreuses et fines, ce qui tend à valider l'hypothèse du noyau composé.

Les expériences ont confirmé l'intérêt des résonances à 8 et 27 keV, et peut-être à 36 keV également, pour produire des champs neutroniques monoénergétiques de qualité. Comme le rendement et la qualité des neutrons produits par la réaction ^{7}Li(p,n) augmentent avec l'énergie, les résonances du scandium aux plus hautes énergies semblent moins attractives.

La détermination des paramètres de résonances et de la structure nucléaire pourrait être réalisée en employant des méthodes de déconvolution du spectre obtenu, ou par l'utilisation de simulations basé sur des modèles théoriques (matrice de réaction). Les mesures pourraient être répétées à des angles choisis pour discriminer les processus (niveaux d'énergie en jeu) et modes (noyaux composé, réaction directe) d'interaction.

Ces expériences ont aussi été une source d'information précieuse pour la mesure de section efficace : elles ont permis la caractérisation de la composition multi-résonance des pics observés, et donné des indices sur l'isotropie dans le centre de masse de la réaction.

Détermination de sections efficaces différentielles de résonances sélectionnées

Sur l'ensemble de son domaine monoénergétique, deux résonances de la réaction ^{45}Sc(p,n) présentent un rendement important à leur faible énergie : les résonances à 8 et 27 keV. Cette étude se concentre par conséquent sur ces deux résonances. Comme établi dans le chapitre 2, les sections efficaces différentielles angulaires sont nécessaires à l'estimation des neutrons diffusés par simulation Monte-Carlo. Le but est ainsi la détermination des sections efficaces d'émission des neutrons dans tout l'espace des deux résonances, réalisée en deux mesures : une mesure absolue à un angle spécifique (0° pour plus de commodités) ; la détermination de la variation angulaire de la section efficace par mesures successives à différents angles.

En combinant les résultats des deux expériences détaillées dans cette étude, la section efficace différentielle absolue de la réaction ^{45}Sc(p,n) a été caractérisée dans tout l'espace pour les deux résonances principales, 8,15 et 27,24 keV.

Comme prévu, les valeurs obtenues sont faibles, même à 0° : respectivement 3,39 ± 0,08 et 2,93 ± 0,07 mb.sr^{-1}. Cependant, la réaction est effectivement isotropique dans le centre de masse, ce qui permet de prendre avantage du poids du scandium pour une meilleure homogénéité à la surface des détecteurs.

Des problèmes de contamination n'ont permis de réaliser des mesures de sections efficaces qu'avec la plus épaisse des cibles préparées. L'emploi de cette cible n'a pas permis de séparer les neutrons produits par plusieurs résonances simultanément. L'expérience pourrait être répétée avec une cible plus fine pour couvrir comme souhaité une résonance à la fois, et s'affranchir de la contribution due à la contamination au lithium 7. Une autre façon de déterminer la section efficace de la résonance principale du pic serait la déconvolution des résultats par la structure résonante déterminée lors des expériences précédentes.

Cependant, et comme les paramètres du faisceau et de cibles employés correspondent au dispositif expérimental habituel dans l'optique d'étalonnage, les résultats obtenus sont suffisants pour l'utilisation courante des champs neutroniques produits par la réaction ^{45}Sc(p,n).

La suite logique de ces résultats est leur implémentation dans les codes de simulation. Ainsi il sera possible de calculer la contribution des neutrons diffusés et l'homogénéité en fluence et en énergie à la surface de l'instrument irradié.

Investigation expérimentale d'autres réactions

Le but de la comparaison des réactions sélectionnées était l'investigation de réactions pour la production de champs neutroniques monoénergétiques en dessous de 50 keV. La comparaison des résultats avec les précédentes mesures ont validé le dispositif expérimental. Les fonctions d'excitation des réactions ^{45}Sc(p,n), ^{65}Cu(p,n), ^{51}V(p,n), ^{57}Fe(p,n), ^{49}Ti(p,n), ^{53}Cr(p,n) et ^{37}Cl(p,n) ont été mesurées sur l'installation AMANDE. Toutes les réactions étudiées possèdent une section efficace à structure résonante, ce qui permet une résolution fine de l'énergie des neutrons. La réaction ^{45}Sc(p,n) reste le meilleur candidat pour la production de neutrons de basse énergie à 0°, particulièrement au moyen des résonances à 8 et 27 keV qui présentent les meilleures rendements des réactions étudiées. La réaction ^{65}Cu(p,n) est intéressante pour sa résonance bien définie à une très faible énergie de 1,17 keV, bien que le champ produit ne soit pas purement monoénergétique. Le rendement neutronique des autres réactions étudiées est trop faible et ne justifie pas leur utilisation.

Un autre résultat de cette étude est la validation de la méthode de production de cibles solides par l'implantation d'éléments gazeux, comme elle a été mise en œuvre pour la réaction ^{37}Cl(p,n).

5 UTILISATION DE CHAMPS NEUTRONIQUES MONOENERGETIQUES DE L'ORDRE DU KEV

Suite aux études expérimentales portant sur les champs monoénergétiques neutroniques dans le domaine du keV détaillées précédemment, plusieurs applications ont ou auraient été intéressantes à réaliser.

Implémentation des résultats expérimentaux dans les codes de simulation

Ce travail, qui n'a pu être réalisé faute de temps, aurait consisté à introduire les valeurs des observables mesurées dans les différents codes de calcul employés par les laboratoires de la collaboration scientifique IRMM-IRSN-NPL-PTB.

Etalonnage de débitmètres dans le domaine 1-100 keV

La sur-réponse de débitmètres et dosimètres dans le domaine 1-100 keV a été démontrée précédemment par des simulations et des campagnes de mesures (Al94, Kl97). Elles justifient les recommandations CEI et ISO pour l'étalonnage d'instruments sensibles aux neutrons au moyen de sources délivrant des neutrons dans ce domaine.

C'est une des raisons principales d'étude des champs neutroniques monoénergétiques de basse énergie, c'est pourquoi des mesures de principe ont été conduites, avec succès, sur les installations de l'IRSN et du NPL sur trois débitmètres en utilisant les résonances à 8 et 27 keV de la réaction ^{45}Sc(p,n).

CONCLUSION ET PERSPECTIVES................................**137**

La réponse d'un détecteur de neutron varie avec l'énergie des neutrons. Cette fonction de réponse est couramment calculée au moyen de codes Monte-Carlo et déterminée expérimentalement sur des installations délivrant des champs neutroniques monoénergétiques. L'importance de l'étalonnage à basse énergie est illustrée par la sur-réponse des débitmètres et dosimètres entre 10^{-5}-10^2 keV.

Il existe plusieurs méthodes de production des champs monoénergétiques ou quasi-monoénergétiques de l'ordre du keV. Les sources radioactives émettrices de neutrons dans ce domaine en énergie sont difficilement disponibles et de courte demi-vie. L'utilisation de réacteurs nucléaires n'a pas été abordée dans cette étude du fait de leur faible disponibilité dans le monde pour l'étalonnage de détecteurs. C'est pourquoi cette étude s'est concentrée sur les sources de neutrons produites par réaction nucléaire entre des ions accélérées et une cible : le but était de prospecter les réactions nucléaires à même de produire des champs neutroniques monoénergétiques de basse énergie adaptée à l'étalonnage de détecteurs de neutron.

Plusieurs réactions nucléaires sont couramment employées sous 100 keV, telles que la réaction ^{7}Li(p,n) aux angles supérieurs et dans une moindre mesure la réaction ^{45}Sc(p,n). L'utilisation de la bien-connue réaction ^{7}Li(p,n) pour le domaine du keV a plusieurs inconvénients, principalement en terme d'homogénéité en énergie et en fluence des neutrons à la surface du détecteur. Malgré ses nombreuses qualités, l'emploi de la réaction ^{45}Sc(p,n) était jusqu'alors limitée par son faible rendement et des lacunes dans sa caractérisation, tout particulièrement en terme de sections efficaces différentielles pour la simulation des neutrons diffusés.

Les expériences réalisés au cours de ce projet ont confirmé l'intérêt de la réaction ^{45}Sc(p,n) pour l'étalonnage de détecteurs. Il a été démontré que son faible rendement neutron peut être compensé en augmentant le courant du faisceau incident jusqu'à plusieurs dizaines de μA sans dommage pour la cible avec un support de tantale.

Des mesures de temps de vol sur cible épaisse et de fonction d'excitation ont été conjointement réalisées afin de détailler la structure résonnante de la section efficace. De nombreuses et nouvelles résonances ont été caractérisées sur l'intégralité du domaine en énergie monoénergétique de la réaction, en termes d'énergie des protons/neutrons et de rendement relatif. Ces résultats sont en excellents accord avec les études passées. Ils pourraient encore être raffinés, notamment en déterminant les paramètres de résonances tels que les largeurs effectives et les modes d'interaction préférentiels. Des méthodes de déconvolution ou des simulations basées sur des modèles théoriques pourraient être appliquées aux données. Les mesures par temps de vol ont aussi permis la vérification de la monoénergéticité de la résonance à 8 keV.

Les sections efficaces différentielles (p,n) ont été déterminées pour les deux résonnances les plus utiles, dans tout l'espace, c.à.d. pour tout angle d'émission des neutrons. Les sections efficaces différentielles des résonances à 8 et 27 keV sont respectivement de 3,39 ± 0,8 et 2,93 ± 0.7 mb.sr^{-1} dans la direction du faisceau incident. L'isotropie dans le centre de masse de la réaction a été vérifiée expérimentalement *a priori*. Un bilan des incertitudes complet a été mené, et les incertitudes particulièrement réduite par la mesure précise de l'épaisseur

des cibles et la sélection fine des résonances étudiées. Les valeurs obtenues sont à comparer à celle de la réaction ^{7}Li(p,n) utilisée aux grands angles, qui sont respectivement de 8,3 et 25,4 mb.sr^{-1} aux mêmes énergies de neutrons (l'énergie du faisceau incident étant fixée à 1936 keV).

Combinée à l'étude de la section efficace, l'étude des cibles conduite démontre que des débits de fluence neutronique comparable à ceux de la réaction ^{7}Li(p,n) sont accessibles si l'on emploie un dispositif expérimental adapté. Des mesures de la contribution des photons à l'équivalent de dose total ont été réalisées. Des problèmes de contamination ont empêché toute analyse de la structure nucléaire par le biais de ces mesures. Cependant elles ont permis de conclure que le rapport entre dose neutron et dose gamma était adapté à des applications telles que l'étalonnage de détecteurs de neutrons.

La prospection d'autres réactions a principalement permis d'écarter les réactions inadaptées. Elle a davantage permis la validation de méthodes (pour la production de cibles par exemple) et de réactions déjà connues. Malgré sont très faible rendement, le cuivre 65 pourrait être une option intéressante pour le développement de champs neutroniques monoénergétique de référence autour d'un keV.

En conclusion, la réaction ^{45}Sc(p,n) a déjà prouvé être un candidat plus que valable pour la production de champs neutroniques monoénergétiques, comme alternative à la réaction 7Li(p,n), particulièrement à 8 keV neutron. Cette réaction est dès lors disponible pour son emploi en routine permettant l'étalonnage d'instruments sensibles aux neutrons, et sera intégrée au prochain exercice de comparaison international en fluence neutron organisé par le BIPM. Elle peut être utilisée pour le développement d'instruments de mesure de référence dans ce domaine inhabituel en énergie, tels que des détecteurs à protons de recul basé sur l'étude des traces ou la discrimination gamma/neutron.

Un des perspectives de ces mesures et études est la possible implémentation des données obtenues dans des codes Monte-Carlo, tels que *TARGET* et/ou *NeuSDesc,* et dans diverses simulations pour reproduire les données expérimentales (par exemple la convolution de la dispersion en énergie du faisceau et de l'épaisseur de la cible). Les sections efficaces et les paramètres de résonances devront être ajoutés aux bases de données nucléaires internationales.

Parallèlement aux études de réactions nucléaires pour abaisser l'énergie neutron accessible tout en maintenant un rendement suffisant, les efforts pourraient être concentrés sur la prospection de réactions produisant des neutrons dans le domaine en énergie entre 50 et 100 keV à 0°, tel que le permet la réaction ^{11}B(p,n). De nouvelles méthodes pourraient être envisagées telles que le filtrage de réactions pour obtenir un nouveau compromis entre qualité du champ produit et importance du rendement neutronique.